Beyond 5G White Paper
6G Radio Technology Project
“Advanced MIMO Technology”

Version 1.0

May 7, 2025

XG Mobile Promotion Forum

【Revision History】

Ver.	Date	Contents	Note
1.0	2025.5.7	First version	

Preface

The fifth-generation mobile communication system (5G), introduced around 2020, plays a crucial role in today's society. 5G serves as a social infrastructure connecting people to people, people to things, and things to things, becoming indispensable for both everyday life and industrial sectors. The next-generation mobile communication system, 6G, is expected to act as a foundational infrastructure to build cyber-physical systems (CPS) and digital twins in the AI era, further increasing its significance. As mobile traffic continues to grow, 6G will not only need to provide a larger-capacity communication environment but also deliver optimal quality of experience for human and application performance for AI across entire areas. On the other hand, for 6G to become a widespread infrastructure, it is vital to deploy networks cost-effectively. From a sustainability perspective, it is also necessary to maintain communication quality while ensuring low power consumption. To achieve this, efficient use of lower frequency bands such as the congested Sub6 GHz, as well as effectively utilizing higher-frequency bands like millimeter waves, which are sensitive to blockage, and the newly anticipated Frequency Range 3 (FR3), will be important. Therefore, 6G needs to significantly enhance communication performance over 5G, taking various requirements into account.

In 5G, Multi-Input Multi-Output (MIMO) technology has played a significant role in enhancing communication performance. Massive MIMO was introduced in 5G, allowing for increased communication capacity through multi-user MIMO (MU-MIMO) and enabling coverage expansion for high-frequency bands with beamforming technology. Additionally, multi-Transmission Reception Point (TRP), which employs multiple base station (BS) antennas at different sites for transmission, allows for communication with a greater number of spatial multiplexing layers, enabling high-speed communication.

The progress of MIMO technology has evolved from single-user MIMO (SU-MIMO) to MU-MIMO, which involves spatial multiplexing communication between a single BS and multiple users, and further to multi-TRP using multiple BSs. In contrast, 6G will require not only a significantly larger number of antenna elements per BS compared to 5G's massive MIMO, but also spatial multiplexing transmission with more BSs and a greater number of user equipment devices (UEs). In essence, both massive MIMO and distributed MIMO technologies will need to evolve and be integrated. Moreover, enhancements in MIMO technology through AI/ML and advancements in control technology utilizing digital twin spaces beyond the traditional concept of MIMO are anticipated. This means that the concept of MIMO will expand to optimize spatial transmission for entire systems, transmitting between spaces in configurations that include intermediate nodes such as relays and reflectors. In this white paper, the evolved

MIMO technologies from traditional massive MIMO and multi-TRP are broadly defined as Advanced MIMO technologies.

This white paper has been crafted with support from many participants in the Advanced MIMO Working Group of the 6G Radio Technology Project in XGMF. The members consist of mobile network operators, network equipment vendors, device vendors, and university experts. In the next chapter, we will outline the evolution of Advanced MIMO towards Beyond 5G/6G and the challenges associated with this progression. Following this overview, we will introduce the specific research and development activities related to Advanced MIMO that each member is engaged in.

Among various activities for Advanced MIMO introduced in the following chapters, a particularly distinctive aspect in Japan is the emphasis on research and development of distributed MIMO. This focus is characterized by extensive research and development efforts for Beyond 5G/6G, targeting a broad range of frequency bands such as Sub-6 GHz, millimeter-wave, and Sub-THz, involving the development of elemental technologies and large-scale experimental demonstrations as well as extensive studies for FR3. Research initiatives also explore network architectures leveraging Radio over Fiber (RoF) technologies to achieve antenna distribution, a critical configuration for realizing distributed MIMO. The heightened interest and activity in distributed MIMO research in Japan can possibly be attributed to the necessity of network deployment in densely built environments, as well as a cultural propensity for seeking high-quality communication and fine-grained coverage.

We hope this white paper will promote global research and development related to Beyond 5G/6G, aid in solving societal issues and create new value in the Beyond 5G/6G era, and ultimately contribute to a prosperous society in Japan. Note that this paper includes the content of the previous Beyond 5G White Paper Supplementary Volume "Cell-Free Distributed MIMO" published by XGMF.

Kazushi Muraoka, NEC Corporation

Daisei Uchida, NTT Corporation

Shunsuke Kamiwatari, KDDI Research, Inc.

I. Evolution and Challenges of Advanced MIMO Towards Beyond 5G/6G

Kazushi Muraoka, NEC Corporation
Daisei Uchida, NTT Corporation
Issei Kanno, Shunsuke Kamiwatari, KDDI Research, Inc.
Satoshi Suyama, Kiichi Tateishi, Yuta Hayashi, NTT DOCOMO, INC.
Takashi Dateki, Fujitsu Limited
Takahisa Fukui, SHARP Corporation
Hiroki Iimori, Ericsson Research Japan
Fumiyuki Adachi, Tohoku University
Kenichi Higuchi, Kazuki Maruta, Tokyo University of Science
Koji Ishibashi, The University of Electro-Communications

I-1. Current Status and Challenges of Massive MIMO

Massive MIMO is a representative wireless technology of 5G and is essential for addressing increasing traffic and ensuring stable coverage. A key technical feature of massive MIMO is the use of TRPs with a large number of antenna elements. By fully utilizing these numerous antenna elements, several advantages can be achieved, as outlined below.

- By using beamforming with multiple antenna elements, beam gain can be improved, and coverage can be extended. This is particularly effective in higher frequency bands, where beamforming compensates for significant propagation losses associated with those frequencies.
- Utilizing multiple antenna elements enables spatial multiplexing communication with numerous UEs. Compared to traditional MIMO, achieving a greater number of spatial multiplexing layers enhances the system capacity.
- Beamforming allows for highly directed communication in specific directions, resulting in increased power efficiency.
- The large number of antenna elements can also be used to direct nulls towards UEs belonging to different cells, thereby reducing interference.

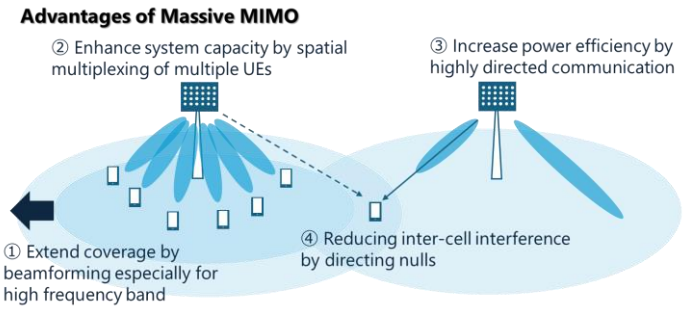

Fig.1-1 Advantages of Massive MIMO

For Beyond 5G/6G, it will be essential to evolve massive MIMO by utilizing an even greater number of antenna elements and transceiver circuits to achieve more spatial multiplexing layers and increase capacity. Additionally, it will be necessary to apply these advancements to new frequency bands, including FR3. However, there are still several challenges that need to be addressed to further develop massive MIMO.

- Challenges related to BS deployment and frequency
  - Securing new sites for BSs incurs costs. To make it easier to introduce new BS sites, the size and weight of the BS equipment need to be reduced.
  - For repurposing existing low-frequency BS sites for higher frequency bands including FR3, it is necessary to expand the BS's coverage. Additionally, in environments with many obstacles, high-frequency bands like the millimeter wave can suffer from limited signal penetration, potentially resulting in restricted coverage.
- Challenges concerning equipment for BSs and UEs
  - An increase in the number of antenna elements and transceiver circuits leads to an expanded circuit size.
  - As the number of spatial multiplexing layers increases, signal processing becomes more complex, and power consumption rises.
- Challenges in transmission methods
  - In actual propagation environments and commercial equipment, when performing SU-MIMO or MU-MIMO, the current control mechanisms do not always allow for the full utilization of the large spatial multiplexing capacity that the BS or UE is technically capable of.
  - In MU-MIMO, as the number of spatially multiplexed UEs increases, channel variations caused by the movement of UEs can significantly deteriorate performance.

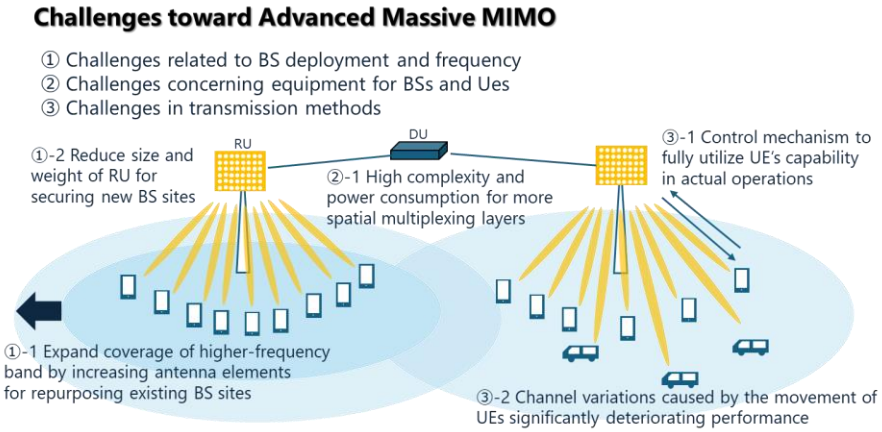

Fig.1-2 Challenges toward Advanced Massive MIMO

The challenges mentioned above are part of the overall issues facing massive MIMO, but they also represent implementation challenges for BSs and UEs that need to be resolved as we advance towards Beyond 5G/6G.

I-2. Current Status and Challenges of Distributed MIMO

Distributed MIMO, where TRPs (also known as distributed antennas) installed in different sites collaborate to transmit, is being considered as a promising solution to improve radio quality degradation caused by weak signal areas at cell edges and inter-cell interference. This approach is also referred to as cell-free massive MIMO. The primary advantages of distributed MIMO include the following four points:

- Improves radio quality at cell edges (such as 95-percentile of cumulative distribution function (CDF) of user throughput within the cell) and equalizes radio quality across the area.
- By coordinating TRPs for MU-MIMO, it reduces user interference and enables capacity enhancements proportional to the number of antennas. This means it is also expected to improve capacity per area.
- The multiple TRPs allow for site diversity, providing a solution for signal blockage and offering enhanced stability and reliability in high-frequency bands.
- By designating some TRPs as receive-only, it is possible to improve the uplink communication link budget without increasing the number of high-cost, high-power-consuming BS transmit units like high-power amplifiers.

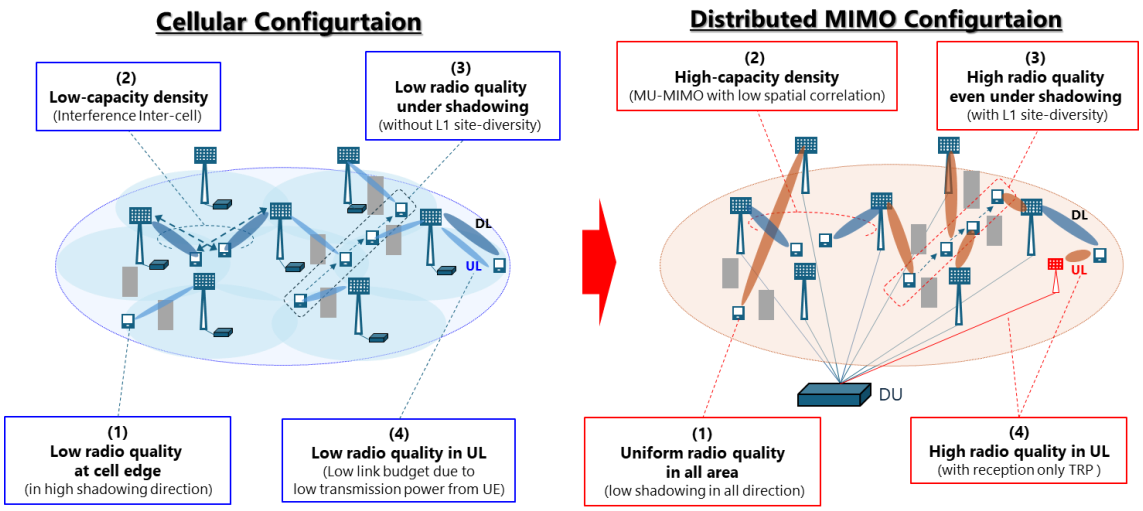

Fig.2-1 Advantages of Distributed MIMO

On the other hand, to Advanced distributed MIMO towards Beyond 5G/6G, the following technical challenges need to be considered:

- Complexity of control at BSs
  - As radio resource control includes TRP selection for optimization, Modulation and Coding Scheme (MCS) selection and the rank adaptation of MIMO layers also becomes more complex. The challenge is balancing the simplicity and feasibility of BS control with the maximization of system capacity.
- Feasibility of implementation as a system
  - When switching TRPs within the scheduling processing time unit (TTI: Transmission Time Interval), high-precision frequency and timing synchronization between TRPs are required. Additionally, if performing coherent joint transmission between TRPs, phase synchronization is also necessary. Thus, the implementation of these types of synchronization and the establishment of those control sequences are required.
  - The number of TRPs used in coordinated distributed MIMO needs to be limited based on the total number of orthogonal reference signals and the maximum number of digital signal processing circuits in Distributed Units (DUs). A challenge is to develop a mechanism and configuration that allows TRPs used in coordinated distributed MIMO to be flexibly altered according to the distribution of UEs and the radio propagation environment.
  - To enable the flexible expansion of TRP numbers according to area requirements, it is necessary to have a mechanism that allows the fronthaul capacity to be expanded flexibly, or a system that enables distributed processing of multiple TRPs across multiple DUs.

- Since TRP installation density could potentially be higher than that of conventional BS sites, there is a challenge in reducing equipment, installation, and operational costs per TRP through miniaturization, weight reduction, and lower power consumption. Additionally, developing a flexible RAN configuration that realizes distributed MIMO while maintaining the same installation density as traditional BS sites is another challenge.

- Application to high-frequency bands
  - In high-frequency bands, both the TRP and UEs use analog beams. Consequently, frequent TRP switching at the Layer 1 level is necessary due to the movement and rotation of the UEs. During TRP switching, changes in Doppler frequency and reception timing occur discontinuously, making it challenging to achieve stable communication quality without significantly enhancing the capabilities of UEs.
  - A mechanism is needed to rapidly optimize the combination of the transmitting TRP, the beam used at each TRP, and the beam used by the UE in response to the terminal's movement.
  - Proactive control to switch TRPs before experiencing blockages is necessary, as sudden decreases in reception levels can occur due to obstructions.
- Deployment scenarios from existing BS configurations
  - Transitioning from the current BS site configurations to a distributed MIMO setup poses challenges in terms of deployment scenarios. Various deployment strategies could be considered, such as implementing distributed MIMO by modifying fronthaul connections using currently deployed TRPs, or adopting a distributed MIMO configuration for TRPs that will be added in the future.
  - In high-frequency bands, relay, repeaters, reconfigurable intelligent surfaces (RIS), and inter-terminal relay are also promising solutions for coverage improvement. Considering these as additional radio propagation paths, challenges include integrating distributed MIMO transmission with these mechanisms, as well as managing the expansion of MIMO layers.

The challenges mentioned above need to be addressed to fully leverage distributed MIMO as we move towards Beyond 5G/6G.

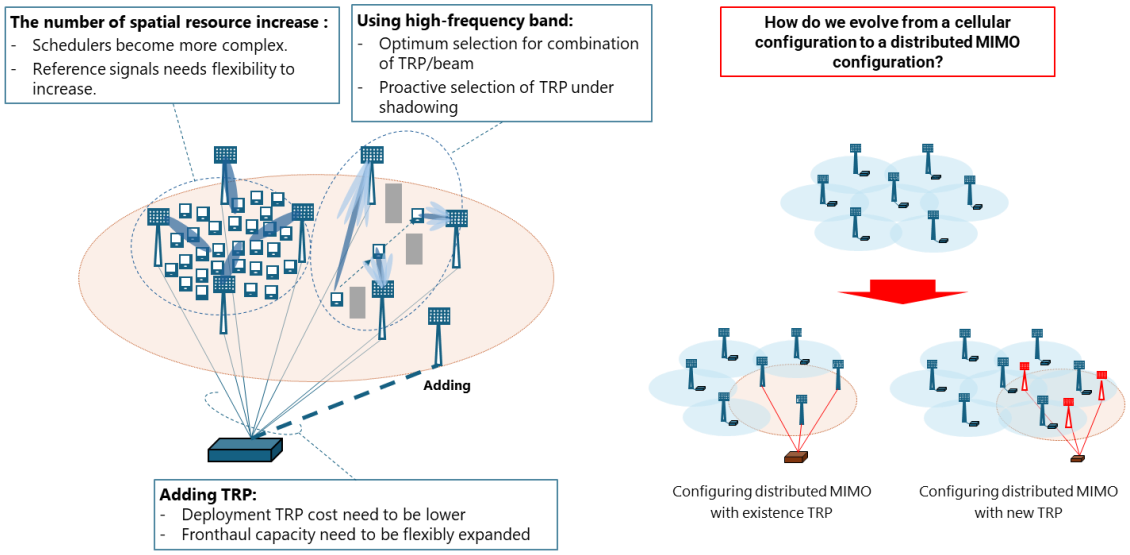

Fig.2-2 Challenges toward Advanced Distributed MIMO

I-3. Recent Activities related Advanced MIMO in 3GPP

The Third Generation Partnership Project (3GPP), which is responsible for the development and specification of mobile communication systems, is also working on realizing Advanced MIMO. Massive MIMO, which was fully introduced starting with Release 15, the first release of 5G, utilizes a large number of antenna elements on planar arrays to spatially multiplex numerous UEs using the same time-frequency resources, thereby improving signal to interference and noise ratio (SINR). Subsequent releases, such as Release 16 and Release 17, have seen enhancements in the codebooks used for transmission and reception, as well as the introduction of a feature known as multi-TRP, which uses multiple transmission-reception points. This section discusses trends in the standardization activities for Releases 18 and 19, known as 5G-Advanced, which serve as precursors to Advanced MIMO, and the outlook for standardization leading up to 6G.

In Release 18, extensive enhancements to MIMO technology were implemented. Firstly, in the multi-TRP feature, signaling overhead from multiple TRPs was a significant challenge, but the expansion of the Transmission Configuration Indicator (TCI) state facilitated more effective data transmission. This improved spectrum resource efficiency when multiple TRPs operate in coordination. For the uplink, the extension beyond the traditional 4-layer limit to a maximum of 8 layers and the introduction of Simultaneous Transmission with Multiple Panels (STxMP) were realized. This anticipates larger UEs, such as Fixed Wireless Access (FWA) and Customer Premises Equipment (CPE), being equipped with more than four antenna panes, significantly enhancing uplink throughput. Additionally, to increase the spatial multiplexing capability of MIMO, reference signals were expanded: Sounding Reference

Signal (SRS) was expanded from a maximum of 4 ports to 8 ports, and Demodulation Reference Signal (DMRS) from a maximum of 12 ports to 24 ports. This allows for the spatial multiplexing of more layers in MIMO.

In Release-19, further advancements are being made to accommodate larger antenna arrays, beam management in FR2, and enhancements related to multi-TRP functions. To enable beamforming with more antenna elements, the number of ports for Channel State Information Reference Signal (CSI-RS) is being expanded from a maximum of 32 to 128. Additionally, stabilizing beamforming remains a critical issue, especially in FR2, and a user-driven beam switching method is being considered. This approach is expected to balance beamforming agility with reduced overhead. For multi-TRP enhancements, calibration between TRPs has been newly standardized to address phase and frequency discrepancies between BSs in real environments. Furthermore, to improve uplink quality—a noted issue in 5G—reference signals are being expanded to accommodate the introduction of small TRPs (uplink-only TRPs) that do not have downlink transmission capabilities. Additionally, to support an increase in the number of transmission antennas in commercial UEs, a new standard for 3 transmission antennas is being developed, broadening support for a wider variety of devices.

Furthermore, in anticipation of the full-scale introduction of 6G, standardization of AI/ML-based air interfaces is underway. This includes functions related to MIMO, such as beam management and CSI prediction. As mentioned earlier, the standardization of MIMO in 3GPP is continuously evolving to realize Advanced MIMO. However, there are still regulatory limitations that exist for realizing Advanced MIMO, such as the number of ports for reference signals and the number of TRPs in multi-TRP. Additionally, 6G brings with it new elements of consideration, such as optimization of communication based on AI/ML, further improvement in energy efficiency, and the use of new frequency bands, i.e. FR3.

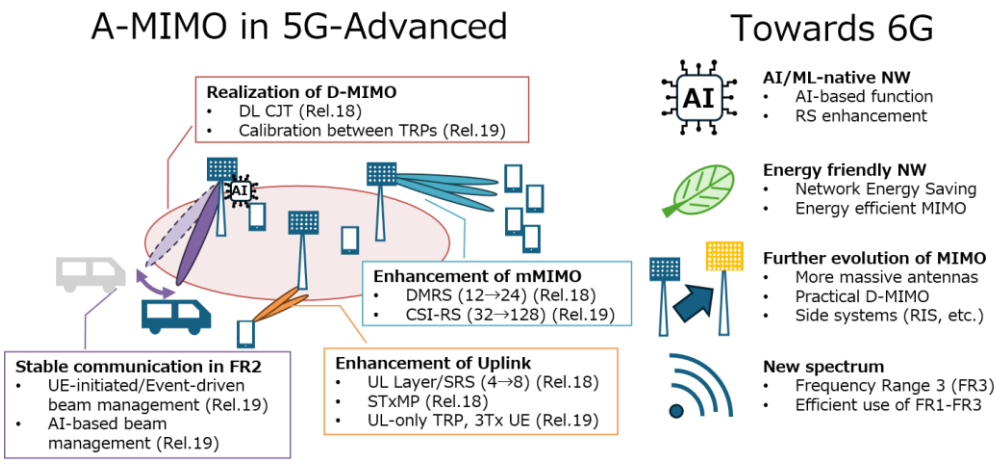

Fig. 3-1 Recent activities related Advanced MIMO in 3GPP

II. Recent Activities of Advanced MIMO Technologies in Japan

This section introduces some of the MIMO technologies being researched by members of this Advanced MIMO Working Group.

II-1. Research Activities for MIMO Evolution in Each Frequency Range towards 6G

Shunsuke Kamiwatari, Shuto Fukue, Masahiro Takigawa, Yu Tsukamoto,
Issei Kanno, and Hiroyuki Shinbo,
KDDI Research, Inc.

***Abstract*— In mobile communication systems, various frequency bands are combined to support diverse use-cases. 5G utilizes frequency ranges (FRs) called FR1 (410 MHz to 7.125 GHz) and FR2 (24.25 GHz to 52.6 GHz), with FR1 offering wide coverage due to low propagation loss, and FR2 supporting high-speed, high-capacity communication. For 6G, an additional frequency band, called FR3 (7 GHz to 24 GHz), is attracting attention. The evolution of massive MIMO technology, pivotal in 5G, is crucial for optimizing these FRs. This article explores MIMO technology advancements across these FRs, outlining use-cases, technical challenges, and the potential of a new 6G-enabled MIMO technologies.**

II-1.1. Introduction

In 5G, frequency ranges FR1 (410 MHz to 7.125 GHz) and FR2 (24.25 GHz to 52.6 GHz) are used, with FR1 providing wide coverage due to low propagation loss, and FR2 offering high data rates thanks to wider bandwidths. For 6G, the use of a new band, FR3 (7 GHz to 24 GHz), is being considered. Each FR has unique characteristics and technical challenges, requiring tailored communication technologies. Massive MIMO (mMIMO), developed further in 5G, is key for utilizing these FRs effectively. Optimizing MIMO for each FR enables to support a wide range of use-cases. This section discusses MIMO technology for 6G frequency bands, outlines use-cases and challenges, and presents findings on the potential of 6G networks and the evolution of MIMO technology.

II-1.2. Challenges related to MIMO technology in FR1 and our activities

FR1 is used for coverage in 5G due to its lower frequency, which has lower propagation loss, but it struggles to provide wide bandwidths necessary for high data rates. mMIMO was introduced in 5G to improve frequency efficiency through spatial multiplexing by using massive antennas. However, larger panels can hinder the scalability of base stations, and communication quality at cell edges can degrade due to interference.

A promising solution is cell-free mMIMO, which coordinates multiple access points (APs) to extend spatial multiplexing user equipment devices (UEs) without enlarging APs and reduces cell edge interference, enhancing communication quality. On the other hand, in realizing cell-free mMIMO, there are challenges such as scalability in signal processing and the increase in fronthaul capacity for cooperation among APs. In this section, we show our activities for realizing cell-free mMIMO in FR1.

II-1.2.1. User-centric RAN for scalable cell-free mMIMO and actual proof with prototype

One of the challenges with large-scale cell-free mMIMO systems is ensuring scalability. Large networks, such as mobile operator networks, require support for numerous APs and UEs. The complexity of radio signal processing, e.g., precoding and multi-user detection, becomes unmanageable by a single central processing unit. Additionally, as the number of antennas increases, more radio signals must be exchanged in fronthaul links between APs and operator facilities such as distribution units.

To address this, KDDI Research is studying a "User-centric RAN" approach aimed at ensuring scalability and maintaining radio quality. This involves two main components: (a) developing a new RAN radio signal processing architecture, and (b) devising control schemes to minimize radio signal processing while guaranteeing radio quality. In the new architecture as shown in Fig. 1-1, radio signal processing functions are distributed and hierarchically organized per user through RAN virtualization. This allows the processing tasks, such as precoding and multi-user detection, to be distributed on a per-user basis, thus ensuring scalability. The hierarchy of CPUs as radio processing units stabilizes radio quality for each UE and reduces the total capacity needed for fronthaul. For instance, upper layer CPUs at the central site handle UEs with rapidly changing radio quality, like those moving at high speeds. In contrast, lower layer CPUs at the edge site manage UEs with stable radio conditions, decreasing the need for communication with central site CPUs and thus reducing fronthaul traffic. The (b) control scheme as shown in Fig. 1-2, based on the User-centric RAN architecture, achieves both high communication quality and reduced computation for radio signal processing.

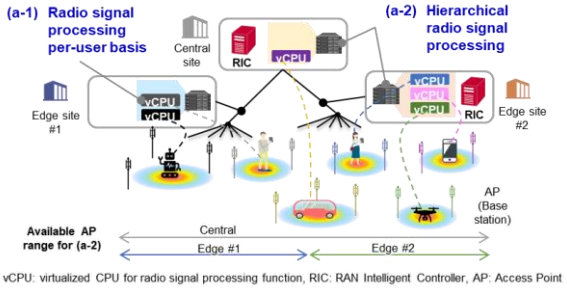

Fig. 1-1 User-centric RAN architecture.

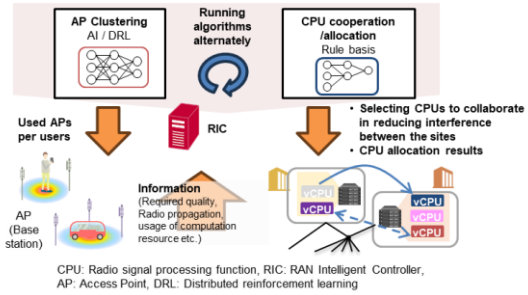

Fig 1-2 Main control schemes.

Key methods include AP clustering [1], CPU placement [2], and inter-CPU coordination [3]. These methods are adapted to meet user quality requirements, computational resources, and fronthaul capacity constraints. AI, specifically distributed reinforcement learning, is employed for AP clustering due to its ease of learning and effectiveness in optimizing AP combinations. Rule-based algorithms are used for CPU placement and

coordination, which simplifies control-related learning and balances processing loads. Our (b) control scheme utilizes AI and rule-based algorithms in appropriate contexts.

A prototype of the User-Centric RAN was implemented to demonstrate its feasibility. This upgraded version from [4] features 10 APs, 20 antennas, a frequency of 4.8 GHz, 100 MHz bandwidth, and supports 8 terminals as shown in Fig. 1-3. The hierarchical structure includes one Central Site and two Edge Sites, with a total of 12 CPUs allocated to each UE according to moving. The RAN Intelligent Controller (RIC) uses the integrated control method to select CPUs and AP inputs based on terminal movement and quality requirements. This prototype was developed at the KDDI Research site, employing widely available technology for practical implementation.

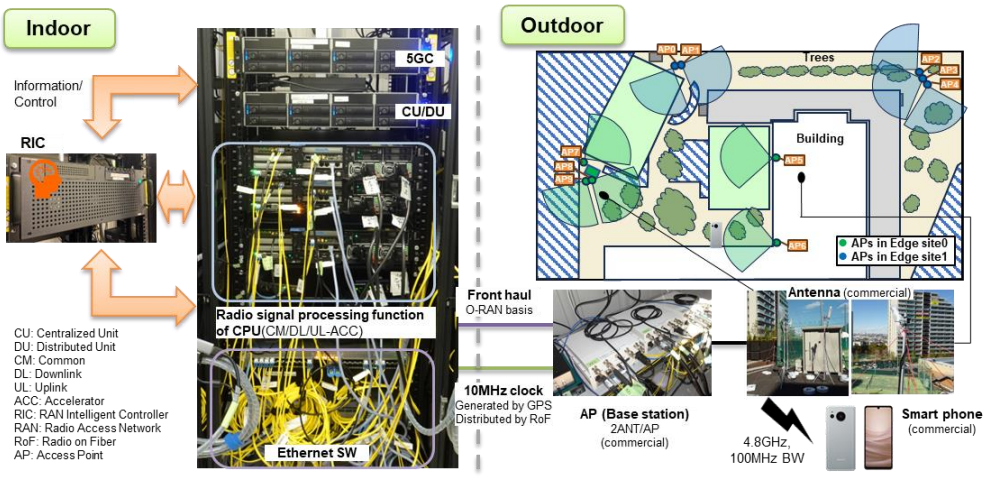

Fig. 1-3 User-centric RAN prototype.

User throughput was evaluated using this prototype, comparing User-centric RAN with our (a) architecture and (b) control scheme, cell-free as all APs in Edge site are used for cell-free mMIMO, and conventional cellular systems. The moving UE in User-centric RAN indicated superior throughput, averaging 4.4 times higher than cellular systems as shown in Fig. 1-4(a). The cumulative distribution function of user throughput indicated higher performance for User-centric RAN compared to both cell-free and cellular systems as shown in Fig. 1-4(b). The User-Centric RAN's integrated control method allows for optimal AP selection and interference suppression, enhancing communication quality.

These results highlight the potential for realizing radio quality assurance through User-centric RAN. Future steps include advancing practical verification and initiating international standardization efforts in O-RAN and 3GPP started from 2025 for 6G. We have made the research report of use-case [5] and architecture [6] for User-centric RAN in O-RAN nGRG with mobile operators and vendors. Collaboration with mobile operators and vendors is ongoing to further develop and apply User-centric RAN solutions.

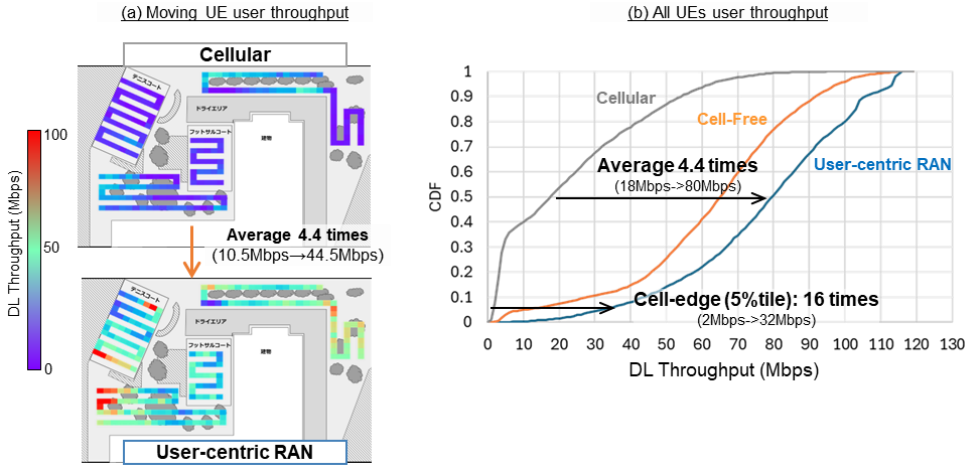

Fig. 1-4 Moving UE user throughput comparison.

II-1.2.2. IFoF based mobile fronthaul for cell-free mMIMO

A significant challenge for large-scale cell-free mMIMO systems is deploying fronthaul cost-effectively while its capacity and link requirements increase. Analog Radio-over-Fiber (ARoF), which converts analog RF waveforms to optical signals, is gaining attention for its potential in wideband transmission, particularly for 6G. ARoF's advantage is that it eliminates the need for ADC/DAC at each AP site, reducing power consumption and implementation scale, thus easing installation requirements. One ARoF type, Intermediate Frequency over Fiber (IFoF) [7] as shown in Fig. 1-5, converts RF waveforms to intermediate frequency (IF), then to optical signals. These signals are later converted back to RF at the AP site. By applying different IFs for each MIMO layer, they can be multiplexed via Frequency Division Multiplexing (FDM) on a single optical fiber, enhancing efficiency. In cell-free mMIMO, this multiplexing cuts down the number and length of fibers needed, and reduces costs associated with E/O and O/E converters.

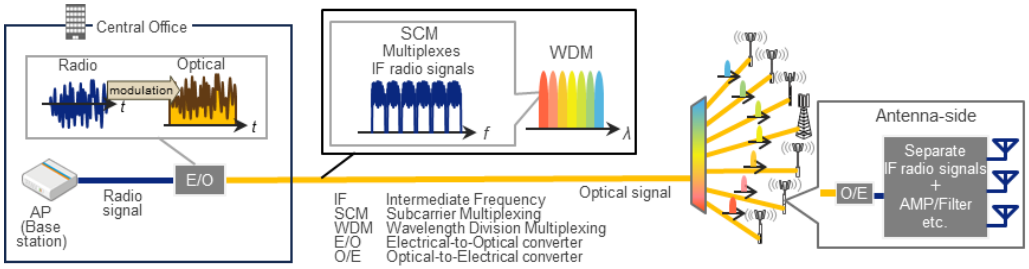

Fig. 1-5 Concept of IFoF based mobile fronthaul.

We evaluated the applicability of IFoF to previous User-centric RAN prototype [4], [8]. In cell-free mMIMO, a phase difference exceeding 15 degrees between antennas is known to impact radio communication quality. We conducted a continuous 48-hour measurement of the phase across 8 antennas with IFoF applied. Despite an external temperature variation of over 16 degrees, the phase difference remained within 5 degrees

in Fig.1-6. Additionally, user throughput was measured in the same radio environment with and without IFoF, showing no significant differences in Fig.1-7. These findings confirm that applying IFoF does not affect the radio communication quality in cell-free mMIMO. The use of IFoF is expected to enhance the flexibility of antenna placement and contribute to the large-scale deployment of cell-free mMIMO.

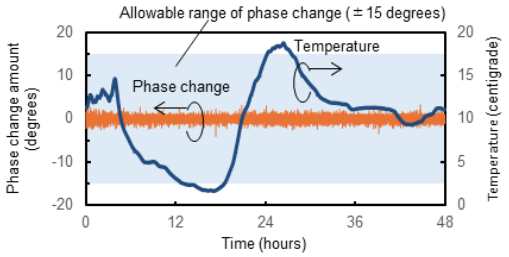

Fig. 1-6 Phase measurement with IFoF.

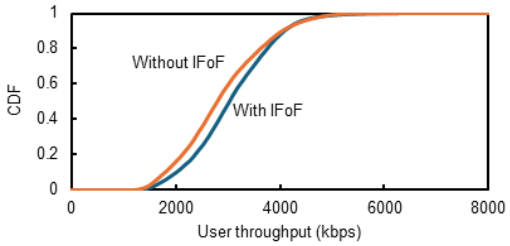

Fig. 1-7 Throughput with/without IFoF.

II-1.3. Challenges of MIMO in FR2 and our activities

From 5G, FR2 is introduced to support high-capacity communication with wide bandwidth. However, FR2 faces limited coverage due to propagation loss and blockage. A key technology is beamforming (BF) via mMIMO, where analog BF is common due to cost. To achieve stable BF, we have been researching antenna panel selection, fast beam switching [9],[10], predicting blockages, and handovers for UE mobility [11]. For 6G, enhanced MIMO technologies in FR2 are needed to meet rising traffic demands. Cell-free mMIMO is considered to mitigate blockages using multiple APs, but requiring systems tailored for analog BF [12]. This section covers our activities in FR2, including clustering for cell-free mMIMO and BF methods for line of site (LoS) MIMO to enhance FR2 capacity.

II-1.3.1. Clustering method for cell-free mMIMO in FR2

For FR2, a cell-free mMIMO with centralized hybrid BF is being considered. Moreover, to maintain scalability at the CPU, AP-wise clustering scheme has been considered in which multiple APs are selected as AP cluster for each UE, and signal processing is performed based on these clusters. However, in hybrid BF, which AP employs multiple RF chains with different analog beams, the coupling loss (the sum of the path loss and analog BF gain) of each RF chain may differ even between the same AP and UE. For cell-free mMIMO with hybrid BF, AP-wise clustering is not well suited because RF chains with high coupling loss may be included in the cluster for each UE. To address this issue, we have proposed RF chain-wise clustering. The concept of the proposed scheme is shown in Fig. 1-8. In this way, RF chains with lower coupling loss can be selected for each UE regardless of to which AP an RF chain belongs. Through simulation (in Fig. 1-9), we show that the proposed scheme can achieve superior spectral efficiency [13], [14].

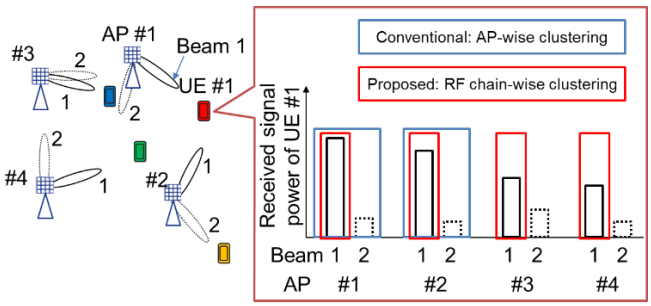

Fig. 1-8 Concept of RF chain-wise clustering.

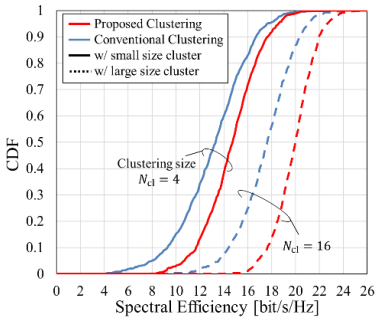

Fig. 1-9 Simulation results.

II-1.3.2. Technology for enhancing FR2 capacity

FR2 with wide bandwidth, has been utilized in order to satisfy higher data rates required in 5G, and beyond. In 5G, FR2 is being used not only for mobile communications in hotspots and factories, but also in FWA and backhaul globally. In addition, it is expected that spectrum efficiency will be enhanced as the use-cases become widespread in the future, particularly in the 6G era, where higher-layer MIMO transmission will be required. However, the FR2 channel is dominated by the LoS path, and the MIMO channel can be rank deficient. It has been revealed that maximum spatial multiplexing gain is obtained even in LoS environment when the antenna arrangement is optimally designed. The optimal arrangement is derived for uniform linear arrays, uniform planar arrays, and uniform circular arrays. However, the antenna arrangement is optimized for a specific transmission distance and the channel capacity degrades due to its higher spatial correlation depending on the transmission distances. To overcome the degradation depending the transmission distance in LoS-MIMO systems, we have proposed an antenna design based on genetic algorithm [15]. Moreover, we have proposed beam training (BT) algorithms for robust LoS-MIMO using phased array [16]. Fig. 1-10 and Fig. 1-11 show the experimental setting and result. From the figure, the throughput is increased by the proposed BT at the communication distance of 14.25m where the throughput degradation occurs due to the higher spatial correlation. We also study a fast BT algorithm using true time delay array for robust LoS-MIMO [17].

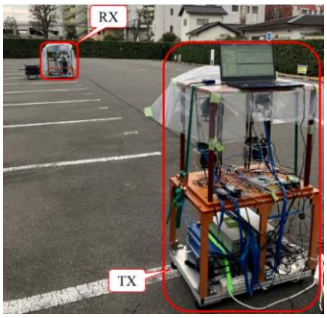

Fig. 1-10 Experimental setting.

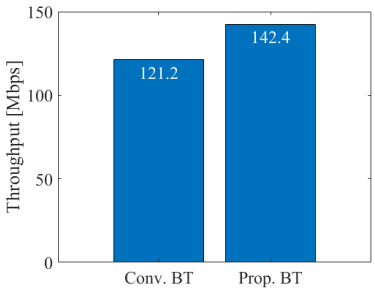

Fig. 1-11 Experimental result.

II-1.4. Challenges of MIMO in FR3 and our activities

Towards 6G, the new frequency band FR3 (7 to 24 GHz) is gaining attention for its balanced compromise between coverage and high-capacity communication. For mMIMO in FR3, a hybrid beamforming approach is being considered, involving dividing large antenna panels into sub-arrays for analog beamforming, combined with digital beamforming through RF chains. FR3 has wider bandwidth than FR1 and lower propagation loss than FR2. Therefore, FR3 may be a promising frequency band for cell-free mMIMO, which aims to deliver high-quality communication across entire areas. In this section, we show our evaluation on FR3's area performance compared to FR1 and suitable sub-array configurations for cell-free mMIMO in FR3.

II-1.4.1. Performance evaluation of large-scale MIMO (Extreme MIMO) in FR3

The propagation loss of FR3 increases compared with that of FR1 due to increasing in frequency. On the other hand, as the frequency increases, more antennas can be mounted on the same aperture area. Therefore, mMIMO in FR3 with hybrid BF may be able to ensure same coverage as FR1. However, the coverage of FR3 in the actual environment has not been revealed. Therefore, we compared the downlink coverage of FR1 (3.7GHz) and FR3 (7.4GHz) through area simulations based on realistic deployments.

Fig. 1-12 illustrates the coverage maps for (a) FR1 and (b) FR3. This result suggests that increasing the array size at FR3 cannot fully compensate for propagation loss. Specifically, in non-LoS (NloS) areas, FR3 tends to reduce SNR. This is because analog BF has directivity, but NloS UEs may not have dominant path. Fig. 1-13 compares SNR and SINR. SNR for FR3 is slightly lower than that of FR1, while SINR of FR3 exceeds that of FR1. Since the target of the evaluation is coverage, we assume that MRT as digital BF, so interference mitigation is only achieved by analog BF. Thus, hybrid BF contributes to improve SINR by interference mitigation [18].

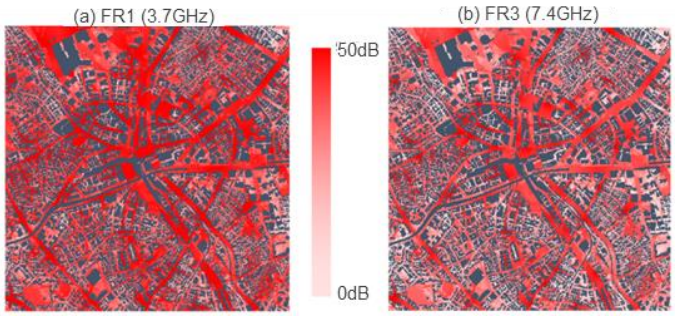

Fig. 1-12 Heatmap of SNR with each FR.

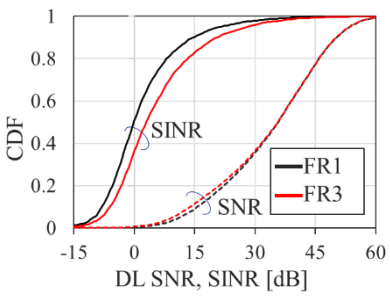

Fig. 1-13 Simulation results.

II-1.4.2. Evaluation of the applicability of cell-free mMIMO in FR3

Cell-free mMIMO is one of the potential technologies for the 6G to provide excellent wireless quality everywhere in a service area. In addition, utilization of FR3, has been

expected as a candidate new spectrum in 6G. In such FR, a hybrid BF architecture, which combines digital and analog BF, has been employed considering the power consumption and implementation cost of APs. In this research, we evaluate the impact of the antenna configuration in sub-array architecture on the spectral efficiency of cell-free mMIMO hybrid BF in the FR3. Fig. 1-14 shows sub-array configuration in AP. We clarify a suitable sub-array configuration in CF mMIMO deployed mainly towards terrestrial Ues through comparative study with simulations (Fig. 1-15) [19], [20].

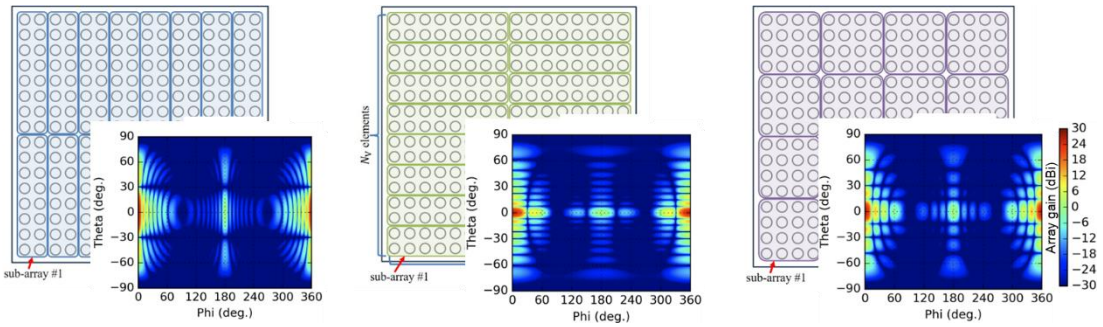

(a) Horizontally long (HL) configuration. (b) Vertically long (VL) configuration. (c) Square (SQ) configuration.

Fig. 1-14 Sub-array configurations and their analog beam patterns.

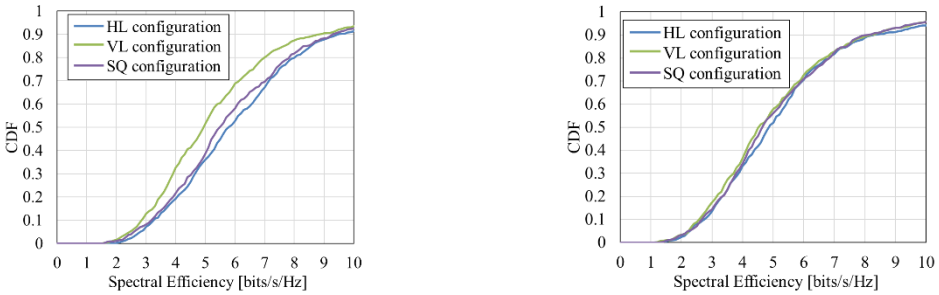

(a) 7 GHz. (b) 14 GHz.

Fig. 1-15 Simulation result of cell free mMIMO with each frequency in FR3.

II-1.5. Conclusion

In this section, we have discussed the trends and challenges of MIMO technology across FR1 to FR3 and highlighted our activities for these challenges. Towards 6G, applying the appropriate MIMO technologies to each of these FRs will enable the development of networks capable of supporting the enhanced and diverse use-cases anticipated in 6G.

Acknowledgements

A part of contents in Section [a]II-2.1, [a]II-3.1, [b]II-2.2, and [c]II-3 are obtained from the commissioned research ([a]JPJ012368C00401 / [b]JPJ012368C01401 / [c]JPJ010017C07501) by National Institute of Information and Communications Technology (NICT), Japan, respectively. A part of this research in Section II-3.2 was supported by the Ministry of Internal Affairs and Communications in Japan (JPJ000254).

REFERENCE

[1] Y. Tsukamoto, A. Ikami, T. Murakami, A. Amrallah, H. Shinbo and Y. Amano, "Scalable AP Clustering With Deep Reinforcement Learning for Cell-Free Massive MIMO," in IEEE Open J. of the Commun. Soc., vol. 6, pp. 1552-1567, 2025.

[2] A. Ikami, Y. Tsukamoto, N. Aihara, T. Murakami and H. Shinbo, "Interference suppression for distributed CPU deployments in Cell-Free massive MIMO," 2022 IEEE 96th Vehicular Technology Conference (VTC2022-Fall), London, UK, Sep. 2022, pp. 1-6. [Best paper award].

[3] A. Ikami, Y. Tsukamoto, N. Aihara, T. Murakami, H. Shinbo and Y. Amano, "User-centric Virtualized CPU Deployment and AP Clustering for Scalable Cell-Free Massive MIMO," 2023 IEEE 98th Veh. Technol. Conf. (VTC2023-Fall), Hong Kong, Oct. 2023, pp. 1-6.

[4] Beyond 5G Promotion Consortium, "Beyond 5G White Paper Supplementary Volume 'Cell-Free / Distributed MIMO '," Section 1.2, Version 1.0, Mar. 2024.

[5] KDDI, LGU+, "Use Case and Gap Analysis for Radio Quality Assurance," O-RAN next Gener. Res. Group (nGRG) Contributed Res. Rep. RR-2024-05, Aug. 2024.

[6] KDDI, LGU+, NVIDIA, "Research Report on scalable and user-centric RAN Architecture and Service Requirements," O-RAN next Gener. Res. Group (nGRG) Contributed Res. Rep. (Draft).

[7] S. Ishimura, B. G. Kim, K. Tanaka, K. Nishimura, H. Kim, Y. C. Chung, et al., "Broadband IF-over-fiber transmission with parallel IM/PM transmitter overcoming dispersion-induced RF power fading for high-capacity mobile fronthaul links", IEEE Photon. J., vol. 10, no. 1, Feb. 2018.

[8] S.Nimura, Y.Tsukamoto, T.Murakami, K.Tanaka, K.Y.Yazdandoost, H.Shinbo, Y.Amano, and R.Inohara,"Field Demonstration of Cell-Free Massive MIMO System Utilizing Analog IfoF-Based Fronthaul Link," in Proc. Opt. Fiber Commun. Conf., Los Angeles, CA, USA, Mar. 2025, Paper Th2A.55.

[9] M. Ito, et al., "Performance Evaluation of Multi-TRP Selection Methods in QoS-Mixed V2X Environments," IEICE General Conf. 2025, B-5A-27, Mar. 2025.

[10] S. Kamiwatari, et al., "Throughput Evaluation of Overhead Reduction by UE-initiated Beam Management in Millimeter Wave Band 5G NR," IEICE Tech. Rep., vol. 124, no. 366, pp.128–133, Jan. 2025.

[11] N. Osawa, et al., "A Study on Characteristic Analysis of Blockage in Millimeter Wave V2X Communication," IEICE Tech. Rep., vol. 125, no. 5, pp.20-24, Apr. 2025.

[12] S. Fukue, I. Kanno and Y. Kishi, "Evaluation of Clustering and Beam-Selection for MmWave Distributed MIMO With In-Band Full-Duplex," IEICE General Conf. 2024, B-5A-59, Mar. 2024.

[13] S. Kamiwatari, I. Kanno, T. Ohseki, K. Yamazaki, and Y. Kishi, “RF chain-wise Clustering for Centralized mm-wave Cell-Free massive MIMO with Hybrid Beamforming,” GLOBECOM 2022 – 2022 IEEE Global Commun. Conf., Rio de Janeiro, Brazil, Dec. 2022, pp. 764-769.

[14] S. Kamiwatari, I. Kanno, T. Hayashi and Y. Amano, “RF Chain-Wise Clustering Schemes for Millimeter Wave Cell-Free Massive MIMO With Centralized Hybrid Beamforming,” in IEEE Access, vol. 12, pp. 19682-19693, 2024.

[15] M. Takigawa, R. Kataoka, I. Kanno and Y. Kishi, “Antenna Design for Robust Millimeter Wave LoS-MIMO Link in Mobile Analog Repeater Achieving Low Latency and High Capacity,” 2024 IEEE 21st Consum. Commun. & Netw. Conf. (CCNC), Las Vegas, NV, USA, Jan. 2024, pp. 912-917.

[16] M. Takigawa, R. Kataoka, I. Kanno and Y. Kishi, “Beam Training of LoS-MIMO Systems Using Subarray-Based Beamforming in the Presence of Ground Reflection,” 2024 18th Eur. Conf. on Antennas and Propag.(EuCAP), Glasgow, UK, Mar. 2024, pp. 1-5.

[17] M. Takigawa, R. Kataoka, I. Kanno, and T. Hayashi, “Fast Beam Training for Higher-Rank LoS-MIMO Using True-Time-Delay Arrays,” in 2025 IEEE 22nd Consum. Commun. Netw. Conf. (CCNC), Jan. 2025, Las Vegas, NV, USA, to be published.

[18] S. Kamiwatari, S. Fukue, I. Kanno and Y. Kishi, “A study on FR3 Area Deployment With Hybrid Beamforming Towards 6G,” IEICE Tech. Rep., vol. 125, no. 5, pp.7-12, Apr. 2025.

[19] S. Kamiwatari, S. Fukue, M. Ito, and I. Kanno, “Impact of Sub-array Configuration on Spectral Efficiency of Cell-Free Massive MIMO with Hybrid Beamforming in FR3,” IEICE Trans. Commun., Vol.E108-B, No.10, 2025, to be published.

[20] S. Kamiwatari, M. Ito, and I. Kanno, “A Study on AP Antenna Configuration for Cell-Free Massive MIMO with Hybrid Beamforming in the Upper-mid Band,” IEICE Tech. Rep., vol. 123, no. 76, pp.212–217, June 2023.

II-2. Performance Evaluation of FR3 Distributed MIMO Using 6G Simulator

Kiichi Tateishi, Yuyuan Chang, Yuta Hayashi, Satoshi Suyama, and Huiling Jiang,
NTT DOCOMO, INC.

***Abstract*—The 6th generation mobile communication system (6G) aims to meet new demands that exceed the capabilities of the 5th generation (5G), focusing on ultra-high performance, including peak data rates over 100 Gbps. To achieve this, the use of the sub-terahertz band (92 to 300 GHz), which offers greater bandwidth, is being explored, although it presents technical challenges such as increased wave directivity and higher propagation loss. Additionally, the mid-band (7 to 24 GHz) is emerging as a viable option, providing advantages in bandwidth and coverage due to lower propagation losses compared to 5G's Sub-6 frequencies. This article introduces a 6G system-level simulator to evaluate the performance of these high-frequency bands in urban environments, incorporating distributed MIMO technology. The findings will elucidate the impact of distributed MIMO and New Radio Network Topology (NRNT) on system performance and operational feasibility, essential for advancing 6G communications.**

II-2.1. Introduction

The 6th generation mobile communication system (6G) is expected to accommodate new combinations of demands that surpass the high speed and large capacity, high reliability and low latency, and simultaneous connections of numerous devices characteristic of the 5th generation mobile communication system (5G), as well as use cases that require ultimate extreme-high performance, which are difficult to achieve even with 5G [1], [2]. Specifically, with peak data rates exceeding 100 Gbps in 6G, it is anticipated that new experiential services will be realized, providing a quality of experience comparable to or exceeding that of real-life sensory experiences. To achieve ultra-high-speed communication exceeding 100 Gbps in 6G, the utilization of the so-called sub-terahertz band, which ranges from 92 to 300 GHz and offers significantly broader signal bandwidth compared to 5G, has been considered. However, the sub-terahertz band poses technical challenges, such as increased directivity of radio waves and greater propagation loss compared to the millimeter waves used in 5G. To address these challenges, NTT DOCOMO is advancing the conception of solution technologies and validating their effectiveness [3]-[6].

Fig. 2-1　6G Simulator in an Outdoor Urban Environment

Furthermore, the frequency band known as the mid-band, ranging from 7 to 24 GHz, is attracting attention as a candidate frequency band for 6G. At the WRC (Wireless Radiocommunication Conference) -23 [7], it was also decided to allocate the 6 GHz band and the 7 GHz band as new frequency bands for mobile communication, and discussions on the 7.125 GHz to 8.4 GHz and 14.8 GHz to 15.35 GHz bands will be held at WRC-27. The mid-band is being considered as a frequency range that can offer wider bandwidth than the Sub-6 frequencies used in 5G (which are below 6 GHz), and due to its lower frequency compared to the millimeter wave bands at 28 GHz, it has the potential to achieve high-speed and large-capacity communication while ensuring a certain level of coverage, thanks to reduced propagation loss [8].

When utilizing high frequency bands such as the sub-terahertz band and mid-band within the system, it is necessary to conduct early evaluations of system performance when multiple base stations (BS) and user equipment (UE) are deployed, in addition to validating individual technologies. This will help clarify the performance improvement effects of the system as a whole and identify any issues. However, device development typically requires a considerable amount of time and cost, and to ensure flexibility in making changes to configurations and parameters, the authors have developed a 6G system-level simulator (hereafter referred to as *6G simulator*) to clarify the feasibility of achieving ultra-high-speed communication through the utilization of the sub-terahertz band and mid-band. They have also been progressing with performance verification of this simulator [9]-[11].

This work aims to further enhance the 6G simulator by introducing the mid-band in an outdoor urban environment, as shown in Fig. 2-1, and evaluating the simulator that incorporates distributed MIMO technology. The effects of applying distributed MIMO and distributed network enhancement technology (NRNT: New Radio Network Topology) will be clarified.

II-2.2. Overview of 6G Simulator

This work evaluates the functions developed based on the 6G simulator reported in reference [11]. The 6G simulator was developed to quantitatively verify the requirements and technical concepts of 6G as described in the NTT DOCOMO 6G white paper [1], as well as to examine the potential for utilizing the sub-terahertz band and mid-band within the system [9]. In this simulator, it is assumed that the sub-terahertz band and mid-band will be applied to the system to achieve ultra-high-speed communication exceeding 100 Gbps more reliably, under the constraint of having the same BS antenna size as those used for Sub 6 and millimeter waves, along with the same transmission power as 5G. In high frequency bands, including the sub-terahertz band, it is possible to significantly increase the number of antenna elements in Massive MIMO antennas (hereafter referred to as elements), thereby achieving high beamforming (BF) gain [12], which can compensate for the considerable propagation loss in high frequency bands.

In 6G, NRNT [13] is becoming one of the key technological areas, focusing on ensuring coverage in high frequency bands, improving connectivity, and reducing power consumption by constructing a spatially distributed wireless network topology [1], [2]. In NRNT, various approaches are being examined for the configuration of nodes and the technologies adopted by those nodes, including the use of existing objects such as streetlights and lighting fixtures as antennas, advancements in wireless relay technology, the utilization of Reconfigurable Intelligent Surfaces (RIS) [14]-[16] that can dynamically control reflection intensity and direction, the employment of mobile BS, and cooperation between UE. In this simulator, RIS and mobile BS are utilized as NRNT technologies to improve the received power of the sub-terahertz band in non-line-of-sight areas and ensure coverage, enabling the evaluation of system performance in outdoor urban environments.

In an outdoor urban environment, distributed MIMO will be introduced for both downlink (DL) and uplink (UL) at the BS. In distributed MIMO, multiple Transmission and Reception Points (TRPs) corresponding to the BS antennas and an aggregation point to consolidate them form the BS. By enabling coordinated transmission and reception (sending and receiving the same or different MIMO streams to and from the same UE) across multiple TRPs, throughput can be improved. In traditional methods that do not apply distributed MIMO, coordinated transmission and reception do not occur between different TRPs, meaning that the UE communicates only with a single TRP. In this simulator, multiple TRPs fixed at pre-set locations are installed, allowing for the evaluation of the DL and UL throughput characteristics of each UE during both coordinated and uncoordinated transmission and reception. Furthermore, to improve propagation loss due to obstruction, a drone TRP will provide service while moving along a specific path. Additionally, UEs will include not only devices carried by people but also robots and autonomous vehicles.

Table 2-1 Simulation parameters

	Sub-6	Mid-band	mmW
Center frequency	4.7 GHz	15 GHz	28 GHz
Bandwidth	100 MHz	400 MHz	400 MHz
Number of antenna elements in TRP (V × H × sub-array)	144 (4 × 4 × 9)	2304 (16 × 16 × 9)	2304 (16 × 16 × 9)
Sub-array spacing	0.5 λ	4 λ	4 λ
Transmission power in TRP	30 dBm		
TRP antenna element gain	5 dBi		
UE transmission power	23 dBm		
Number of antenna elements in UE (V × H × sub-array)	144 (4 × 4 × 9) / 384 (4 × 4 × 24)		
UE antenna spacing	0.5 λ		
Precoder	SVD		
Receiver	MMSE-IRC		
Number of MIMO layers / UE	1, 2, 3, 4, 8, 16, 24		

Compared to the millimeter wave band, the sub-terahertz band experiences even greater effects from propagation loss and shielding loss. Therefore, in this simulator, Massive MIMO antennas composed of multiple sub-arrays are introduced at each TRP to compensate for the increasing propagation loss. Additionally, based on the relative positions of the sub-terahertz TRPs and UEs, as well as the presence or absence of obstructions between the TRP and UE, propagation loss and shielding loss are calculated to determine the received power of each UE. The combinations of each TRP (fixed one or a drone) and RIS with the UE are then determined based on this received power. When using RIS, propagation loss is calculated using the path length from the TRP to the RIS and from the RIS to the UE. For simplification of the evaluation, it is assumed that the control of the reflection direction by RIS operates ideally, and for the purpose of evaluation, RIS is regarded as a virtual fixed TRP for beamforming. Based on the received power calculated from the above, it is assumed that the TRP that communicates with the UE switches ideally without delay.

II-2.3. Simulation Evaluations

This simulator simulates an outdoor urban environment where 5G and 6G are deployed for system-level simulation evaluations. In this work, two scenarios are established: Scenario A evaluates the throughput improvement effects of applying distributed MIMO technology and NRNT technology to the mid-band, while Scenario B assesses the throughput improvement effects of adaptive TRP selection based on the communication environment of UEs with the introduction of AI-ML technology.

The simulation parameters for both scenarios are shown in Table 2-1. The center frequencies for the Sub-6, mid-band, and millimeter wave frequency bands are set at 4.7 GHz, 15 GHz, and 28 GHz, respectively, with bandwidths of 100 MHz, 400 MHz, and

400 MHz. The Massive MIMO antennas at the TRPs use planar arrays composed of 9 sub-arrays, where each sub-array forms one beam through analog beamforming using analog circuits. The total transmission power of the fixed TRPs and drone TRPs is kept constant at 30 dBm, regardless of the number of elements in the sub-arrays. The duplexing scheme is Time Division Duplex (TDD), with a time ratio of DL to UL of 7:3 for Scenario A and 10:0 for Scenario B. A total of 21 UEs are placed throughout the urban environment area, consisting of 18 individuals carrying UEs, one robot equipped with a UE, and two autonomous vehicles. The individuals and the robot move at a speed of 3 km/h, while the autonomous vehicles travel at a speed of 60 km/h. The number of MIMO layers is selected based on the propagation environment, choosing the maximum number possible from the candidates of 1, 2, 3, 4, 8, 16, or 24 per UE. The radio propagation environment follows a multipath Rayleigh fading model or Spatial Channel Model (SCM) [17], and when applying SCM, antenna correlation is only considered between the sub-arrays within the same TRP. Precoding control is performed using Singular Value Decomposition (SVD) precoders, and channel estimation is assumed to be ideal. In the receiving process at each TRP and UE, signal detection is carried out using an Interference Rejection Combining (IRC) receiver based on the Minimum Mean Squared Error (MMSE) criterion using the propagation channel matrix (MMSE-IRC). In this simulator, the block error rate is derived from the received SINR of the detected signals, and the throughput for both DL and UL is calculated.

The urban environment area realized in this simulator is shown in Fig. 2-1. This environment features an open plaza surrounded by high-rise buildings, with obstructions such as electronic billboards and trees lining the plaza. The Blockage model B [18] is applied to the obstructions, calculating and adding attenuation based on the distance difference between the straight-line distance between the transmission point and the receiving point and the distance traveled through the upper and lower sides of the planar obstructions. Individuals, robots, and autonomous vehicles can either be stationary or moving. UEs are expected to connect to the TRP that has the highest received power in the downlink, wiFigureth a TRP selection cycle set at 1 ms (1 slot). Fixed TRPs and RIS are installed on building walls or streetlights, while the drone TRP regularly moves back and forth in the air above the roadside to provide service to UEs located away from the buildings in the plaza. It is assumed that the backhaul for the drone TRP is ideally constructed.

Fig. 2-2 shows the percentage of throughput for each UE when distributed MIMO is not applied. The graphs on the left and right of the figure display the DL and UL throughput, respectively. The throughput is represented in five color ranges: 0–1 Gbps, 1–10 Gbps, 10–50 Gbps, 50–100 Gbps, and over 100 Gbps. The horizontal axis represents time (slot), while the vertical axis indicates the percentage of UEs achieving throughput in the respective color ranges. The colors of the lines connecting TRPs and UEs in

Figure 1 correspond to the colors in Fig. 2-2. From Fig. 2-2, it is confirmed that all UEs achieve a DL throughput of over 1 Gbps. This is because all UEs in the urban environment can secure broadband transmission coverage by connecting to the mid-band, which has a bandwidth comparable to that of millimeter waves but operates at a lower frequency. Additionally, more than 90% of UEs achieve UL throughput exceeding 1 Gbps. Furthermore, around 65% of UEs achieve DL throughput in the range of 1–10 Gbps, and approximately 35% of UEs achieve DL throughput of over 10 Gbps.

Next, the results when applying distributed MIMO and NRNT technologies, while maintaining the same fixed TRP installation positions as in Fig. 2-2, are shown in Fig. 2-3. When applying NRNT technology, it is assumed that the electronic billboards present in the plaza can control reflection direction by applying films or similar materials to their surfaces, treating them as a type of RIS. From the figure, about 60% of UEs achieve DL throughput in the range of 1–10 Gbps, and approximately 40% of UEs achieve DL throughput exceeding 10 Gbps. Additionally, nearly all UEs achieve UL throughput exceeding 1 Gbps.

At this point, let us focus on UE #22, which is in front of a high-rise building and is marked by a yellow circle in Fig. 2-1. Figs. 2-4 and 2-5 show the throughput for UE #22 without and with the application of distributed MIMO technology and NRNT technology, respectively, with the horizontal axis representing time and the vertical axis indicating throughput. From Fig. 2-4, it can be observed that the introduction of the mid-band, in addition to Sub-6 and millimeter waves, increases the DL throughput from approximately 18 Gbps to about 24 Gbps. Furthermore, Fig. 2-5 confirms a peak DL throughput of around 40 Gbps when applying distributed MIMO technology and NRNT technology from the state shown in Fig. 2-4. From the above, it is clarified that UEs with transmission speeds below 50 Gbps can improve DL and UL throughput by realizing higher-order MIMO transmission with the application of distributed MIMO and NRNT technologies. Thus, it is also demonstrated that even in urban environments, where reflections are relatively scarce and line-of-sight conditions are abundant, and where spatial multiplexing effects from MIMO are not expected, applying distributed MIMO and NRNT technologies can significantly improve throughput for both DL and UL.

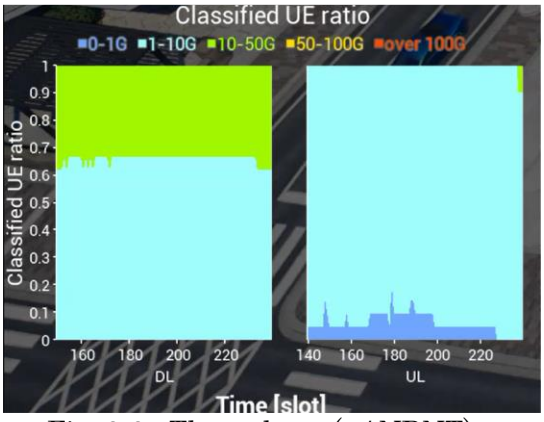

Fig. 2-2 Throughput (w/ NRNT)

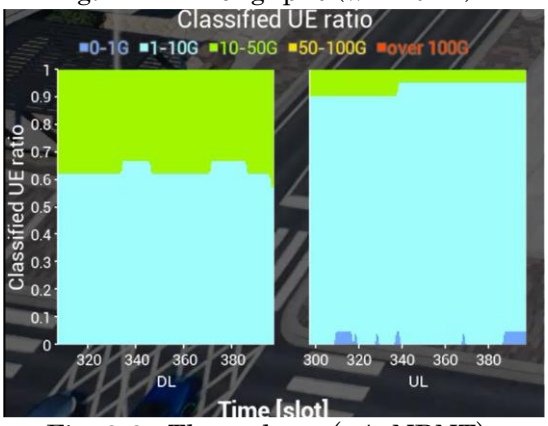

Fig. 2-3 Throughput (w/o NRNT)

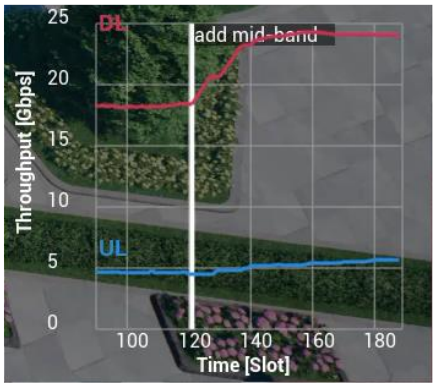

Fig. 2-4 Throughput of UE#22 (effect of adding mid-band)

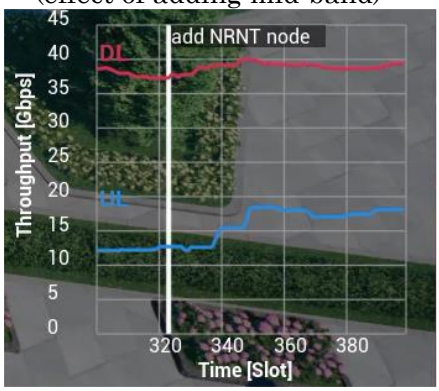

Fig. 2-5 Throughput of UE#22 (effect of adding NRNT)

II-2.4. Conclusions

This work has discussed the development of a simulator that significantly improves both DL and UL throughput by introducing the mid-band and applying distributed MIMO and NRNT technologies in an outdoor urban scenario as part of enhancing the 6G simulator. Specifically, it was confirmed that with the application of distributed MIMO and NRNT technologies using the mid-band, all UEs achieve DL and UL throughput of over 1 Gbps, and approximately 40% of UEs achieve DL throughput of over 10–50 Gbps. In the future, the simulator will continue to be expanded to enable the performance evaluation and visualization of various 6G technologies as a system, and to provide a virtual experience of use cases suited to the 6G era based on this performance.

REFERENCE

[1] NTT DOCOMO, Inc., 5G Evolution and 6G White Paper (Version 5.0), Jan. 2023. https://www.docomo.ne.jp/english/binary/pdf/corporate/technology/whitepaper_6g/DOCOMO_6G_White_PaperEN_v5.0.pdf

[2] Y. Kishiyama, S. Suyama, S. Nagata, “Trends and Target Implementations for 5G evolution & 6G,” NTT DOCOMO Technical Journal, vol. 19, no. 11, pp. 18–25, Nov. 2021.

[3] S. Suyama, T. Okuyama, Y. Kishiyama, S. Nagata, and T. Asai, “A study on extreme wideband 6G radio access technologies for achieving 100 Gbps data rate in higher frequency bands,” IEICE Trans. Commun., vol. E104-B, no. 9, pp. 992-999, Sep. 2021.

[4] S. Suyama, T. Okuyama, N. Nonaka, and T. Asai, “NTT DOCOMO’s Efforts Towards the Utilization of Sub-Terahertz Waves in 6G,” IEICE General Conf., CI-7-6, Mar. 2022.

[5] S. Suyama, K. Kitao, T. Tomie, and M. Nakamura, “Propagation Simulations and Experiments in Sub-terahertz Band toward 6G,” NTT DOCOMO Technical Journal, vol. 25, no. 2, Oct. 2023.

[6] NTT DOCOMO Press Release Document, “DOCOMO and NTT Expand 6G Collaborations with World-leading Vendors Including Ericsson and Keysight Technologies,” Feb. 2023.
https://group.ntt/en/newsrelease/2023/02/27/230227a.html

[7] MIC ICT Policy Press Release, “Results of the International Telecommunication Union (ITU) 2023 World Radiocommunication Conference (WRC-23),” Dec. 2023.
https://www.soumu.go.jp/main_sosiki/joho_tsusin/eng/pressrelease/2023/12/27_7.html

[8] Y. Hayashi, D. Mohri, Y. Chang, S. Suyama, and H. Jiang, “Evaluation of Transmission Performance of Mid-Band Massive MIMO by Computer Simulation,” IEICE Tech. Report, RCS-2024-141, Oct. 2024.

[9] T. Okuyama, S. Suyama, N. Nonaka, T. Asai, “6G System-level Simulator: Toward 100 GHz Band, 100 Gbps Extreme-high-data-rate Communications,” NTT DOCOMO Technical Journal, vol. 23, no. 3, pp. 13–26, Jan. 2022.

[10] K. Tateishi, K. Kitao, S. Suyama, T. Yamada, “Advancement of 6G System-Level Simulator,” NTT DOCOMO Technical Journal, vol.31, no.2, Jul. 2023.
https://www.docomo.ne.jp/corporate/technology/rd/technical_journal/bn/vol31_2/004.html

[11] K. Tateishi, S. Suyama, H. Jiang, “Real-Time Simulator for Sixth-Generation Mobile Communications System,” IEICE Tech. Report, RCS2023-143, Oct. 2023.

[12] 3GPP, TR 37.840 V12.1.0 (2013-12), “Study of Radio Frequency (RF) and Electromagnetic Compatibility (EMC) requirements for Active Antenna Array System (AAS) base station”.

[13] M. Iwabuchi, S. Suyama, T. Arai, M. Nakamura, K. Goto, R. Ohmiya, D. Uchida, T. Yamada, T. Ogawa, “Concept and Issues of New Radio Network Topology for 5G Evolution & 6G,” IEICE Tech. Report, RCS2022-148, Oct. 2022.

[14] D. Kitayama, Y. Hama, K. Miyachi, and Y. Kishiyama, “Research on Transparent RIS Technology for 5G Evolution and Toward 6G,” NTT DOCOMO Technical Journal, vol.23, no.2, Oct. 2021.

[15] Y. Hama, D. Kitayama, H. Takahashi, and H. Ochiai, “A Study on Multi-Beam Formation Based on Discrete Phase Control for Single Users in Reconfigurable Intelligent Surfaces,” IEICE General Conf., B-5A-35, Mar. 2024.

[16] D. Mohri, S. Suyama, Y. Chang, and H. Jiang, “Beam Selection Algorithm with BS Digital Null Beamforming in RIS-empowered 6G System,” IEICE Tech. Report, RCS2024-79, June 2024.

[17] 3GPP TR 38. 901 v14. 1. 1, “Study on channel model for frequencies from 0.5 to 100 GHz (Release 14),” July 2017.

II-3. Performance Evaluation of FR3 Massive MIMO in Real Urban Areas through Link-Level Simulation

Yuta Hayashi, Yuyuan Chang, Takahiro Tomie, Satoshi Suyama, and Huiling Jiang,
NTT DOCOMO, INC.

Abstract—**In the sixth-generation mobile communication system (6G), the objective is to achieve extreme high-speed communication exceeding 100 Gbps, along with ultra-low latency, surpassing the capabilities of the fifth-generation system (5G). To facilitate this, the utilization of the sub-terahertz band, above 100 GHz, is being explored; however, challenges such as strong directivity and significant obstruction impacts must be addressed. In 5G, the millimeter wave bands (24-43 GHz) face similar coverage issues, leading to a combined approach with lower frequency Sub-6 bands (3-7 GHz). For 6G, the mid-band (7-24 GHz) is considered a promising option, providing greater bandwidth and flexibility for different use cases. Furthermore, to counteract the high propagation loss in 5G and 6G, hybrid beamforming methods are being investigated that combine analog and digital techniques. This study employs the color image method (CIM) for radio wave propagation analysis in a model of Yokosuka city, evaluating the transmission characteristics and coverage performance of mid-band Massive MIMO in an urban environment. The findings will help optimize antenna configurations for improved performance in future 6G implementations.**

II-3.1. Introduction

In the sixth-generation mobile communication system (6G), the goal is to achieve extreme-high-speed and high-capacity communication exceeding 100 Gbps, as well as extreme-low latency communication, surpassing the fifth-generation mobile communication system (5G) [1], [2]. To achieve this goal, the utilization of the sub-terahertz band, which refers to frequency bands above 100 GHz, is under consideration. However, high-frequency radio waves face the challenge of strong directivity and significant impacts from obstructions. In fact, in 5G, frequency bands known as millimeter waves in the range of 24 GHz to 43 GHz are being utilized, but securing coverage is difficult for similar reasons, and as a result, the expansion of these areas has not progressed rapidly.

To address this, 5G employs the combined use of the lower frequency Sub-6 band (3 GHz to 7 GHz) to ensure coverage. Similarly, for 6G, the mixed use of frequency bands below the sub-terahertz band is being considered. The use of the “mid-band”, which refers to frequency bands ranging from 7 GHz to 24 GHz, is being explored for 6G [3]. The mid-band is expected to provide a wider bandwidth compared to Sub-6 and is attracting attention. Different frequency bands can be utilized according to use cases,

such as using the mid-band when coverage is essential along with high-speed and large-capacity communication, and the sub-terahertz band when ultra-high-speed and large-capacity communication is needed in limited areas.

As previously mentioned, since 5G and 6G handle high-frequency bands with significant propagation loss, beamforming (BF) through Massive MIMO is employed. Traditionally, analog beamforming, which controls the phase using RF elements, has been used due to device cost and computational load considerations. However, to accommodate the increase in the number of streams and connected devices, digital beamforming based on digital signal processing, which can suppress inter-stream interference and generate multiple beams, is being investigated. Nonetheless, implementing Massive MIMO purely with digital beamforming raises concerns about increased circuit scale, signal processing load, implementation cost, and power consumption. Therefore, hybrid beamforming [4], [5], which combines analog beamforming capable of generating multiple high-precision beams with digital signal processing while avoiding the complexity of digital signal processing systems, is receiving attention.

When applying hybrid beamforming, the characteristics vary based on antenna configurations such as the number of antenna elements and digital ports, necessitating the identification of the optimal configuration for specific applications. The authors have previously conducted studies utilizing 3GPP channel models and other resources to evaluate basic transmission characteristics and consider the optimal hybrid beamforming antenna configuration for mid-band Massive MIMO [6], [7]. In this paper, the color image method (CIM) of radio wave propagation analysis [8], [9] is applied to a model simulating the city of Yokosuka, and the obtained radio wave propagation channel is used to evaluate transmission characteristics in the urban area of Yokosuka, verifying the coverage performance when mid-band Massive MIMO is deployed in the urban environment [10].

II-3.2. Mid-band Massive MIMO

At WRC-23 (World Radiocommunication Conference) held in November 2023, it was decided to newly allocate the 6 GHz and 7 GHz bands as frequencies for mobile communication, and discussions regarding the 7.125–8.4 GHz and 14.8–15.35 GHz bands will take place at WRC-27 [11]. These frequency bands, as mentioned earlier, are referred to as mid-band or “centimeter waves”, and may also be called “FR3”, following the FR1 designation for Sub-6 frequency bands and FR2 for millimeter wave frequency bands. The mid-band is characterized by lower signal attenuation compared to millimeter waves and sub-terahertz waves, and it is expected to provide a wider bandwidth than Sub-6, allowing for area coverage while ensuring high communication

capacity. Meanwhile, in 5G and 6G, the examination of beamforming (BF) using Massive MIMO is being conducted to achieve higher capacity and lower propagation loss, with a particular focus on hybrid BF, which combines analog BF and digital signal processing to reduce implementation costs and computational loads. The utilization of hybrid BF for Massive MIMO antenna configurations is also being explored for the mid-band.

Hybrid BF characteristics can vary greatly depending on antenna configurations, such as the number of antenna elements, the number of digital ports, and sub-array configurations. For example, if the total number of antenna elements remains constant and beams are formed per sub-array, increasing the number of digital ports allows for more beams to be generated, but with fewer elements per sub-array, the beam width becomes wider. While this increase in the number of beams allows for connections to more devices, the overlapping beams may interfere with each other, potentially degrading throughput. Conversely, reducing the number of digital ports increases the number of elements per sub-array, leading to a decrease in the number of beams and a narrowing of the beam width. With more elements within a sub-array, it becomes feasible to create sharper beams, but the focus shifts to analog BF processing, which reduces design flexibility. Additionally, beam width also varies based on the frequency band used, so the choice of frequency band must be considered.

To fully leverage hybrid BF, it is essential to consider the optimal antenna configuration and beam control based on the frequency band being used, the use case, and the environment. Failing to do so may result in an inadequate utilization of spatial multiplexing through MIMO, complicating the realization of high-speed and high-capacity communication as well as coverage assurance. Therefore, it is necessary to investigate the optimal antenna configurations and beam control strategies to achieve the high-speed, large-capacity communications intended for the mid-band while ensuring broad coverage.

II-3.3. color image method (CIM)

CIM is a method that simplifies the calculation of wall surface scattering as an alternative to the radar equation. Specifically, different RGB colors are assigned to the walls of all buildings in the evaluation area. As shown in Fig. 3-1, these buildings are then transformed into images from the perspectives of the transmission and reception points. The matching color codes on the respective wall surfaces in both images are identified as scattering wall surfaces, and the number of pixels on those walls is counted (to determine the visible surface area of the walls). Similar calculations are performed for all scattering walls, and by summing these results, the received power is calculated. The received power P_R at the receiving point can be expressed mathematically as follows:

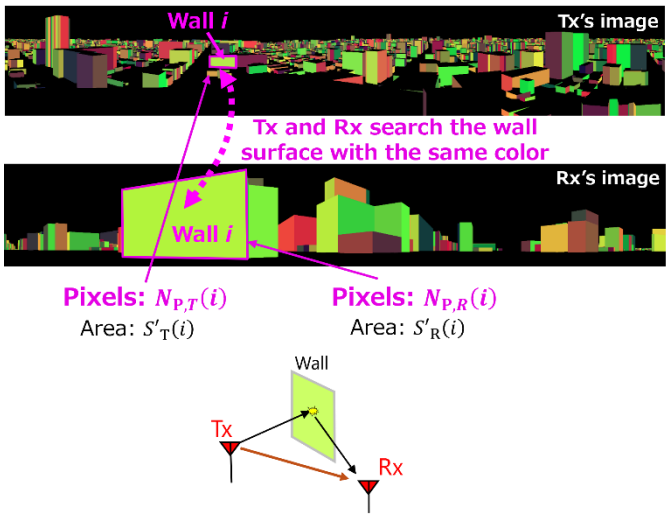

Fig. 3-1 An example of a color image of a building as viewed from the transmission and reception points.

$$P_R = \sum_i k(i) \cdot N_{P,T}(i) \cdot N_{P,R}(i),$$

where $N_{P,T}(i)$ and $N_{P,R}(i)$ represent the number of pixels corresponding to scattering wall i in the images as viewed from the transmission and reception points, respectively. Additionally, $k(i)$is a coefficient that represents the material properties of scattering wall i, as well as the gain of the transmitting and receiving antennas and the frequency. Since CIM calculates scattering based on surfaces, it assumes that the surfaces are larger than the first Fresnel zone, resulting in smaller estimation errors compared to ray tracing methods (RTM), particularly when using commercially available rough building models, with an error of approximately 9 dB [8], [9]. Naturally, using more detailed structural models is expected to provide higher estimation accuracy. Furthermore, by creating images from all receiving points, conducting color analysis, and pre-storing the results in a database (DB), referred to as preprocessing, while separately handling the creation of the image from the transmission point, color analysis, and matching with the analysis results of the receiving points stored in the DB, referred to as postprocessing, the estimation of propagation characteristics can omit preprocessing. This results in the estimation time being equal to the time required for postprocessing (approximately 20 seconds), allowing for speed increases of over 100 times compared to RTM [8], [9].

Table 1　Simulation parameters

Center frequency [GHz]	7	14
Band width [MHz]	200, 400	400
No. of BS antennas	256	1024
No. of digital ports of BS	64	
No. of MS antennas	64	256
No. of digital ports of MS	16	
No. of stream	16	
Beam scanning range (horizontal, both BS and MS)	±60°	
Beam scanning range (vertical, both BS and MS)	±20°	
Beam space	10°	

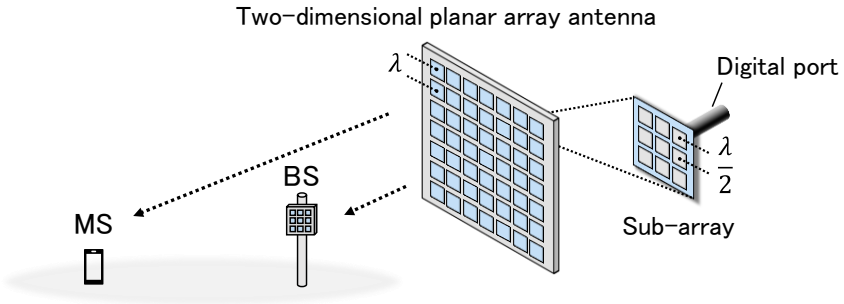

Fig. 3-2　BS and MS Antenna Configuration

II-3.4. Coverage Evaluations of the Mid-Band

Table 1 shows the simulation parameters. For the mid-band frequency range, we adopted two frequency bands: 7 GHz and 14 GHz. The bandwidth is set to two types for 7 GHz, namely 200 MHz and 400 MHz, whereas it is set to 400 MHz for 14 GHz. The height of the base station (BS) is set at 26 m and the height of the mobile station (MS) at 2.5 m, with one of each being placed.

As shown in Fig. 3-2, both the BS and MS are equipped with two-dimensional planar array antennas with multiple sub-arrays. The element spacing within the sub-array is set to half a wavelength, while the spacing between the sub-arrays is set to one wavelength. Additionally, the number of antenna elements is configured so that the aperture areas are equal for 7 GHz and 14 GHz. Fig. 3-3 displays the movement path of the MS. In this simulation, the MS calculates throughput at various points while moving through the streets of Yokosuka, following the arrows indicated in the figure.

Two movement routes, Course A and Course B, are prepared for this simulation. Course A traverses an area densely populated with buildings, including many tall structures like skyscrapers. In contrast, Course B is a residential area with fewer large buildings compared to Course A, and part of the route faces the sea. The BS is installed

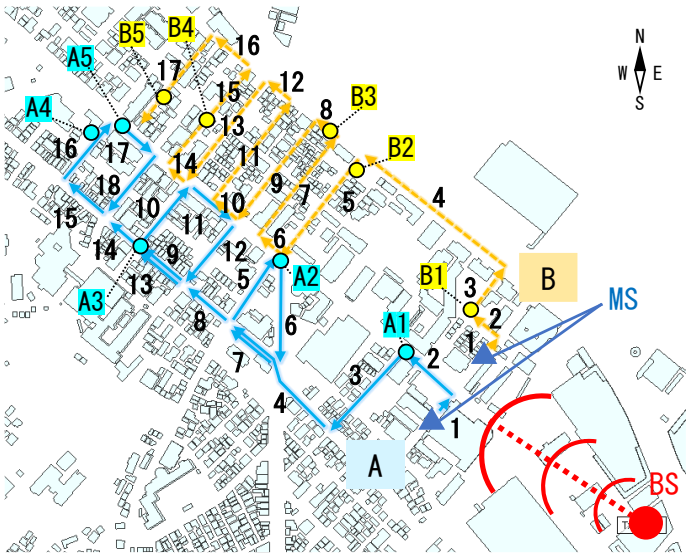

Fig. 3-3 The location of BS and the movement paths of MS

at the locations marked with circles in the figure, oriented to face the direction of the dashed and arch-shaped lines. Furthermore, the front of the MS is fixed to always face east (to the right on the map).

II-3.5. Coverage Evaluation of Mid-Band Massive MIMO

Fig. 3-4 shows the transition of throughput when moving along Course A. The horizontal axis represents the distance traveled by the MS from the starting point, ranging from 0 to 2000 m. The trend indicates that high throughput can be achieved in locations that are unobstructed and closer to the BS. Conversely, in areas with many obstructions and greater distances from the BS, throughput significantly decreases. However, there are locations within densely built areas where high throughput can still be achieved, likely due to the arrival of reflected waves at the MS from buildings. Fig. 3-5 depicts the transition of throughput when moving along Course B. The distance traveled in Course B ranges from 0 to 1815 m. The trend is like that observed in Course A.

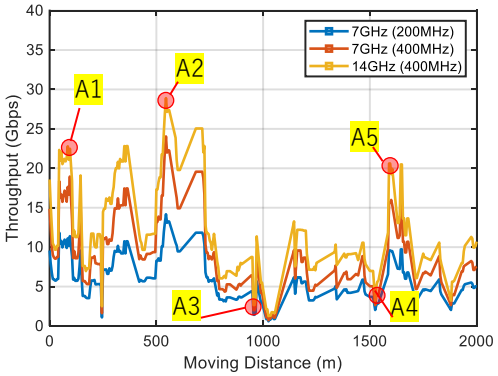

Fig. 3-4 Throughput over Course A

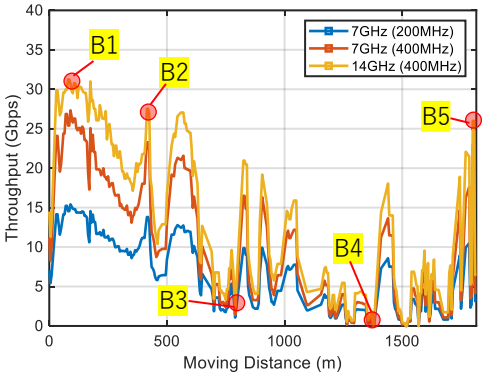

Fig. 3-5 Throughput over Course B

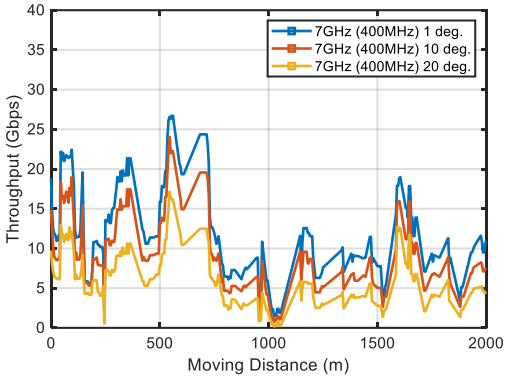

Fig. 3-6 Throughput vs. beam space (Course A, 7 GHz, bandwidth 400 MHz)

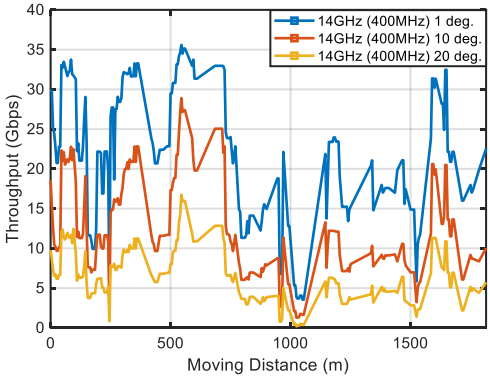

Fig. 3-7 Throughput vs. beam space (Course A, 14 GHz, bandwidth 400 MHz)

II-3.6. Coverage Evaluation When Changing Beam Spacing

The hybrid beamforming algorithm used in this simulation generates numerous beam candidates within the search range and selects the beams with higher received power from among them. By narrowing the spacing between beams during the generation of beam candidates, a denser exploration of beams is possible, while widening the spacing allows for a sparser search. While narrowing the beam spacing enables a more refined search for optimal beams, the number of beam candidates increases, thus increasing the computational load. Conversely, widening the beam spacing may lead to a coarser search but reduces the number of beam candidates, allowing for a decrease in computational load. Therefore, we investigate the impact of changes in beam spacing on coverage performance.

Figs. 3-6 and 3-7 present the throughput characteristics for different beam spacings at 7 GHz (with a bandwidth of 400 MHz) and 14 GHz, respectively. In this simulation, beam spacings of 1°, 10°, and 20° were tested along Course A. Other parameters, such as the number of antenna elements, used values shown in Table 1. For both Figs. 3-6 and 7, the results indicate that throughput characteristics improve with narrower beam

spacings. Notably, 14 GHz is sensitive to changes in beam spacing. Comparing the maximum throughput when the beam spacing is set to 1° versus 20° in Fig. 3-7 shows a difference of approximately 20 Gbps. In contrast, 7 GHz is less sensitive to variations in beam spacing compared to 14 GHz. The difference in responsiveness to changes in characteristics based on the frequency band is likely due to the difference in beam width; since 14 GHz has a narrower beam width compared to 7 GHz; it necessitates a more thorough beam exploration.

II-3.7. Conclusion

In this work, we investigated the coverage performance when deploying mid-band Massive MIMO in the urban area of Yokosuka. Since the mid-band operates at lower frequencies compared to millimeter waves and sub-terahertz waves, it is possible to achieve a certain level of throughput even in locations surrounded by buildings due to the influence of reflected waves. Additionally, to maximize the benefits of hybrid beamforming, we examined antenna configurations and beam control methods. While narrowing the beam spacing showed improvements in performance, it is necessary to balance this with the associated computational load. Furthermore, changes in the number of digital ports also affect throughput characteristics; without ensuring a certain degree of beam sharpness and number of beams, high throughput cannot be achieved. Looking ahead, we plan to conduct similar analyses for Sub-6 and millimeter waves to facilitate comparisons with mid-band performance.

REFERENCE

[1] NTT DOCOMO, Inc., 5G Evolution and 6G White Paper (Version 5.0), Jan. 2023. https://www.docomo.ne.jp/english/binary/pdf/corporate/technology/whitepaper_6g/DOCOMO_6G_White_PaperEN_v5.0.pdf

[2] M. Iwabuchi, S. Suyama, T. Arai, M. Nakamura, K. Goto, R. Ohmiya, D. Uchida, T. Yamada, T. Ogawa, “Concept and Issues of New Radio Network Topology for 5G Evolution & 6G,” IEICE Tech. Report, RCS2022-148, Oct. 2022.

[3] 3GPP, 3GPP Technology Trends, Jan. 2024. https://www.5gamericas.org/wp-content/uploads/2024/01/3GPP-Technology-Trends-WP.pdf?trk=public_post_comment-text

[4] R. A. Stirling-Gallacher and M. S. Rahman, “Multi-user MIMO strategies for a millimeter wave communication system using hybrid beam-forming,” IEEE ICC 2015, Jun. 2015.

[5] N. Nonaka, S. Suyama, T. Okuyama, and T. Asai, “Performance Evaluations of Transmitter and Receiver Hybrid Beamforming in Massive MIMO at 100 GHz-band,” IEICE Tech. Report, RCS-2021-179, Dec. 2021.

[6] Y. Hayashi, D. Mohri, Y. Chang, S. Suyama, and H. Jiang, “Evaluation of Transmission Performance of Mid-Band Massive MIMO by Computer Simulation,” IEICE Tech. Report, RCS-2024-141, Oct. 2024.

[7] Y. Hayashi, H. Tomie, S. Suyama, D. Mohri, Y. Chang, and H. Jiang, “Coverage Evaluation of Mid-Band Massive MIMO Simulation in Yokosuka City Urban Area,” IEICE General Conf., B-5A-64, March 2025.

[8] H. Tomie, S. Suyama, K. Kitao, N. Kuno, M. Inomata, W. Yamada, and M. Sasaki, “Performance Evaluation of Color Images Method for Path Loss Estimation in High Frequency Bands,” IEICE Tech. Report, AP2023-179, Jan. 2024.

[9] H. Tomie, S. Suyama, K. Kitao, N. Kuno, “Study on Propagation Emulation Method for 6G Using Dynamic Control by CPS,” IEICE Tech. Report, RCS2023-170, Nov. 2023.

[10] Y. Hayashi, H. Tomie, D. Mohri, Y. Chang, S. Suyama, and H. Jiang, “Evaluation of Transmission Performance of Mid-band Massive MIMO in Yokosuka City Urban Area by Computer simulation,” IEICE Tech. Report, RCS2025-1, April 2025.

[11] MIC ICT Policy Press Release, “Results of the International Telecommunication Union (ITU) 2023 World Radiocommunication Conference (WRC-23),” Dec. 2023. https://www.soumu.go.jp/main_sosiki/joho_tsusin/eng/pressrelease/2023/12/27_7.html

II-4. High-frequency Band Distributed Antenna System

Daisei Uchida, Takuto Arai, Shuki Wai, Hibiki Tsukada, and Mizuki Suga
NTT Access Network Service Systems Laboratories
Satoshi Suyama, Juling Huiling, and Kiichi Tateishi
NTT DOCOMO, INC

Abstract— **This article introduces a high-frequency band distributed antenna system that yields the extreme communication capacity for 6G. Specifically, we describe the system concept and the required technologies. Moreover, we introduce a demonstration experiment of analog radio over fiber, analog-beam selection, and antenna selection technologies.**

II-4.1. Introduction

6G is expected to have even greater high-capacity communication than 5G for high density terminal environments [1]. As one of the means achieving such high-capacity, we focus on the combination of high frequency bands and distributed antenna systems that well utilize the high frequency bands for mobile communication and inter-cell interference suppression. This paper introduces the concept, the required technologies, and a study of the issues with high-frequency band distributed antenna systems.

II-4.2. High-frequency Band Distributed Antenna System

To stably utilize high frequency resources such as millimeter waves for mobile communications, it is necessary to carefully arrange base stations to ensure "line of sight (LoS)" rather than "proximity". Distributed antenna systems are expected to achieve this [2][3]. Fig. 4-1 shows the system concept. Multiple antennas are set in a distributed manner such that radio waves can propagate in multiple directions to provide terminal coverage; and the radio signals transmitted or received at any antenna can be modulated and demodulated by one base station (BS). By switching antennas on the L1 layer, this system can achieve stable high-frequency band wireless transmission even in the fluctuating shielding environments created by moving human bodies and cars, etc.

We believe that three technologies are required to realize this system [2]. Fig. 4-2 shows conceptual diagrams of these technologies. The first, distributed antenna (DA) deployment, ensures line-of-sight propagation paths, with high probability, for mobile terminals. The second is distributed propagation realized by the switching of communication paths established on narrow beams to follow the movement of user terminals. The third is distributed cooperative MIMO, which utilizes path control

technology to realize the large-capacity simultaneous transmission demanded by many user terminals. In the next chapter, we describe a study on these technologies.

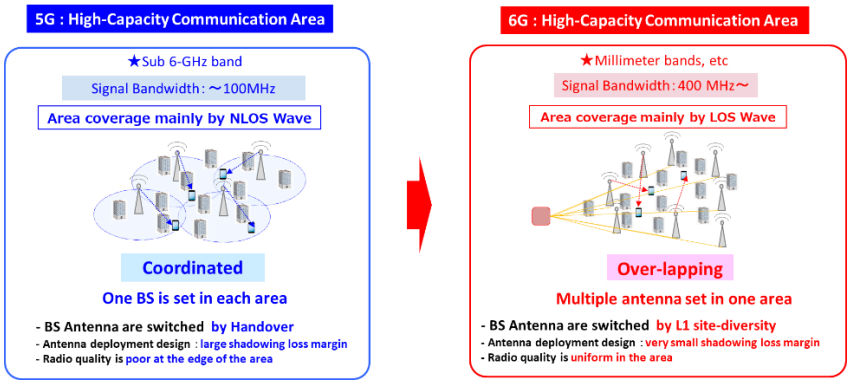

Fig. 4-1 High-Frequency Band Distributed Antenna System

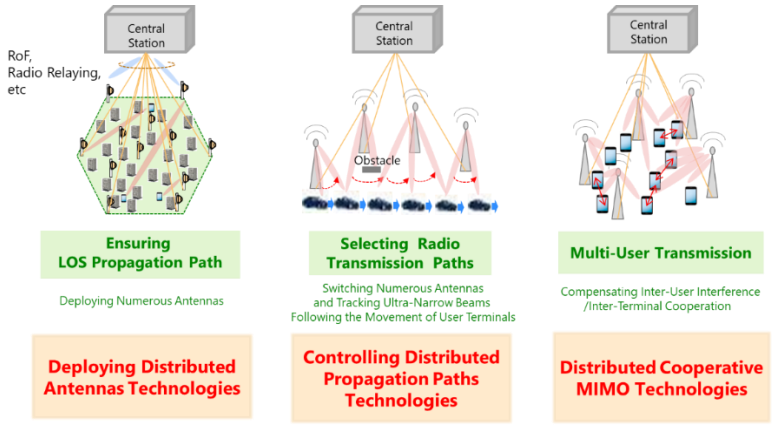

Fig. 4-2 Technologies needed for high-frequency band distributed antenna system

II-4.3. Analog Radio over Fiber (A-RoF) technologies

We describe analog radio over fiber (A-RoF) as an approach to DA implementation. An RoF is seen as a highly effective way of connecting a large number of DAs to a central station (CS). Compared to coaxial cables, connecting DAs and CS with optical fiber offers the significant advantages of low attenuation and long-distance transmission of wireless signals, especially in the high frequency bands. Furthermore, analog-digital conversion functions can be reduced, because wireless signals are directly converted into optical signals without analog to digital conversion. This is expected to realize DAs that have lower power consumption than digital RoF [4].

To achieve DAs with A-RoF, it is necessary to synchronize clocks, support time division duplex (TDD), and realize analog beamforming. We have proposed a control signal transmission method for use with subcarrier multiplexing (SCM) [5]. Properly designing the input power balance between the analog main signal and control signal is important

to avoid falls in signal quality. We demonstrated this in an experiment. Experimental overview and results are shown in Fig. 4-3. Optical signals containing an analog main signal and a control signal were transmitted over a 20km single mode fiber (SMF) using one carrier in the C band. The wireless signals used the 5G FR2 signal format, and so had 28.25GHz center frequency, 100MHz bandwidth, 60kHz subcarrier spacing and 256QAM modulation format.

The measured results confirmed the impact on analog main signal quality from control signal transmission with SCM. The error vector magnitude (EVM) value after 20km A-RoF transmission was 1.14%, which means that EVM degradation from original signal was less than 1%. This reveals that the measured EVM values of analog main signal multiplexed with the control signal needed meet the 3GPP requirement of 3.5% or less for the 256QAM format. The experiments confirm that SCM with a properly designed input power balance his highly attractive as an effective control signal transmission method.

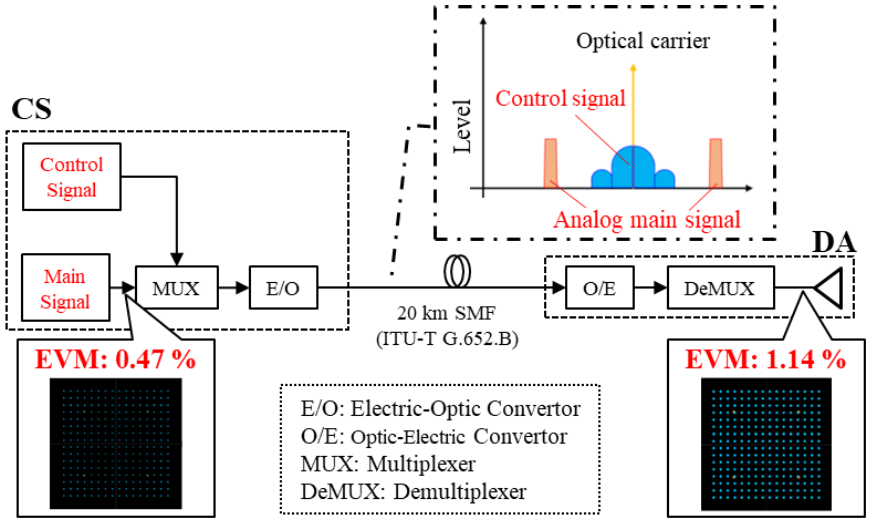

Fig.4-3. Experimental setup and result.

II-4.4. Simultaneous beam search on all DAs

In the case of a high-frequency band DA system, since both DAs and the UE antennas perform analog-beamforming, it is necessary to determine appropriate combinations of DA and analog beams (hereafter called “beam”) for each UE antenna. The simplest convention method is to search beams for each DA in turn for each UE antenna (Exhaustive search). However, as the number of DAs increases, the search time explodes.

To solve this problem, we proposed simultaneous beam search on all DAs [6]. Fig. 4-4 overviews the proposed method. The beam reference signals of all DAs are the same and transmitted simultaneously. An example of the reference signal is SS/PBCH. It selects

the beams with the 1st-Mth highest reception levels of the superimposed reference signal from all DAs (1st Stage in Fig. 4-4). Then, beam sweeping is performed for just the selected beams for each DA in turn, for example, by using CSI-RS as reference signal; this yields detection of the 1st-Mth optimal combinations of DAs and beams for each UE (2nd Stage in Fig. 4-4).

This proposed method can limit the number of searches for all beams of each DA to one regardless of the number of DAs and the optimal combination of DA and beam can be detected rapidly even if the number of DAs is high.

We have evaluated the effectiveness of this proposed method by a demonstration experiment. Fig. 4-5 shows the experimental set up and specifications, and Fig. 4-6 shows the measured results. The experiment was conducted in an indoor laboratory; the 4 DAs were placed at 3m intervals. A UE equipped with 2 antennas was moved at approximately 4km/h along 3 routes and the starting position was 2m from the wall. The number of MIMO layers was 2 on the downlink (DL), and the DL throughputs with either the conventional or proposed method were measured. Other experimental parameters were a carrier-frequency band of 40.8GHz, a signal bandwidth of 100MHz, an OFDM signal with a subcarrier spacing of 60KHz, and DA EIRP of 22dB.

The beam search was assumed to be performed by using SS/PBCH in 5G NR, which is transmitted up to 64 times every 40 ms. The total search time for the conventional method was 440 ms (with 16 beams for 4DA and 9 beams for the UE antenna). On the other hand, the proposed method could suppress the total search time to 120 ms. Assuming a 10-fold higher UE moving speed, approximately 40 km/h, the total search time was set to 10 times the real speed. Fig. 4-6 (1) shows the DL throughput performance on route B. The conventional method updated the beam at intervals of approximately 4.4 m, so although DL throughput is high immediately after the update, it falls as the UE moves. On the other hand, the proposed method achieves almost the same DL throughput as the conventional method immediately after the update, and since beam update occurs at intervals of approximately 1.2 m, the DL throughput can be held high with no long-term degradation. Fig. 4-6 (2) shows the cumulative distribution function (CDF) of DL throughput on all three routes. The DL throughput of the proposed method is 2.88 times higher at the 5%-tile CDF, 1.35 times higher at the CDF of 50%-tile compared with the conventional method. These results demonstrate that the proposed method suppresses the degradation in DL throughput compared the conventional method when a UE moves.

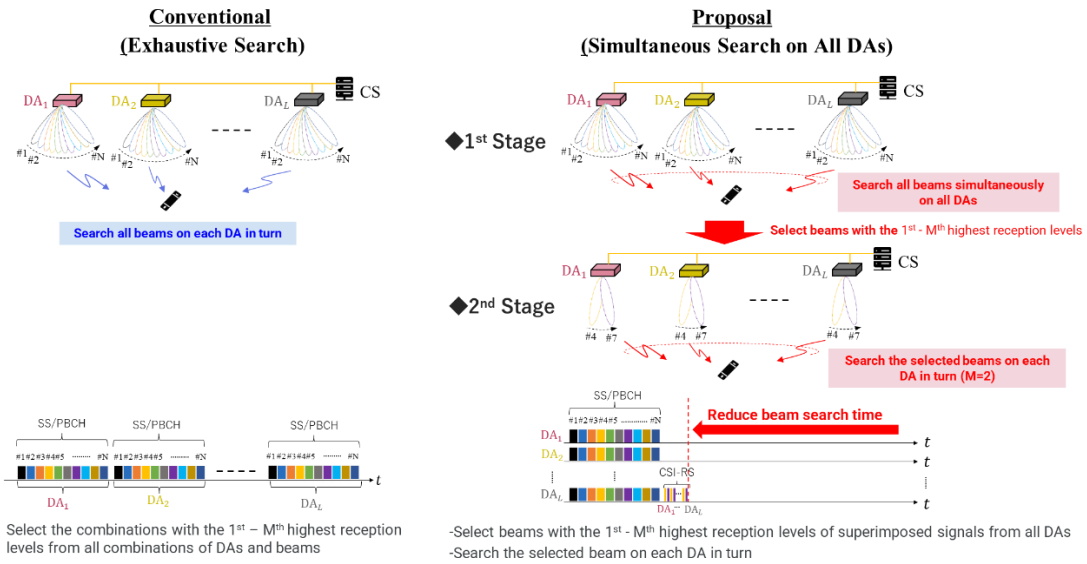

Fig. 4-4 Overview of proposed method

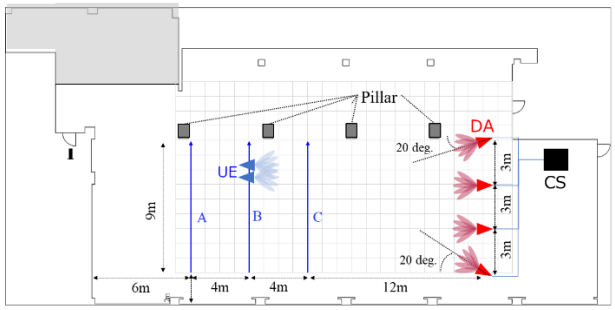

Parameters	Values
Carrier frequency	40.8 [GHz]
Channel bandwidth	100 [MHz]
Modulation Scheme	OFDM
Subcarrier spacing	60 [kHz]
Target radio link	Downlink (DL)
EIRP (DA)	22 [dBm]
NF (UE)	10 [dB]
Number of DA	4
Number of UE ant.	2
Number of antenna elements	8 (8 x 1)
Beam width	16 degrees
Number of analog beams (DA)	16
Number of analog beams (UE)	9
Number of MIMO layers	2
Post-coding (UE)	MMSE

Fig. 4-5 Experimental setup and specifications

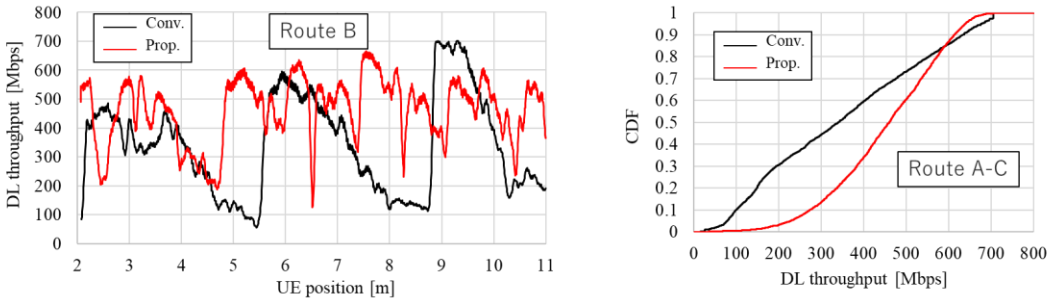

(1) The DL throughput on UE position (2) The CDF of DL throughput

Fig. 4-6 Measured results

II-4.5. A DA selection method when the DA is configured as a sub-array

We are also studying a DA selection method for each UE antenna when the DA consists of the sub-array configuration and multiple antennas are installed in the UE. When selecting the DA based on the reception level, multiple antennas on the same UE tend to select DAs at the same site that is the nearest for the UE antennas (the conventional method shown in Fig. 4-7). In the case of high frequency bands, since both the DA and UE antenna need analog beamforming, a rich multipath environment cannot be expected. Therefore, when antennas on the same UE select DAs at the same site, the spatial correlation among them is high and the SU-MIMO transmission performance may degrade. To solve this problem, we have proposed a method that allows antennas on the same UE to select DAs at different sites even if the reception level is low (the proposed method is shown in Fig. 4-7) [7].

This proposal can reduce spatial correlation in SU-MIMO transmission based only on the received level. This makes control possible simply by observing the reception level of each beam during analog beamforming and does not require the observation of crosstalk between UEs and solving complex optimization problems based on SINR (Signal-to-Interference Ratio). Therefore, while the control is simple, it is expected to improve SU-MIMO transmission performance by extracting the inherently low spatial correlation of the DAs.

We demonstrated the effectiveness of proposed method in an experiment. Fig. 4-8 shows the experimental configuration and specifications, and Fig. 4-9 shows the measured results. The experiment was conducted in an indoor laboratory, with DAs installed at 2 locations 5 m apart; each had a 2-subarray configuration. There was one UE equipped with 2 antennas. The carrier frequency band, signal bandwidth, modulation method, DA EIRP, and UE receiving NF were the same as those in Chapter Section II.4-4. As in Section II.4-4, the UE moved along 3 routes facing the DA. The number of MIMO layers was 2 on the DL, and DL throughputs of the conventional and the proposed methods were measured. The post-coding for SU-MIMO on the UE was MMSE. Fig. 4-9 (1) shows the measured DL throughput performance at each time on UE movement. The proposed method avoided the DL throughput degradation of the conventional method for most of the time. Fig. 4-9 (2) shows the CDF of DL throughput performance. The proposed method improved the 5%-tile CDF value by about 2.5 times compared to the conventional method. These results demonstrate that the proposed method can, through simple control using only the reception level of each beam observed in analog beamforming, significantly improve SU-MIMO transmission performance by taking advantage of the characteristics of DA configuration.

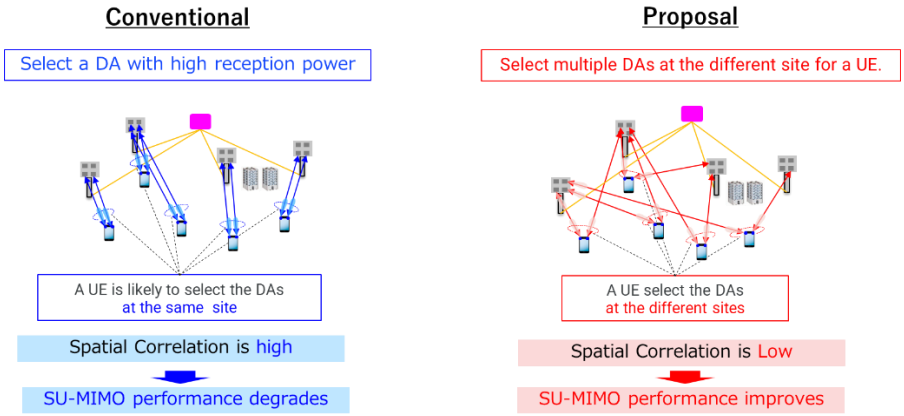

Fig. 4-7 Overview of proposed method

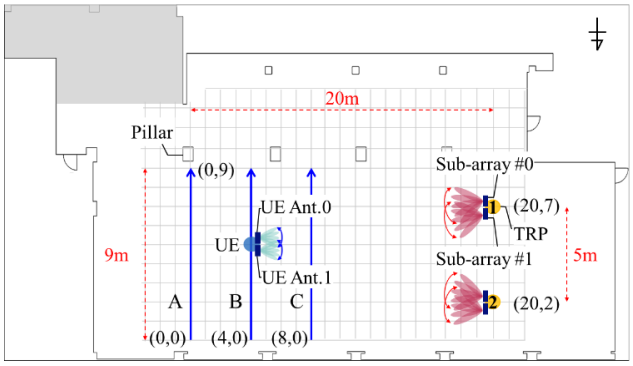

Parameters	Values
Carrier frequency	40.8 [GHz]
Channel bandwidth	100 [MHz]
Subcarrier spacing	60 [kHz]
Target Radio Link	Downlink (DL)
EIRP (DA)	22 [dBm]
NF (UE)	10 [dB]
Number of DA	2
Number of sub-array	2
Number of UE ant.	2
Number of antenna elements	8 (8 × 1)
Beam width	16 [deg.]
Number of beams / Sub-array	15
Number of beams / UE ant.	7
Beam select period	120 [ms]
Number of MIMO layer	2
Post-coding	MMSE

Fig. 4-8 Experimental setup and specifications

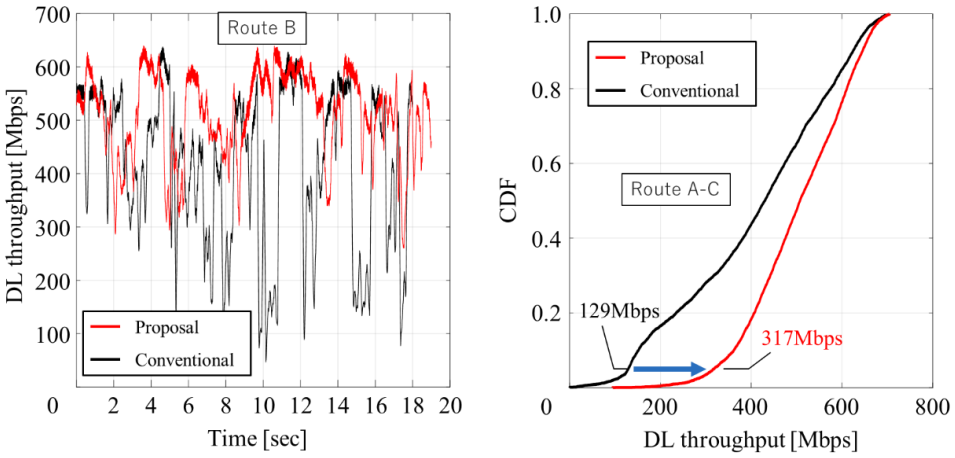

(1) DL throughput (vs time) (2)The CDF of DL throughput

Fig. 4-9 Measured results

II-4.6. Conclusion

We described a high-frequency band distributed antenna system as one means of realizing the extremely high speed and large communication capacity wireless transmission needed for 6G. We introduced and described its required technologies and studied their issues.

Specifically, we introduced a method for multiplexing transmission of the control signals and communication signals on A-RoF which is a promising approach to deploying DA, a method for rapidly detecting the optimal DA, and beam selection when both the DA and the UE perform analog beamforming, and a method to select the DA for SU-MIMO transmission when the DA has the sub-array configuration. We quantitatively showed the effectiveness of our proposed methods by experiments.

Acknowledgements

We are grateful to NEC Corporation for their collaboration in these works.

REFERENCE

[1] Beyond 5G Promotion Consortium White Paper Subcommittee, “Beyont 5G White Paper -Message to the 2030s- ver3.0“, March 7, 2024
https://b5g.jp/en2/wp-content/uploads/2024/03/whitepaper_3-0.pdf

[2] NTT DOCOMO, INC, ”White Paper 5G Evolution and 6G”, January 2023
https://www.docomo.ne.jp/english/binary/pdf/corporate/technology/whitepaper_6g/DOCOMO_6G_White_PaperEN_v5.0.pdf

[3] S.Buzzi, et al., “Cell-Free and User-Centric Massive-MIMO at Millimeter Wave Frequencies”, PIMRC, 2017.

[4] Kota Ito, et.al, “Efficiently Accommodating High-frequency-band Wireless Systems by Using Analog Radio-over-fiber,” NTT Technical Review, vol. 18, no. 5, May 2020.
https://doi.org/10.53829/ntr202005fa3

[5] Yasuyoshi Yamamoto, et.al, “Experimental Results of Multiplexing Transmission of 256-QAM 5G NR Signal with Control Signal by SCM over 20 km Analog RoF Link,” Optics Communications, vol. 570, Nov. 2024.

[6] S. Wai, et.al, " Experimental Evaluation of Simultaneous Beam Search with Multiple Distributed Antenna on Distributed Antenna Systems using High Frequency Bands," IEICE General Conference, B-5A-14, Mar. 2025.

[7] T.Arai, et.al, "Experimental Evaluation of Spatial Resources Control in Distributed Antenna Systems Using High Frequency Bands," IEICE General Conference, B-5A-15, pp.250, Mar. 2025.

II-5. Distributed MIMO Technology for Efficient Utilization of Millimeter-Wave Bands

Kazushi Muraoka, Daichi Shirase, Jun Shikida,
Masaaki Tanio, Toshiki Takeuchi, Yasushi Maruta
NEC Corporation

Abstract—**Millimeter-wave bands offer the potential for high-capacity communication but are characterized by high directivity and susceptibility to signal degradation due to blockage. To effectively leverage these bands, we explore two use cases: (a) a radio access network designed for millimeter-wave band to mobile terminals, and (b) millimeter-wave band backhaul for high-velocity vehicles. For these use cases, we introduce key technologies: (1) Radio over fiber transmission, (2) inter-access points coordinated transmission, (3) antenna-beam coordination based on mobility prediction, and (4) pre-compensation schemes for Doppler frequency offset. Integrating these technologies will realize stable high-capacity communication in millimeter-wave bands.**

II-5.1. Introduction

The use of high-frequency bands, such as millimeter waves, is necessary for accommodating growing mobile traffic as low-frequency band has a limited available spectrum. Use of millimeter wave for mobile network was introduced in the fifth-generation mobile communication system (5G). However, as of 2025, its use has not yet achieved widespread adoption. There might be several reasons, but one of the reasons is difficulty to ensure coverage with the millimeter-wave band which has high directivity and susceptibility to signal degradation due to blockage. Solving challenges for utilization of the millimeter-wave band is a key in the era of 6G.

Distributed MIMO, which generates line-of-sight (LoS) paths from access points (APs) to mobile terminals (MTs) by deploying multiple APs, is a promising concept for overcoming the challenges. Leveraging the distributed MIMO to utilize the millimeter-wave band, we present two use cases: (a) radio access network (RAN) designed for millimeter-wave band to deliver stable high-capacity communication to MTs, and (b) millimeter-wave band backhaul for high-velocity vehicles. To realize these use cases, we introduce four key technologies: (1) Radio over fiber (RoF) transmission enabling low-cost and high-quality signal transmission, (2) inter-AP coordinated transmission to mitigate increasing interference, (3) antenna-beam coordination based on mobility prediction to minimize the impact of blocking, and (4) pre-compensation schemes for Doppler frequency offset (DFO) which increases with higher frequencies. Integrating these technologies will lead to stable high-capacity communication in millimeter-wave bands.

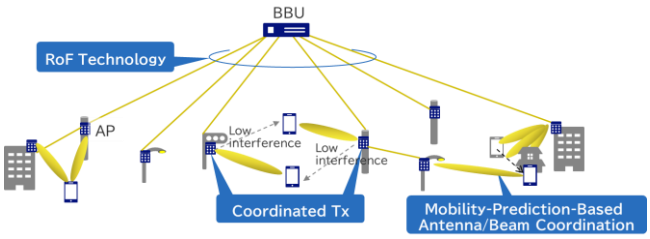

Fig. 5-1 Overview of RAN utilizing millimeter-wave Distributed MIMO.

II-5.2. Millimeter-Wave Use Cases Enabled by Distributed MIMO

We introduce two millimeter-wave use cases utilizing distributed MIMO. The first one is RAN designed for a millimeter-wave band, whose concept is shown in Fig. 5-1. Multiple APs deployed over a wider area are connected to a centralized baseband unit (BBU). These APs can be installed outdoors on utility poles, traffic signals, streetlights, etc., and indoors on walls and ceilings. With distributed MIMO, MTs can redundantly have LoS paths from multiple APs, enhancing the communication stability of high-frequency bands. For each AP, employing analog beamforming is assumed to compensate large path loss due to high frequency. To deploy distributed MIMO over a wide area, it is necessary to install numerous APs. Securing installation sites for APs is not easy, as it can be both time-consuming and costly. Thus, it is critical to miniaturize the APs and increase the number of potential installation sites. The low-layer functional split, in which the digital signal processing functions traditionally handled by the 5G radio units (RUs) transferred to a BBU, is suitable for AP miniaturization. In this case, communication between the fiber-optic connected APs and the BBUs requires RoF transmission, which transmits radio signal waveforms over optical fibers. If commercial-off-the-shelf (COTS) optical transceivers can be used for RoF transmission, the installation cost can be reduced. In Section II-5.3.1, we discuss RoF technology [1][2][6] that achieves high-quality transmission using COTS optical transceivers.

While installing a large number of APs over a wide area can redundantly secure the LoS paths, excessive interference may occur in some locations. Therefore, distributed MIMO requires transmission technology that coordinates multiple APs to suppress interference. To coordinate transmission from the multiple APs, BBUs need to understand the received signal level of each AP and each beam at the MTs. However, in actual mobile communication systems, there is a limit to the number of reports of the received power from MTs. In Section II-5.3.2, we discuss inter-AP coordinated transmission [3] that is achievable even with a limited number of reports.

Furthermore, in high-frequency bands, if an MT goes behind an obstacle, the received power may suddenly drop, and the connection may be disrupted. If MTs could always connect to multiple APs, received power could be maintained, but it would also result in

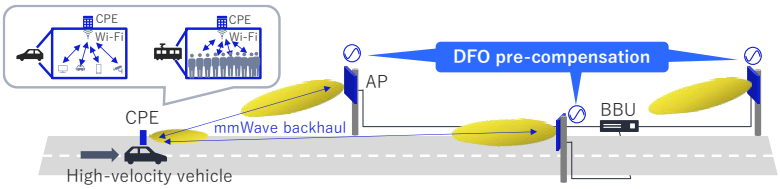

Fig. 5-2 Overview of millimeter-wave backhaul for high-velocity vehicles.

wasting radio resources. Hence, we introduce the mobility-prediction-based antenna-beam coordination [4][5], which selects the combination of APs and beams based on prediction of the reception quality degradation and allows for joint transmission from multiple APs only when necessary, in Section II-5.3.3.

The second use case for millimeter-wave utilizing distributed MIMO is wireless backhaul for vehicle-mounted customer premise equipment (CPE) at high-velocity vehicles such as cars or trains. The concept is shown in Fig. 5-2. It is envisioned that devices like smartphones will connect to the CPE via Wi-Fi, allowing communication with outside APs using millimeter-wave. Given that cars and trains travel in linear paths, they lend themselves well to LoS communication with APs installed along roadsides or rail tracks, making millimeter-wave a suitable option. Distributed MIMO configuration, where multiple APs connect to the same BBU, is expected to reduce the frequency of handovers due to high-speed movement and decrease interference between APs. Conversely, the use of millimeter waves in high-speed scenarios results in significant DFO. Notably, at the moment of AP switchover, the DFO can change drastically, leading to a degradation in communication quality. To mitigate this effect, Section II-5.3.4 will introduce DFO pre-compensation method on the network side. The subsequent section will describe the four aforementioned technologies.

II-5.3. Key Technologies for Distributed MIMO

II-5.3.1. RoF Transmission

Among the low-cost RoF methods using COTS optical transceivers, Delta-Sigma RoF is one of the promising approaches. To make Delta-Sigma RoF more practical, we introduce the pulse distortion model (PDM)-embedded Delta-Sigma RoF, which compensates for signal quality degradation caused by waveform distortion. Delta-Sigma modulation is a modulation technique that outputs quantized signals, with a feedback configuration that prevents quantization errors from occurring within the desired signal bandwidth. Delta-Sigma RoF is a RoF transmission method that applies Delta-Sigma modulation. Specifically, the radio signal is converted into a 1-bit signal sequence using Delta-Sigma modulation, then transmitted to the AP through an optical fiber as an optical signal sequence using a 1-bit COTS optical transceiver. At the AP, the original radio signal is

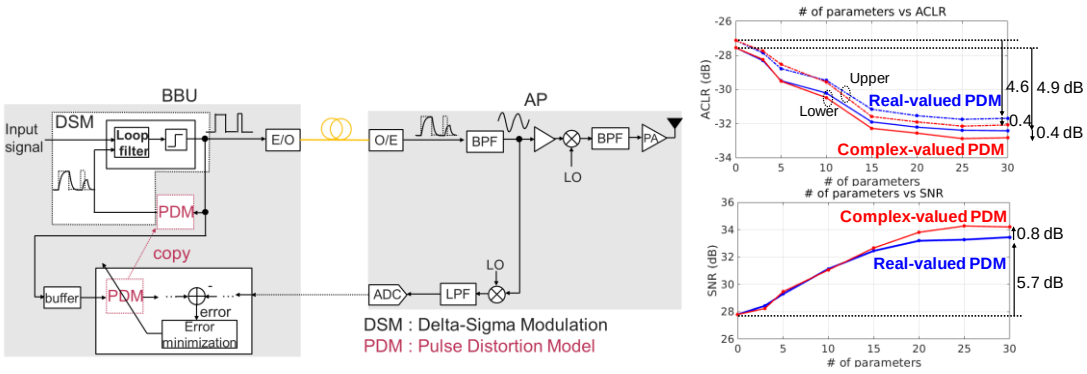

(a) Concept of PDM embedding. (b) Number of parameters vs ACLR and SNR.

Fig. 5-1 PDM-embedded Delta-Sigma RoF

regenerated by removing out-of-band quantization errors with a bandpass filter (BPF). While this method is effective in reducing costs owing to the use of COTS optical transceivers, there is a challenge of signal quality degradation at the BPF in the AP, caused by waveform distortion, such as asymmetric pulse distortion, during the RoF transmission process.

To address this challenge, we present the concept of PDM-embedded Delta-Sigma RoF in Fig. 5-3 (a). In the first step of this method, the radio signal passed through the BPF is sent back from the AP to the BBU, and the PDM is generated by comparing it with the original 1-bit signal sequence of the Delta-Sigma modulation. In the second step, the PDM obtained in the first step is embedded within the feedback loop of the Delta-Sigma modulation. This approach allows for compensation of not only quantization errors but also the waveform distortion, enabling 1-bit modulation that prevents the distortion from affecting the signal quality of the demodulated radio signal.

Furthermore, to enable wideband modulation with low adjacent channel leakage, we additionally propose an extended PDM that generalizes its parameters from real numbers to complex numbers, which allow for fine-tuned delay adjustments in the PDM. In an RoF transmission experiment using a 400-MHz bandwidth orthogonal frequency division multiplexing (OFDM) signal, we evaluated the adjacent channel leakage ratio (ACLR) and Signal to Noise Ratio (SNR). As shown in Fig. 5-3 (b), compared to the conventional RoF design without the PDM, we confirmed that by embedding the real-valued PDM, ACLR improved by up to 4.6 dB (Upper) / 4.9 dB (Lower) and SNR improved by 5.7 dB. Moreover, the proposed Delta-Sigma RoF design with the complex-valued PDM further improved the SNR by 0.8 dB and ACLR by 0.4 dB compared with using the real-valued PDM, respectively. The proposed design satisfies the specification of a 400-MHz bandwidth for 5G millimeter waves.

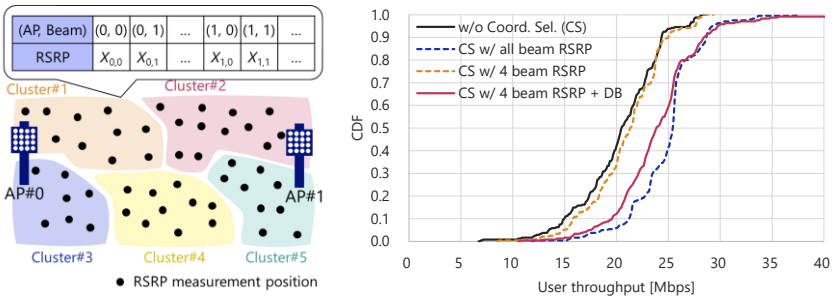

(a) Concept of RSRP DB (b) User Throughput Performance

Fig. 5-2 Coordinated MT and Beam Selection with RSRP DB.

II-5.3.2. Inter-AP Coordinated Transmission

For the inter-AP coordinated transmission method in the distributed MIMO, we adopt an approach that selects MT and beam based on the reported results of beam reception quality. Furthermore, in order to enable appropriate MT and beam selection even under conditions where the number of reports of beam reception quality is limited, we present a method utilizing a database (DB) of beam reception quality [3].

One of the inter-AP coordinated transmission methods in a distributed MIMO system adopting analog beamforming is coordinated user and beam selection. This method selects a combination of an MT and an analog beam for each AP to minimize inter-AP interference. Specifically, the selection process utilizes the beam reference signal received power (RSRP) at the MT. For each AP, the MT and beam are selected such that the difference between the beam RSRP of the serving AP and the that of the interfering AP is greater than a threshold. This allows for reduced interference and improved user throughput performance. However, measuring the RSRP of all beams from all APs at MTs and reporting all of them to the BBU is not feasible from an overhead perspective. Therefore, we estimate the RSRP of all beams from the reported RSRP of a limited number of beams using an RSRP DB, and use the estimated RSRP for the selection.

Fig. 5-4 (a) shows the concept of the RSRP DB. As shown in the figure, the average RSRP value of each beam from each AP in each area is stored in the DB, which is constructed by clustering the RSRP values at multiple positions based on similarity. When selecting MTs and beams for each AP, the appropriate RSRP values corresponding to the target MT are retrieved from the DB by checking the similarity between the reported RSRP of a limited number of beams and the clustered RSRP in the DB. Fig. 5-4 (b) shows the user throughput performance when applying coordinated MT and beam selection using the RSRP DB. It can be seen that when using only the RSRP of four beams without a DB, the interference reduction effect between APs is small, and the performance improvement compared to no coordinated selection is limited. However, when using the proposed RSRP DB, the performances are close to the ideal case where the RSRP of all beams from all APs are assumed to be available.

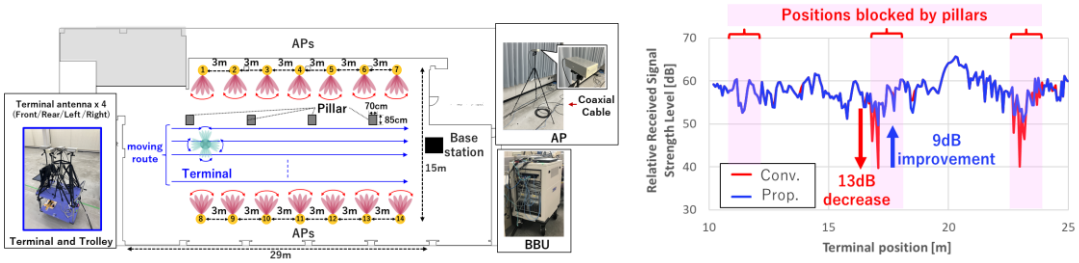

(a) Experimental environment and systems (b) Experimental results

Fig. 5-3 Experiment of mobility-prediction-based antenna-beam coordination.

II-5.3.3. Mobility-Prediction-based Antenna-Beam Coordination

When an MT using high-frequency band moves into an environment with blockage, a sudden drop in radio communication quality or disconnection may occur as radio waves do not diffract easily. For distributed MIMO performing analog beamforming, a mobility-prediction-based antenna-beam coordination predicts the occurrence of sudden radio communication quality degradation due to blocking by predicting the subsequent position of the MT and can select the appropriate APs and beams [5].

In this method, the radio communication quality, such as RSRP, of each AP and beam at each position is measured in advance, and the combination of optimal AP and beam at each position is learned. During actual operation, the communication quality of each AP and beam for an MT is continuously observed, and the position of the MT is estimated using machine learning techniques. Furthermore, the subsequent position of the MT is predicted from the estimated movement track of the MT, and the appropriate APs and beams before obtaining the next communication quality information can be predicted. As a result, even if the transmission performance of the AP and beam selected based on the current communication quality information is drastically degraded due to the blocking triggered by the movement, this method stabilizes communication by selecting the appropriate APs and beams based on the predicted subsequent position of the MT.

In an experimental environment simulating 14 APs shown in Fig. 5-5 (a), we evaluated the relative received signal strength (relative to a predetermined level in the device) of downlink (DL) transmission by using the channel estimate between each AP and terminal antenna. Fig. 5-5 (b) shows the relative received signal strength when the MT moves along the route close to the pillars shown in Fig. 5-5 (a). The received signal strength of the conventional method, which selects the AP and beam based on the current communication quality, decreased by about 13 dB at the position behind the pillar. On the other hand, in the proposed method, which selects APs and beams based on mobility prediction of an MT, the received signal strength at the same position is improved by about 9 dB compared with the conventional method.

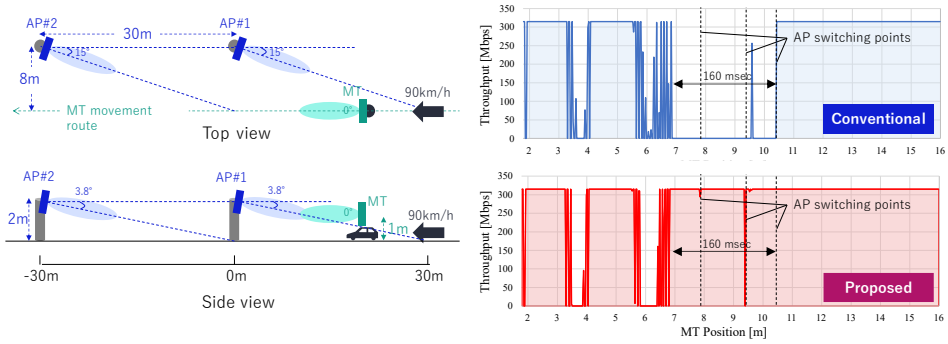

(a) System model for simulations (b) Simulation results

Fig. 5-4 Doppler Frequency Offset Pre-compensation

II-5.3.4. Doppler Frequency Offset Pre-compensation

The use of millimeter waves for high-speed scenarios results in a significant DFO. Since the DFO varies greatly depending on the location of each AP, AP switchover due to high-speed movement of the MT leads to abrupt DFO changes experienced by the MT. This DFO changes cause a deterioration in communication quality. Typically, the DFO caused by the movement of a MT is compensated by automatic frequency control (AFC), which adjusts the local oscillator frequency to synchronize the received signal frequency. However, it is difficult to quickly adapt to such abrupt DFO changes by AFC.

Our proposed method compensates for DFO in coordination among APs, thereby minimizing the DFO experienced by high-speed MTs during AP switching [7]. In this method, the connected AP estimates the DFO between itself and the MT based on the frequency difference between the previously sent DL reference signal and the received uplink (UL) reference signal from the MT. The AP adjusts the frequency of the DL reference and data signals according to the estimated DFO, which helps to converge the received DFO at the MT to around zero. Simultaneously, the MT's frequency after AFC also converges to the original DFO-free carrier frequency. Other APs, assuming the MT's AFC frequency has converged, measure DFO based on the frequency of the received UL reference signal from the MT. When switching APs to transmit signals to the MT, they use the measured DFO to adjust the DL signal frequency.

Fig. 5-6 (a) illustrates the assumed deployment of APs and MT. In the evaluation, the MT traveled at a speed of 90 km/h through a linear area served by two APs, and AP switching was conducted based on received power criteria. Fig. 5-6 (b) presents the throughput for each MT position. The results revealed that with the conventional method, throughput significantly decreased for 160 milliseconds due to the DFO experienced by the MT during AP switching. In contrast, the proposed method successfully mitigated the throughput degradation during AP switching by applying DFO pre-compensation. Based on the results, the proposed method enables user-centric wireless communication by allowing seamless AP switching without requiring special processing by the MT.

II-5.4. Conclusion

We introduced four key technologies that support distributed MIMO for the effective utilization of millimeter-wave bands: RoF transmission, inter-AP coordinated transmission, mobility-prediction-based antenna-beam coordination, and DFO pre-compensation. We believe integrating these technologies within distributed MIMO systems will economically build systems that enable stable high-capacity communication even in millimeter-wave bands.

Acknowledgement

A part of this research was conducted in collaboration with NTT and NTT DOCOMO.

REFERENCE

[1] M. Tanio, N. Ishii, and K. Muraoka, "Wideband delta-sigma radio-over-fiber embedding a pulse-distortion model for beyond 5G," 2022 IEEE 96th Vehicular Technology Conference (VTC2022-Fall), 2022, pp. 1-5.

[2] Y. Kase, S. Hori, N. Oshima, and K. Kunihiro, "Radio-over-fiber system with 1-bit outphasing modulation for 5G/6G in-door wireless communication," IEICE Trans. Electron., vol.E106-C, no.7, pp.405-416, 2023.

[3] J. Shikida, K. Muraoka, T. Takeuchi, and N. Ishii, "Inter-access point coordinated user and beam selection for mmWave distributed MIMO systems," 2022 IEEE 96th Vehicular Technology Conference (VTC2022-Fall), 2022, pp. 1-5.

[4] "World's first successful demonstration of distributed MIMO that continues wireless connections in the 28 GHz band by eliminating shielding issues," https://www.nec.com/en/press/202210/global_20221031_04.html

[5] "Successful 40 GHz band distributed MIMO demonstration of maintaining radio communication quality even when interference occurs due to movement of multiple users," https://www.nec.com/en/press/202310/global_20231031_01.html

[6] M. Tanio, D. Ogasahara, N. Ishii, and K. Muraoka, "Wideband Delta-Sigma Radio-Over-Fiber Embedding Complex-Valued Pulse-Distortion Model for 5G and Beyond," IEEE Access, vol. 12, pp. 130995-131007, 2024.

[7] D. Shirase, T. Takeuchi, and K. Muraoka, "A Study on Doppler Shift Pre-compensation for Antenna Switching in mmWave Backhaul Communication for High-Speed Mobility," IEICE Tech. Rep., vol. 124, no. 311, RCS2024-178, pp. 19-24, Dec. 2024.

II-6. Distributed Antenna Technology (High-density Distributed Antenna System and Transmission Point Sharing Control)

Takashi Dateki,
Fujitsu Limited

Abstract— **This article introduces ultra-high-density distributed antenna technology for higher capacity and technology for sharing radio resources among distributed antennas deployed at multiple locations and among operators for efficient area deployment.**

II-6.1. Introduction

One important aspect of cell-free communication technology is to be able to flexibly provide the high communication performance of 6G when and where it is needed, depending on the user's activity and their environment. It is necessary to provide high-performance communications on demand in each local area. However, in terms of cost and power consumption, the overall processing and power consumption must be reduced to cover the entire area efficiently. This chapter introduces ultra-high-density distributed antenna technology for higher capacity and technology for sharing radio resources among distributed antennas deployed at multiple locations and among MNO for efficient area deployment.

II-6.2. Ultra-High Density Distributed Antenna

From FY2015 to FY2018, we have been engaged in research and development of ultra-high-density distributed antenna systems as a technology to realize high capacity and have performed various simulations and field experiments under the research project of the Ministry of Internal Affairs and Communications [1].

Fig. 6-1 shows an example of a computer simulation of the ultra-high-density distributed antenna system with 16 antennas in an area using the real map and building information for a part of the central Tokyo. The centralized baseband unit provides cooperative control for a large number of distributed antenna units densely located in the area. Significant system throughput improvements can be seen compared to the case where each transmission point is operated as a different cell (conventional uncoordinated system). It can also be confirmed that a good communication area is formed where the user is present without degradation at fixed cell boundaries. In general, a dense cell arrangement is expected to increase capacity, but in practice, inter-cell interference prevents a sufficient capacity increase. Therefore, we have developed a cooperative radio resource control technique that improves signal quality by reducing interference among distributed antennas. The technique is basically distributed multi-user MIMO, in which

the entire signal from many distributed antennas is orthogonalized using algorithms such as ZF and MMSE, and each user receives only the signal component addressed to each user [2]. This algorithm is called "dynamic virtual cell control technology" because of its image of forming individual cells for each user in order to improve communication quality by reducing interference for all users communicating simultaneously. Unlike conventional cell configurations that operate with fixed cell boundaries, this technology can be seen one of cell-free technologies that automatically forms virtual cells based on propagation path estimates between distributed antennas and users.

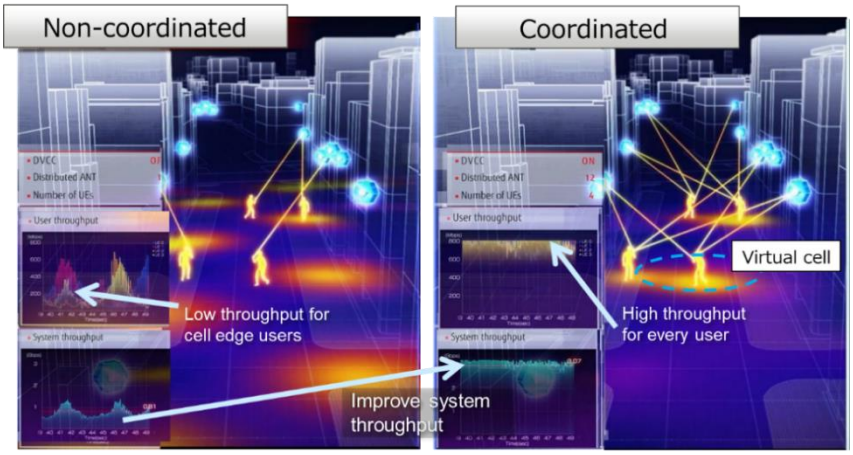

Fig. 6-1 The example simulation results of High density distribute antenna system with and without coordination control (dynamic virtual cell control)

To verify the advantage of the ultra-dense distributed antenna system, we developed the experimental device shown in Fig. 6-2 (a). The base station equipment consists of a central baseband unit and up to 16 RF devices (up to 32 antennas) connected by optical fibers. The central baseband unit uses an over-the-air (OTA) calibration function to perform high accuracy channel estimation using the reciprocity between Uplink and Downlink channel, and performs spatial multiplexing transmission of up to 32 streams. A distributed antenna system using these equipment was constructed in Fujitsu Shin-Kawasaki Technology Square, Kanagawa, Japan, and indoor field experiments were performed [1]. To confirm the effect of capacity increase by coordination control of the radio resource, the system throughput was compared when the number of TPs was varied from 4, 8, to 16 under the condition that the number of TPs and the number of UEs were the same. The results are shown in Fig. 6-2 (b). When cooperative radio resource control is applied, the capacity increase is almost proportional to the increase in the number of TPs, and it can be confirmed that the system capacity at 16 TPs is about 4 times larger than that of a simple small cell system (i.e. without coordination control).

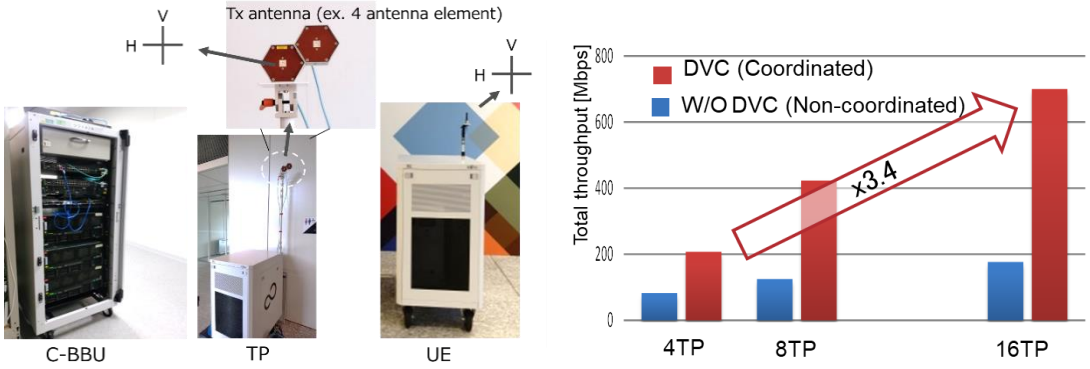

(a) (b)

Fig. 6-2. (a)The developed experimental equipment, (b) The capacity evaluation result for the increasing number of TP.

The evaluation result for the case when TPs and UEs were located at one of the candidate locations is shown in Fig. 6-3 (a). Fig. 6-3 (b) shows the CDF of user throughput measured multiple times. The results show that distributed placement can improve the areal system capacity and that the improvement can be enhanced by appropriately designing the location of the transmission points.

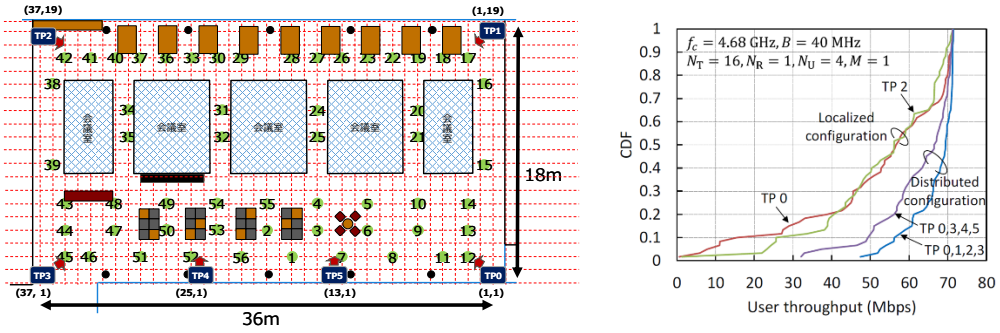

(a) (b)

Fig. 6-3. (a)Area map and the TP location, (b) CDF of the user throughput in the experimental area.

II-6.3. Transmission point Sharing technology

In the R&D project "Research and Development of 5G Base Station Sharing Technology" by the Ministry of Internal Affairs and Communications (MIC), a technology to efficiently achieve high density in urban areas was studied by multiple Mobile Network Operators (MNO) using shared base stations located at many points in the area. In this project, the shared radio units (RUs) for multiple MNO frequencies and the radio resource control techniques that efficiently utilize fronthaul within a limited bandwidth were developed. This radio resource control is an algorithm that optimally allocates a

large number of RUs located at multiple points in multiple MNOs in an area so that high capacity can be achieved in the area while limiting the total fronthaul and radio resources below a certain value. This reduces the maximum capacity required for central baseband unit and fronthaul to process multiple cells to cover the entire area, while focusing resources on the required areas to achieve efficient communication according to data traffic demands [3],[4].

Fig. 6-4 shows an image of the operation of radio resource control in a base station sharing system. if MNO #A and #B have their own base stations in independent locations, UEs that are far from the cell center will have lower field strength. Or, in an interference-limited environment, UEs will have a lower SINR due to interference from other cells communicating in the same band. On the other hand, in a base station sharing system, each MNO allocates and uses a portion of the system bandwidth from its own location, allowing all UEs to communicate with nearby base stations without increasing the total amount of radio resources used by the entire system. This improves system performance without increasing the total amount of overall radio resources and radio transmission energy.

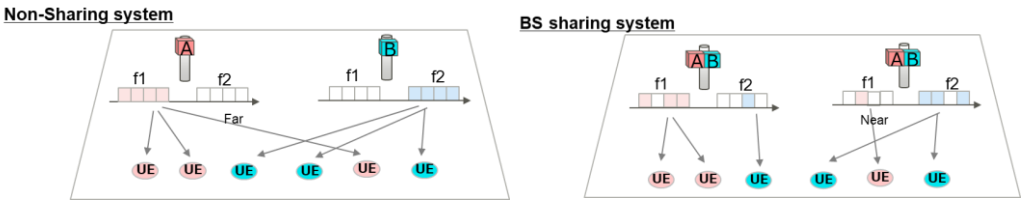

Fig. 6-4. An example of the radio resource control in a base station sharing system.

Fig. 6-5 shows the simulation results of system throughput using the simulation model correspond to urban areas in 3GPP. It can be seen that the average throughput is significantly improved by base station sharing.

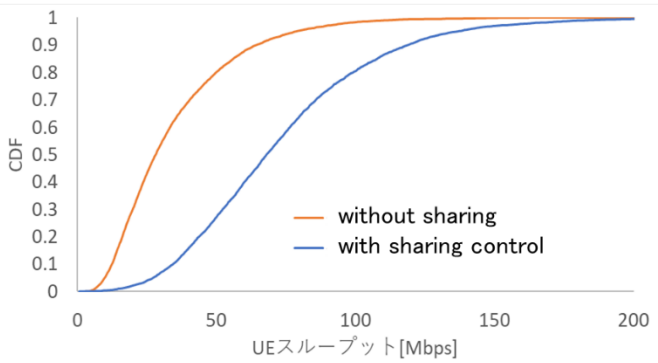

Fig. 6-5. Throughput improvement of radio resource sharing

II-6.4. Conclusion

In this paper, we have introduced ultra-dense distributed antenna technology for high capacity and base station sharing technology for efficient area deployment. In addition, cell free NW is also related to other technologies introduced in this white paper, such as the intelligent reflectors and relay technologies, etc. These technological elements should not only be considered separately to be introduced in different use-cases, but the integrated system including various technologies should adapt to the dynamically changing requirements of the area. The overall picture of such a 6G system has still unclear. Therefor active research and development is expected to continue in the future.

Acknowledgements

This paper includes a part of results of “The research and development project for realization of the fifth-generation mobile communications system” and “The research and development project for 5G Shared Radio Unit (JPJ000254)” commissioned by The Ministry of Internal Affairs and Communications, Japan.

REFERENCE

[1] M. Minowa et al., "5G R&D Activities for High Capacity Technologies with Ultra High-Density Multi-Band and Multi-Access Layered Cells," 2019 IEEE 89th Vehicular Technology Conference (VTC2019-Spring), Kuala Lumpur, Malaysia, 2019, pp. 1-5

[2] Takashi Seyama, Masafumi Tsutsui, Teppei Oyama, Takaharu Kobayashi, Takashi Dateki, Hiroyuki Seki, Morihiko Minowa, Tatsuki Okuyama, Satoshi Suyama and Yukihiko Okumura, “Study of Coordinated Radio Resource Scheduling Algorithm for 5G Ultra High-Density Distributed Antenna Systems,” IEEE Asia Pacific Wireless Communication Symposium (APWCS) 2016, pp.306-310, Aug. 2016.

[3] T. Kobayashi, et.al. “Function Division Type Resource Control Method for 5G Shared Radio Unit,” Proceeding of 2022 IEICE General Conference, B-5-12, Mar. 2022, and B-5-13, B-17-5, B-5-58.

[4] T. Kobayashi, et.al., “Radio Resource Management Algorithms for Implementation in Radio Unit Sharing Systems,” IEICE Transactions on Communications J106-B (5), 327-337, 2023-05-01

II-7. 6G views on Coherent Joint Transmission and Multi-User MIMO

Takahisa Fukui, Kozue Hirata, and Kazunari Yokomakura
SHARP Corporation

Abstract— One of the significant challenges in cellular system is to avoid performance degradation of cell-edge users due to inter-cell interference and severe pathloss. To address this issue, 5G-Advanced, which is specified in 3GPP, supports the deployment of multiple transmission and reception points (TRPs) to realize cell-free network architectures. In particular, coherent joint transmission (CJT) improves cell-edge user performance by coordinating inter-cell radio resources of multi-TRP. However, implementation of CJT on multi-TRP operation leads to excessive consumption of common radio resources as the number of users increases. To solve this issue, we focus on multi-user (MU) MIMO, which is widely recognized as a key technology for enhancing spectral efficiency and has been further optimized in 5G-Advanced. Notably, enhanced MU-MIMO in 5G-Advanced doubles the spatial multiplexing capability compared to 5G. Integration of MU-MIMO with CJT on multi-TRP operation is expected to improve the resource utilization while mitigating the inter-cell interference. In this article, we show views toward 6G on multi-TRP CJT and MU-MIMO technologies and discuss their potentials for future cell-free cellular system.

II-7.1. Introduction

Cellular systems have been essential for people around the world as one of the most important basic infrastructures. In the cellular systems, cellular coverage is constructed by locating multiple base stations, and each user equipment (UE) can enjoy the internet connection anywhere by connecting to one of the base stations and its network. However, because cellular coverage is realized by multiple coverage areas generating by geographically separated multiple base stations, the performance of cell-edge UEs is degraded due to large pathloss and inter-cell interference (ICI). Therefore, one of the significant challenges in cellular system is to avoid such performance degradation of cell-edge UEs.

To address this issue, deployment of multiple transmission and reception points (TRPs) has been considered to realize cell-free network architectures. On the multi-TRP operation, communication areas are formed using multiple transmission points and multiple reception points. The multi-TRP can coordinate to serve data transmission to one UE, and it can improve signal-to-noise-plus-interference (SINR). In particular, coherent joint transmission (CJT) from the multi-TRP improves the cell-edge UE performance by coordinating inter-cell radio resources with beamforming [1],[2].

However, implementation of CJT on multi-TRP operation leads to inefficient resource utilization in high data traffic case because the multi-TRP synchronizes and transmits the same signals simultaneously from multiple coordinated TRPs by using additional resources such as spectrum and power. To solve this issue, we focus on multi-user multiple-input multiple-output (MU-MIMO), which is widely recognized as a key technology for enhancing spectral efficiency and has been further optimized in 5G-Advanced [1], [2]. MU-MIMO enables each TRP to serve multiple UEs simultaneously on the same time-frequency resource using multiple antennas and multiple MIMO layers (i.e., stream). Notably, enhanced MU-MIMO in 5G-Advanced doubles the spatial multiplexing capability compared to 5G. For these reasons, we focus on integration of MU-MIMO with CJT on multi-TRP operation which can realize the cell-free network architectures such that the cell-edge UE performance is improved by the effect of CJT on multi-TRP operation, and also improve the resource utilization by the effect of MU-MIMO.

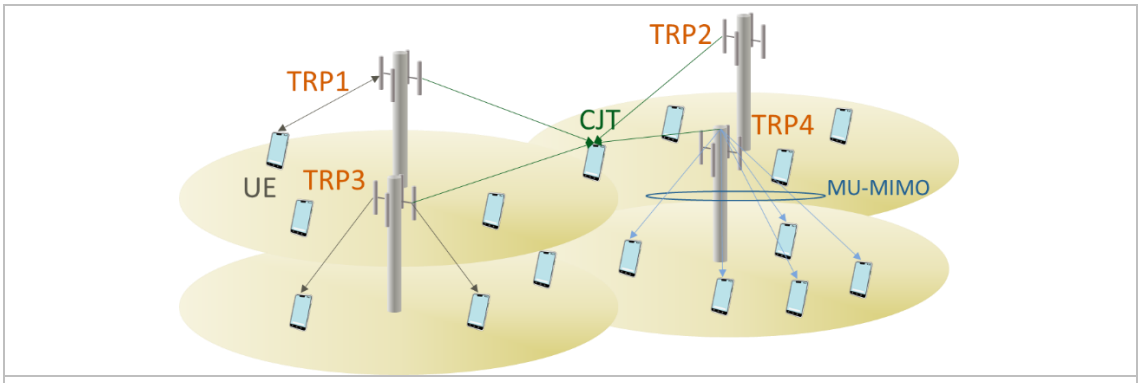

Fig. 7-1 Integration of MU-MIMO with CJT on multi-TRP operation

Fig. 7-1 shows a concept of integration of MU-MIMO with CJT on multi-TRP operation. As shown in this figure, multi-TRP simultaneously transmit the same data to a UE on the same frequency resource in multiple adjacent cells. On the single TRP operation, if different data are allocated to the same frequency resource in different cells, they are regarded as interference to each other. On the other hand, in CJT on multi-TRP operation, the SINR at the cell-edge UE is improved because the desired signal from the adjacent cells can be received instead of the interference. Furthermore, in this figure, each TRP also multiplexes multi-UEs on the same frequency resource within a cell. This effect of MU-MIMO can compensate for resource consumption caused by the effect of CJT on multi-TRP operation.

As mentioned above, the integration of MU-MIMO with CJT on multi-TRP operation is expected to improve the resource utilization while mitigating the ICI. However, one of the most complicated algorithms to realize this integration is a radio resource allocation because both intra-cell and inter-cell resource need to be managed. Hence, in this paper, we show an radio resource allocation algorithm that is the most complicated design for

MU-MIMO with CJT on multi-TRP operation. Furthermore, we provide views toward 6G on multi-TRP CJT and MU-MIMO technologies and discuss their potentials for future cell-free cellular system.

II-7.2. Radio resource allocation

3GPP specifications do not fully define all algorithms required for implementation. Instead, they allow flexibility in some areas, leaving algorithmic choices to vendors, operators, or equipment manufacturers. This approach enables innovation and competition while ensuring compliance with the standard. Particularly, the radio resource allocation by scheduling is one of the most susceptible algorithms. As a general scheduling method, the proportional fairness (PF) scheduling has been widely studied in the cellular system. In this paper, the PF scheduling is applied for the MU-MIMO with CJT on multi-TRP operation.

In PF scheduling, the radio resource is allocated for each UE based on the ratio of instantaneous expected throughput to average throughput, which is called PF metric. This instantaneous expected throughput can be calculated by using a signal-to-noise-plus-interference (SINR), which is derived based on a channel quality indicator (CQI) reported by UE. For MU-MIMO, in order to decide whether to perform MU-MIMO and determine the number of multiplexed UEs, the network can update the SINR of UE#i for MU-MIMO based on the reported SINR of UE#i for SU-MIMO and a MIMO precoder $w_{i,v}$ reported by each UE as the following:

$$SINR_{MU,i} = \frac{1}{r_i}\sum_{v=1}^{r_i} \frac{\frac{1}{K} SINR_{SU,i}}{1 + \frac{1}{K} SINR_{SU,i} \sum_{k=1,k\neq i}^{K} \frac{1}{r_k} \sum_{v'=1}^{r_k} \left| \boldsymbol{w}_{i,v}^{H} \boldsymbol{w}_{k,v'} \right|^2}$$

where r_i is an optimal MIMO rank reported by UE#i, K is the number of multiplexed UEs k. For this, each TRP would switch between SU-MIMO and MU-MIMO subject to the calculated SINR. For example, TRP allocates radio block group (RBG) to UE#i with the highest PF metric on this RBG, and TRP decides to perform MU-MIMO for UE#i when $SINR_{MU,i}$ is larger than $SINR_{SU,i}$. As a result of intra-TRP resource allocation, each TRP can determine the mapping list of UE to RBG e.g., {{RBG#1, UE#x}, {RBG#2, UE#y} …, {RBG#N, UE#z}}.

As a next step, for CJT on multi-TRP operation, inter-TRP resource allocation is performed. For CJT, multi-TRP transmits the same data to single UE within the same RBG. For example, when TRP#1 and TRP#2 transmit the same data to UE#b within RBG#2, the mapping list of TRP#1 is {{RBG#1, UE#x}, {RBG#2, UE#b} …, {RBG#N, UE#z}} and the mapping list of TRP#2 is {{RBG#1, UE#a}, {RBG#2, UE#b} …, {RBG#N, UE#c}}. As inter-TRP resource allocation, the inter-cell interference can be significantly

reduced such that the same RBG is allocated to the cell-edge UE with e.g., lowest SINR [3].

As the above, MU-MIMO with CJT on multi-TRP operation can be performed by two-step resource allocation of intra-TRP and inter-TRP. In intra-TRP resource allocation, a higher PF metric results in a higher priority for resource allocation. The PF metric can be calculated for both MU-MIMO and SU-MIMO, and the higher one can be utilized. According to [4], the 50%ile UE throughput with optimal switching between SU-MIMO and MU-MIMO improves by 34% over that with only MU-MIMO. In inter-TRP resource allocation, a lower SINR results in a higher priority for coordinated TRPs. When different TRPs allocate the same RBG to different UEs in intra-TRP resource allocation, the different TRPs re-allocate the same RBG to one of the different UEs in inter-TRP resource allocation by considering the channel condition. According to [3], the 5%ile UE throughput with CJT improves by 91% over that without CJT.

II-7.3. 6G views

The integration of MU-MIMO with CJT on multi-TRP operation results high reliability, low latency, and high communication service availability. This technology could be applied to 6G delay-critical services even if the traffic extremely grows due to introducing new use cases in addition to the mobile. As examples of 6G delay-critical services, discrete automation, intelligent transport systems, high-voltage electricity distribution, etc., are being considered. Particularly, we focus on the cooperative autonomous driving system as one of 6G use cases in this paper.

As a societal challenge, “The 2024 Problem” is serious and comes from the country’s driver shortage and the Japanese government’s new amendment on labor standards, limiting yearly overtime work of truck drivers to 960 hours [5]. For this reason, the demand for Level 4 and higher autonomous driving has been increasing, and it is anticipated that the number of autonomous vehicles will rapidly grow. Furthermore, cooperative autonomous driving, which leverages V2X (Vehicle-to-Everything) communication, has been identified as an effective approach to share real-time information about the surrounding environment between roadside unities (RSUs) and vehicles. Particularly, it is essential that all vehicles recognize vulnerable road users (VRUs) such as pedestrians and cyclists, who do not have communication capabilities. This involves collecting data from sensors installed on RSUs and in-vehicle sensors, then sharing and complementing this information in real time with vehicles in blind spots or at intersections to ensure stable and immediate vehicle braking. To realize cooperative autonomous driving, we believe that C-V2X (Cellular V2X) communication, which has been standardized in 3GPP, is utilized.

In our view, C-V2X communication is expected to increase demand in 6G due to “The 2024 Problem”. In 6G, even in environments with dense traffic, sufficient system

capacity is required for all vehicles to recognize each other. Furthermore, high reliability and seamless mobility are further required for all vehicles to ensure real-time safety features like collision avoidance. For such requirements, the integration of MU-MIMO with CJT on multi-TRP operation can be highly suitable for C-V2X communication. In terms of mobility, the cell-free network architecture ensures the seamless handover from one cell to another cell. In environments with dense traffic, MU-MIMO allows the system to communicate with multiple vehicles simultaneously, improving not only spectral efficiency but also latency. Furthermore, CJT on multi-TRP operation ensures better coverage and lower ICI to cell-edge vehicles. These mean the integration of MU-MIMO with CJT on multi-TRP for C-V2X systems can ensure consistent and reliable communication even for vehicles in non-line-of-sight conditions, critical for real-time safety features like collision avoidance or autonomous driving.

II-7.4. Conclusion

One of the significant challenges in cellular system is to avoid performance degradation of cell-edge users due to inter-cell interference and severe pathloss. To address this issue, 5G-Advanced, which is specified in 3GPP, supports the deployment of multiple transmission and reception points (TRPs) to realize cell-free network architectures. In particular, coherent joint transmission (CJT) improves the cell-edge user performance by coordinating inter-cell radio resources of multi-TRP. However, implementation of CJT on multi-TRP operation leads to excessive consumption of common radio resources as the number of users increases. To solve this issue, we have focused on multi-user (MU) MIMO, which is widely recognized as a key technology for enhancing spectral efficiency and has been further optimized in 5G-Advanced. Notably, enhanced MU-MIMO in 5G-Advanced doubles the spatial multiplexing capability compared to 5G. Integration of MU-MIMO with CJT on multi-TRP operation is expected to improve the resource utilization while mitigating the inter-cell interference. In this paper, we have shown views toward 6G on multi-TRP CJT and MU-MIMO technologies and discuss their potentials for future cell-free cellular system.

REFERENCE

[1] RP-213598, New WID: MIMO Evolution for Downlink and Uplink, Dec., 2021.

[2] W. Chen et al., ”5G-Advanced Toward 6G: Past, Present, and Future,” in IEEE Journal on Selected Areas in Communications, vol. 41, no.6, pp. 1592-1619, June 2023, doi: 10.1109/JSAC.2023.3274037.

[3] Takahisa Fukui, Taro Kumamoto, Akihiro Sonoda, Kazunari Yokomakura, “Performance Evaluation of Coherent Joint Transmission by using Multi-TRP Coordination,” IEICE society conference, B-5A-12, September, 2024. (Japanese)

[4] Takahisa Fukui, Ryota Morimoto, Kazunari Yokomakura, “Performance Evaluation of Enhanced DL MU-MIMO for 5G-Advanced,” IEICE Technical report, RCS2023-62, vol. 123, no.76, pp.200-205, June 2023. (Japanese)
[5] Nippon Television, “Japan facing “2024 Crisis” – services struggling to fight with changes,” September 2024, https://www.ntv.co.jp/englishnews/articles/2021kxh2kol1axekdx1y.html

II-8. A Study on Advanced MIMO Large Arrays in the 7–15 GHz Spectrum for 6G

Hiroki Iimori, Szabolcs Malomsoky
Ericsson Research Japan

Abstract— **This article explores the potential of the 7–15 GHz centimeter-wave spectrum as a key enabler for 6G networks, balancing coverage and capacity. If current growth trends continue, network traffic is projected to double or even triple by 2030, creating a significant demand for additional spectrum. The centimeter-wave band offers a middle ground between lower frequencies (e.g., sub-6 GHz) and higher-frequency millimeter-wave bands. As wavelength decreases and propagation conditions deteriorate compared to sub-6 GHz bands, advanced multiple-input multiple-output (MIMO) technology with large array systems will play a crucial role in achieving the expected performance improvements. Consequently, transmission challenges, including antenna design and power efficiency, become critical. In this context, we present NR-compliant link-level simulation results comparing fully digital MIMO arrays with beam-sweeping-based hybrid MIMO arrays, showcasing the potential of hybrid MIMO arrays in this promising band.**

II-8.1. Introduction

The rapid evolution of mobile networks reflects an ongoing drive for increased capacity, enhanced energy efficiency, and reduced operational costs [1]. As we gear up to transition from 5G to 6G, the pressure on wireless infrastructures is expected to rise due to surging data volumes and the quest for enhanced spectral efficiency. While 5G has delivered remarkable improvements in mobile broadband, fixed wireless access, and IoT connectivity, it still left room for further improvements from different perspectives. Recognizing this, experts and researchers have rallied around the idea that exploring new frequency bands is imperative for realizing the full potential of 6G. In this pursuit, the centimeter-wave (cmWave) spectrum - spanning roughly 7 to 15 GHz - has emerged as a leading candidate to power the next wave of network innovations.

II-8.2. New Frequency Band for 6G

Looking back, mobile networks have depended on sub-6 GHz frequencies for the reliable propagation condition and expansive coverage. Yet given that emerging applications such as immersive extended reality, holographic communications, and intricate digital twinning as well as unseen future applications encourage different requirements on communications, the challenges of these lower frequency resources become inevitably posed. In contrast, millimeter-wave (mmWave) frequencies offer vast bandwidth and exceptional data rates in some limited scenarios, but they have their own

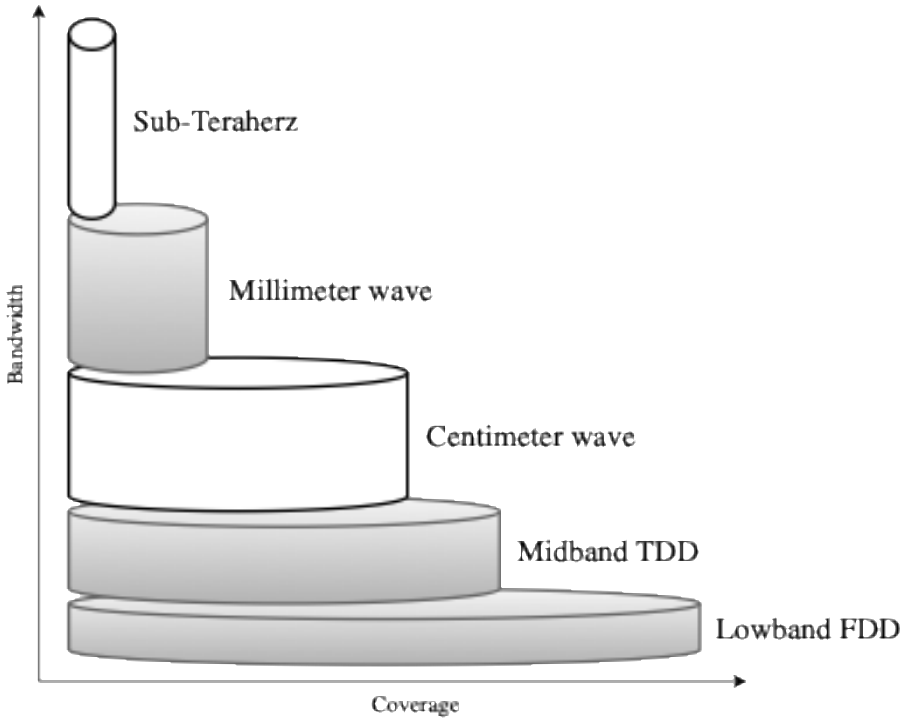

Fig. 8-1: Spectrum Layer Cake Model.

challenges by significant propagation losses and limited reach, necessitating a denser network infrastructure. In light of this, the centimeter-wave band is seen as a promising compromise, providing broader bandwidth than traditional sub-6 GHz bands while offering more favorable propagation characteristics than mmWave frequencies.

Recent industry discussions as well as academic literature, such as Ericsson's blogpost on the cmWave spectrum [2], have highlighted the untapped technical potential of this frequency range. Ericsson's findings articulate that the cmWave band can be integrated into current network infrastructures - particularly those operating around 3.5 GHz – together with massive MIMO technology. This approach facilitates the placement of potentially denser antenna arrays, improving the array gain. For example, 7GHz bands can accommodate nearly four times as many half-wavelength antenna elements within the same physical space as compared to a 3.5 GHz setup. This antenna density effectively mitigates the higher path loss due to higher spectrum, potentially leading to improvements in both spectral efficiency and overall network capacity. Simulation studies conducted in dense urban environments (i.e., London was selected as an example in the study) demonstrates that the strategic incorporation of cmWave spectrum could boost downlink capacity from roughly 5 Gbit/s/km² to over 13 Gbit/s/km² without requiring a complete overhaul of the existing network topology.

Building on industry insights, the paper "6G Takes Shape" presents a comprehensive technical and conceptual view for 6G network development and requirements [3]. Their analysis argues that achieving 6G's ambitious performance objectives such as spanning enhanced data rates, energy efficiency, and cost-effectiveness will require a diverse spectrum strategy. To achieve this goal, the cmWave band stands out as a vital component. It plays a strategic role in the so-called "layer cake" model of spectrum deployment as shown in Fig. 8-1: low-frequency bands secure wider coverage, high-frequency mmWave bands serve for speed in localized hotspots, and intermediate bands (e.g., cmWave) effectively bridge the two counterparts by offering both enhanced coverage and vast bandwidth.

The combined insights from the aforementioned studies lead to convincing reasons why the cmWave spectrum is indispensable for 6G. First, the capacity demands of future networks are expected to grow further by an order of magnitude compared to previous generations. To meet these demands, not only additional spectrum but also deployment strategies that jointly maximize spectral, energy, and cost efficiency are needed. The cmWave band offering wider bandwidths and enhanced spatial manipulation through advanced MIMO technology may provide an effective solution to this challenge. Second, the propagation behavior of cmWave frequencies could serve as the missing piece that bridges the gap between low-speed, wide-coverage sub-6GHz networks and high-speed, short-coverage mmWave networks, thanks to their potential for less susceptibility to the penetration loss, yet for wider bandwidth than the sub-6 GHz bands. Third, the deployment of cmWave spectrum aligns with the other goals of 6G, e.g., integrating additional functionalities like real-time sensing and edge computing. The integration of these services into the cellular network may impose additional challenges that we don't see in the current use cases. The cmWave band is uniquely positioned to meet these requirements thanks to the advantages already mentioned above.

II-8.3. Hybrid MIMO Arrays

Although the prospects are promising, the advantage comes with challenges. For instance, a range of non-cellular applications presently occupies the cmWave spectrum, necessitating advanced strategies for spectrum sharing and coexistence. In addition, the implementation of advanced massive MIMO systems in cmWave bands introduces its own set of technical challenges. Due to elevated frequencies, it needs an increase in the number of antenna elements to overcome the additional path loss, inevitably escalating both hardware complexity and cost. This denser antenna configuration is eager to enhance beamforming techniques and timely accurate channel state information (CSI) acquisition, which become more challenging as the number of transceiver ports scales up. The practical limitations related to mutual coupling between closely spaced antenna

elements and increased overhead over eCPRI further complicate the deployment of massive MIMO solutions.

In summary, 6G represents a shift in how spectrum is utilized. The cmWave band is essential for meeting the demands of data-heavy applications, but unlocking its full potential requires overcoming substantial challenges. In this direction, this paper presents an NR-compliant link-level simulation result comparing fully digital MIMO arrays with beam-sweeping-based hybrid MIMO arrays, showcasing the potential of hybrid MIMO arrays in this promising band.

II-8.4. Experimental Result

This section presents link-level simulation results evaluating the performance of a downlink hybrid beamforming large-array architecture employing beam sweeping and practical channel estimation under 5G New Radio (NR)-compliant setups at 7 GHz. The primary objective is to assess key metrics such as Physical Downlink Shared Channel (PDSCH) throughput with adaptive modulation and coding scheme (MCS) selection, determining whether such systems can serve as a cost-efficient MIMO array architecture in cmWave bands. The results are benchmarked against a fully digital large-array setup with perfect channel state information (CSI), highlighting the potential advantages of the hybrid architecture.

The link-level simulator is based on a cyclic-prefix orthogonal frequency-division multiplexing (CP-OFDM) framework, operating at a carrier frequency of 7 GHz with a subcarrier spacing of 30 kHz and a total bandwidth of 100 MHz, corresponding to 272 physical resource blocks (PRBs). The simulation employs the Clustered Delay Line Model B (CDL-B), as specified in 3GPP TR 38.901, to represent non-line-of-sight (NLoS) propagation conditions. Channel State Information Reference Signals (CSI-RS) are transmitted every 5 slots using a 2-port configuration. Here, the CSI feedback information is used to configure the analog domain beamforming weights, while digital beamforming weights are calculated via SRS-based channel estimation under reciprocity. Key physical layer parameters include a delay spread of 100 ns, an azimuth spread of arrival (ASA) of 45°, an azimuth spread of departure (ASD) of 30°, a zenith spread of arrival (ZSA) of 10°, and a zenith spread of departure (ZSD) of 2°.

The simulation integrates low-density parity-check (LDPC) channel coding with adaptive MCS selection, utilizing a Min-Sum decoding algorithm with 30 iterations. MCS selection is based on NR PDSCH Table 2 256-QAM, and transport block sizes are determined according to 3GPP TS 38.214 version 15.6.0. The user equipment (UE) speed is set to 30 km/h, and the fast Fourier transform (FFT) size is 4096. The base station (BS) employs a dual-polarized planar antenna array with 8 rows and 16 columns per polarization, resulting in a total of 256 antenna elements. The UE is equipped with a

single dual-polarized omnidirectional antenna. In the hybrid array architecture, the number of radio frequency (RF) chains is set to 32.

Fig. 8-2 presents a comparative analysis of the relative PDSCH throughput performance between hybrid large-array and fully digital large-array architectures as a function of SNR. In the figure, the hybrid architecture is represented by black markers, while the fully digital architecture is depicted with white markers. The throughput performances are normalized to the maximum throughput achieved by the fully digital array. As observed, the hybrid architecture demonstrates performance close to that of the fully digital counterpart under the simulated environment with realistic channel modeling. This indicates the potential of employing hybrid array systems in these frequency bands, offering an advantageous performance-cost trade-off.

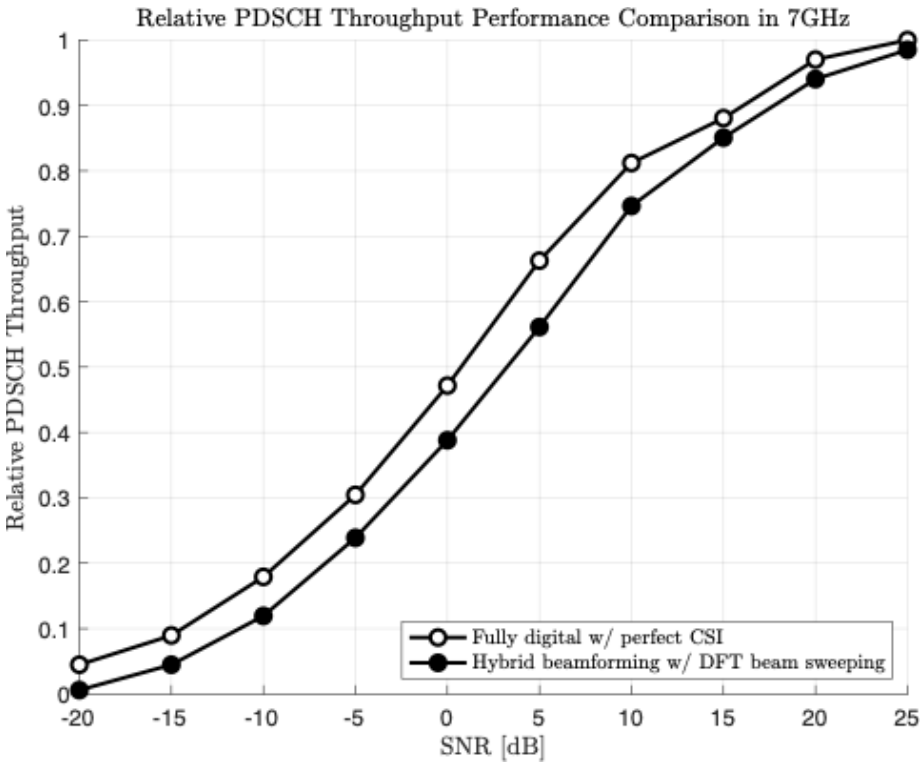

Fig. 8-2 PDSCH Throughput Performance Comparison.

II-8.5. Conclusion

In summary, this article underscores the promise of the cmWave spectrum for advancing next-generation wireless networks. Spanning the 7–15 GHz frequency range, cmWave provides an attractive playground by offering both broader contiguous bandwidth and favorable propagation characteristics. This balance makes it an ideal candidate for meeting the high data rate and connectivity requirements anticipated for 6G applications. Bridging the gap between conventional sub-6 GHz frequencies and

higher-frequency millimeter-wave bands, cmWave can enhance network capacity and extend coverage without overly dense infrastructure deployments. Nevertheless, fully leveraging the benefits of the cmWave spectrum presents its own set of challenges. A pivotal requirement is the adoption of advanced large-array technologies to counteract the inherent increased path loss. This, however, introduces a range of technical obstacles, such as the complexities associated with channel state information (CSI) acquisition, heightened computational demands, and challenges in hardware implementation. Overcoming these hurdles will require collaborative efforts from researchers and engineers across various disciplines, including signal processing and hardware design. As a compromise between performance and efficiency, we have demonstrated through link-level simulations that a hybrid large-array system can perform comparably to a fully digital counterpart in certain reasonable environments. This indicates that hybrid array architectures offer a promising solution for cmWave deployments, balancing the trade-offs between system complexity and performance.

REFERENCE

[1] Ericsson, “Ericsson Mobility Report,” Ericsson AB, Stockholm, Sweden, Nov. 2024. [Online]. Available: https://www.ericsson.com/en/mobility-report.

[2] Stefan Parkvall, Robert Baldemair, Jialu Lun, "CM-wave spectrum: A potent enabler for 6G," Ericsson Blog, June 2023. [Online]. Available: https://www.ericsson.com/en/blog/2023/6/cm-wave-spectrum-6g-potent-enabler

[3] J. G. Andrews, T. E. Humphreys, and T. Ji, "6G Takes Shape," *IEEE BITS the Information Theory Magazine*, pp. 1-38, Nov. 2024, doi: 10.1109/MBITS.2024.3504521.

II-9. User Cluster-centric Approach for Cell-free Massive MIMO Systems

Fumiyuki Adachi
Tohoku University
Ryo Takahashi
Tohoku University and Panasonic System Networks R&D Lab. Co., Ltd.

Abstract— **The user cluster-centric (UCC) approach effectively improves the capacity of cell-free massive MIMO (CF-mMIMO) systems. This approach introduces the spatial multiplexing technique, which involves forming user clusters (or user-centric virtual small cells) consisting of neighboring users. A certain number of omnidirectional distributed antennas are associated with each user cluster to enable cluster-wise spatial multiplexing based on either minimum mean square error (MMSE) or zero-forcing (ZF) criterion. The partial interference suppression multiuser MMSE/ZF (IS-MU-MMSE/ZF) is designed to suppress only the dominant interference from the neighboring user clusters while performing spatial multiplexing of users within each user cluster.**

II-9.1. Introduction

Cell-free massive MIMO (CF-mMIMO), also known as distributed mMIMO, has recently attracted great attention as a key technology for 6G systems [1]. CF-mMIMO is particularly important when the mmWave bands are utilized to ensure sufficient radio bandwidth to provide a variety of new communication services in 6G systems. The mmWave signals have a strong rectilinear propagation nature and thus, can be frequently blocked by buildings and other obstacles between the transmitter and the receiver. CF-mMIMO ensures multiple propagation paths, effectively mitigating the blockage problem and also mitigating the adverse effects of severe multipath fading.

In CF-mMIMO systems, a central processing unit (CPU) provides communication services to users through the cooperative use of a fairly large number of omnidirectional distributed antennas (hereafter simply called antennas) deployed over the communication service area. To ensure system scalability and address the issue of inter-user interference, the user-centric (UC) approach is considered in [2]. In the UC approach, antenna clusters each consisting of a certain number of antennas near each user are formed, and minimum mean square error (MMSE) interference suppression is applied.

However, as the ratio of users to antennas increases, more users cause strong interference, thereby reducing the achievable user capacity. To address this issue, the user cluster-centric (UCC) approach is considered in [3]. This approach utilizes spatial multiplexing based on either MMSE or zero-forcing (ZF) criterion by associating a certain number of antennas with each user cluster, consisting of neighboring users, for performing cluster-wise multiuser spatial multiplexing.

Inspired by the idea of MMSE interference rejection combining (MMSE-IRC) [4], partial interference suppression multiuser MMSE/ZF (hereafter, called partial IS-MU-MMSE/ZF) is designed to suppress only the dominant interference from the neighboring user clusters while performing spatial multiplexing of users within each user cluster.

II-9.2. UCC-based CF-mMIMO

A CF-mMIMO system model is illustrated in Fig. 9-1. A (>>1) antennas are connected with the CPU via an optical mobile fronthaul to provide communication services to $U(\leq A)$ single-antenna users. The UCC and UC approaches are compared with an example in Fig. 9-2. In the UCC approach, a user cluster consists of 3 users, and the minimum required 3 antennas are associated with this user cluster as shown in Fig. 9-2 (a). Any users outside this user cluster are interfering users for this cluster. On the other hand, in the UC approach, each user is an interfering user to other users. An antenna cluster is formed by 2 antennas, located close to each user. This is shown in Fig. 9-2 (b).

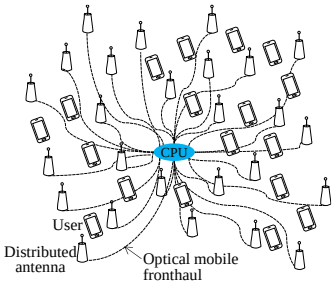

Fig. 9-1 CF-mMIMO system model.

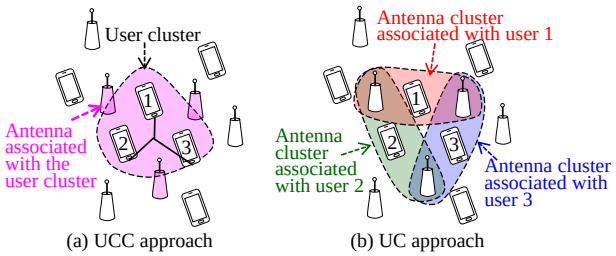

Fig. 9-2 Comparison of UCC and UC approaches.

The UCC approach takes two steps: user clustering and antenna association [3]. User clustering is done by using a constrained K-means algorithm [5],[6]. U users in the communication area are grouped into $K(=U/U')$ user clusters, each consisting of neighboring users, where U' denotes the number of users in each user cluster and is determined based on the computing power of the CPU. Here, for simplicity, $U$is assumed to be an integer multiple of U'. Let $\mathrm{S}_k \subset \{1,\ldots,u,\ldots,U\}$ denote a subset of users ($|\mathrm{S}_k|=U'$) belonging to user-cluster k. Since user clusters do not overlap, $\mathrm{S}_k \bigcap \mathrm{S}_i = \varnothing$.

In antenna association, a certain number A' ($U' \leq A' \leq A$) of antennas are associated with each user cluster to perform cluster-wise spatial multiplexing. Antenna association is based on the maximum pathloss criterion, and the same antenna is allowed to be shared by different user clusters. Let $\mathrm{M}_k \subset \{1,\ldots,a,\ldots,A\}$ with $|\mathrm{M}_k| = A'$

represents the subset of antennas belonging to user cluster k. For detailed user clustering and antenna association procedures, refer to [3].

The uplink transmission model for UCC-based CF-mMIMO is illustrated in Fig. 9-3. The transmitted signal from user $u(=1,\ldots,U)$ belonging to user cluster $k(=1,\ldots,K)$ is received by A' antennas belonging to user cluster k, and they are then weighted and combined. The baseband equivalent received signal y_u after weighted combining is represented as

$$y_u = \mathbf{w}_u^H \mathbf{D}_k \mathbf{h}_u s_u + \sum_{v=1, v\neq u}^{U} \mathbf{w}_u^H \mathbf{D}_k \mathbf{h}_v s_v + \mathbf{w}_u^H \mathbf{D}_k \mathbf{n}, \quad \text{Eq. (9-1)}$$

where $\mathbf{w}_u$ is the partial IS-MU-MMSE/ZF multiplexing weight vector of size $A\times 1$, $(.)^H$ represents the conjugate transpose operation, $\mathbf{D}_k = \mathrm{diag}(d_1,\ldots,d_a,\ldots,d_A)$ with $d_a = 1(0)$ if $a \in \mathrm{M}_k$ (otherwise) is the antenna association matrix for user cluster k, and $h_{u(or\ v)} = \left[h_{u(or\ v)1}\ldots h_{u(or\ v)a}\ldots h_{u(or\ v)A}\right]^T$ is the propagation channel vector with $(.)^T$ representing the transpose operation and $h_{u(\mathrm{or}\ v)a}$ being the propagation channel gain between user u (or v) and antenna a.

$s_{u(\mathrm{or}\ v)}$ is the baseband equivalent transmit signal with the transmit power $p_{u(\mathrm{or}\ v)}$. $\mathbf{n}$ is the additive noise vector of size $A\times 1$ with each element being an independent zero-mean complex Gaussian variable having variance $2\sigma^2$.

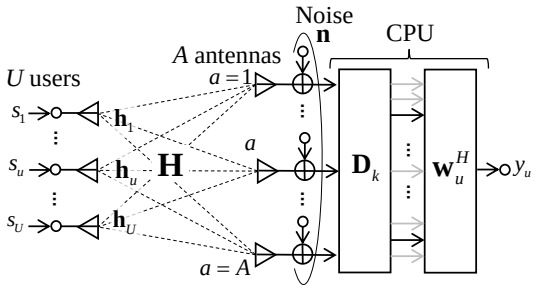

Fig. 9-3 Uplink transmission model for user u belonging to user cluster k.

The partial IS-MU-MMSE/ZF weight vector $\mathbf{w}_u$ for uplink transmission is expressed as

$$\mathbf{w}_u = \begin{cases} p_u \left(\sum_{v\in \mathrm{P}_k} p_v \mathbf{D}_k \mathbf{h}_v \mathbf{h}_v^{\mathrm{H}} \mathbf{D}_k + \mathrm{diag}\left(\sum_{v\in \mathrm{P}_k} p_v \mathbf{D}_k \left[\mathrm{E}\left\{|h_{v1}|^2\right\} \ldots \mathrm{E}\left\{|h_{va}|^2\right\} \ldots \mathrm{E}\left\{|h_{vA}|^2\right\} \right]^{\mathrm{T}} \right) + \sigma^2 \mathbf{D}_k \right)^{\dagger} \mathbf{D}_k \mathbf{h}_u & \text{for MMSE} \\ p_u \left(\sum_{v\in \mathrm{P}_k} p_v \mathbf{D}_k \mathbf{h}_v \mathbf{h}_v^{\mathrm{H}} \mathbf{D}_k \right)^{\dagger} \mathbf{D}_k \mathbf{h}_u & \text{for ZF} \end{cases}, \quad \text{Eq. (9-2)}$$

where P_k represents a set of users of user cluster k to which user u belongs plus dominant interfering users in neighboring user clusters, $\overline{\mathrm{P}}_k$ represents a set of users except P_k, and $\mathrm{E}\{.\}$ and $(.)^\dagger$ represent the expectation operation and the pseudo-inverse operation to address the rank deficiency case. The interference power from user $v \in \overline{\mathrm{P}}_k$ is treated as an equivalent zero-mean noise having the variance $p_v D_k \left[\mathrm{E}\left\{|h_{v1}|^2\right\} \ldots \mathrm{E}\left\{|h_{va}|^2\right\} \ldots \mathrm{E}\left\{|h_{vA}|^2\right\} \right]^T$ with $\mathrm{E}\left\{|h_{va}|^2\right\}$ being the short-term averaged (i.e., averaged over fading) propagation channel gain between user v and antenna a. Note that the weight vector for downlink transmission is given by $\mathbf{w}_u$ when assuming time-division duplex transmission. Also note that when $U' = 1$, the MMSE weight vector representation in Eq. (9-2) becomes equivalent to the weight vector of the UC approach [2].

While the partial IS-MU-ZF is simpler than the partial IS-MU-MMSE because the noise power estimation is not required, the achievable user capacity significantly degrades when the number of considered interfering users becomes equal to or close to the antenna degree of freedom minus the number of multiplexing users in each user cluster. To solve this problem, adaptive partial IS-MU-ZF employing adaptive selection of dominant interfering users is developed in [8]. As a result, note that P_k for ZF is not necessarily the same as for MMSE.

Below the computational complexity of obtaining the weight vector is discussed. The inverse matrix operation of the channel covariance matrix has a significant impact on the computational complexity and the order of computational complexity is $O(A'^3)$ [7]. In the UCC approach, the pseudo-inverse matrix in Eq. (9-2) for the UCC approach is shared by all users in each user cluster. Therefore, if the total computational complexity required for obtaining the inverse matrix for the UCC approach is made equal to the UC approach, the number A'_{UCC} of antennas associated with each user cluster for the UCC approach can be increased to

$$A'_{\mathrm{UCC}} = \left\lfloor \sqrt[3]{U'_{\mathrm{UCC}}} A'_{\mathrm{UC}} \right\rfloor, \qquad \text{Eq. (9-3)}$$

where A'_{UC} is the number of antennas in each user cluster for the UC approach, while U'_{UCC} is the number of users in each user cluster for the UCC approach. Compared to the UC approach, the UCC approach can increase the number of antennas associated with each user cluster. Accordingly, it is made possible to generate the nulls toward more interfering users. This is an advantage of the UCC approach.

II-9.3. Capacity Evaluation

To confirm the effectiveness of the UCC approach, we evaluate by computer simulation the uplink user capacities achievable with UC and UCC approaches. Here, partial IS-MU-MMSE is considered both for UC and UCC approaches. Also compared is the computational complexity, which is the total number of complex multiplications required for the weight computation for all U users. For the detailed simulation procedure, refer to [3]. A antennas and U users are randomly placed in a 1×1 normalized communication area, where A=512 and $U=\{8,16,32,64,128,256,512\}$.

In the UCC approach, the size of user cluster is set to $U'_{UCC}=8$ and a total of K=U/8 user clusters are formed. The number of antennas associated with each user cluster is set to $A'_{UCC}=16$. In the UC approach ($U'_{UC}=1$), the size of antenna cluster is set to $A'_{UC}=8$ according to Eq. (9-3).

The user transmit power (same for all U users) is represented by the normalized transmit signal-to-noise ratio (SNR) Γ_t. This is the received SNR when the transmitter-receiver distance is equal to a normalized distance of 1. In the simulation, Γ_t is set to $\{-60,-50,-40,-30\}$ dB, which provides the received SNR of about 58dB higher, i.e., {–2, 8, 18, 28} dB when the transmitter-receiver distance is equal to half the average distance between two neighboring antennas.

The propagation channel is assumed to be characterized by distance-dependent pathloss with pathloss exponent of 3.5, log-normally distributed shadowing loss with standard deviation of 8 dB, and Rayleigh fading. Assuming perfect knowledge of the propagation channel, the partial IS-MU-MMSE weight is obtained using Eq. (9-2).

The uplink user capacity C_u [bps/Hz] of user $u(=1,\ldots,U)$ is calculated using the capacity formula $C_u=\log_2(1+\Lambda_u)$ for a set of user locations of all U users, where Λ_u

represents the received signal-to-interference plus noise ratio of user u and can be derived from Eq. (1). The cumulative distribution function (CDF) of the user capacity is evaluated by randomly changing a set of user locations.

Fig. 9-4 compares UC and UCC approaches in terms of the user capacity at CDF=50%. The UCC approach provides higher capacity when Γ_t = -30 dB and -40 dB (i.e., relatively high transmit power, sufficient to allow for the cooperation of neighboring antennas for spatial multiplexing). However, when Γ_t = -50 dB and -60 dB, the UCC approach provides slightly lower capacity. This is because such low transmit power makes antenna cooperation difficult for spatial multiplexing. But, even when Γ_t is set to -50 dB and -60 dB, the UCC approach provides slightly higher capacity when U gets larger.

The relationship between the user capacity and the computational complexity is shown in Fig. 9-5 with A' as a parameter when U=512 and Γ_t = -30 dB. The computational complexity assuming the LDL^H decomposition for the inverse matrix operation [7] is shown in Table 9-1. The UCC approach provides higher user capacity than the UC approach at any level of computational complexity.

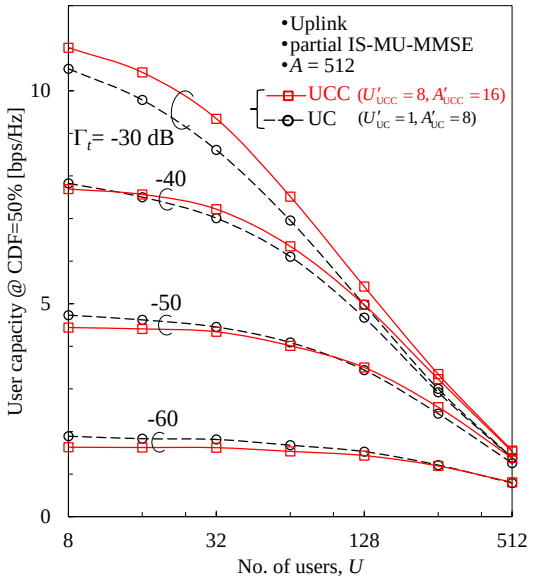

Fig. 9-4 User capacity comparison.

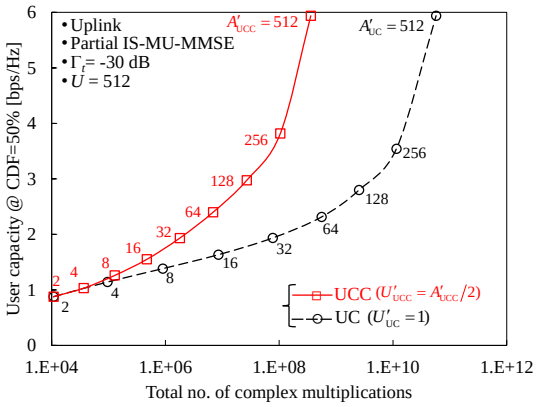

Fig. 9-5 Capacity versus complexity.

Table 9-1. Computational complexity.

Approach	No. of user clusters	The total no. of complex multiplications required for weight computation for all users
UC	$K=\frac{U}{U'_{\mathrm{UC}}}=U$	$\left(\frac{A'^{2}_{\mathrm{UC}}+A'_{\mathrm{UC}}}{2}\left(\frac{1}{K}\sum_{k=1}^{K}\lvert \mathrm{P}_k\rvert\right)+\frac{A'^{3}_{\mathrm{UC}}-A'_{\mathrm{UC}}}{3}+A'^{2}_{\mathrm{UC}}\right)K$
UCC	$K=\frac{U}{U'_{\mathrm{UCC}}}$	$\left(\frac{A'^{2}_{\mathrm{UCC}}+A'_{\mathrm{UCC}}}{2}\left(\frac{1}{K}\sum_{k=1}^{K}\lvert \mathrm{P}_k\rvert\right)+\frac{A'^{3}_{\mathrm{UCC}}-A'_{\mathrm{UCC}}}{3}+A'^{2}_{\mathrm{UCC}}U'_{\mathrm{UCC}}\right)K$

So far, the perfect channel information is assumed to compute the partial IS-MU-MMSE/ZF weight vector $\mathbf{w}_u$ of Eq. (9-2). The channel information is estimated by transmitting the orthogonal pilots from different antennas. When using a limited number of orthogonal pilots, the channel estimation quality degrades due to the so-called pilot contamination. If a sufficiently large number of orthogonal pilots is used, the pilot contamination can be avoided, but it costs significant overhead. A graph coloring algorithm-based pilot assignment method is developed in [8] to mitigate pilot contamination while utilizing a relatively small number of orthogonal pilots. In this pilot assignment method, the available orthogonal pilots are divided into different exclusive pilot groups. The relationship among user clusters is represented by an undirected graph consisting of vertices (user cluster centroids) and edges (the relationship between two user clusters sharing the same antenna). Then, different pilot groups (colors) are assigned to the neighboring user clusters (connected vertices) for channel estimation. The well-known least-square estimation is employed.

An example of graph coloring algorithm-based pilot assignment is shown in Fig. 9-6, where 32 clusters of 8 users and 16 antennas are represented as colored vertices at their centroids' locations. 32 orthogonal pilots are used, and they are grouped into 4 pilot groups, each consisting of 8 pilots. In Fig. 9-7, partial IS-MU-MMSE and adaptive partial IS-MU-ZF (with adaptive selection of dominant interfering users [8]) in the UCC-based CF-mMIMO system are compared in terms of user capacity at CDF=50% for the cases of perfect and estimated channel information. The user capacity with estimated channel information decreases compared to that with perfect one, but the capacity degradation is marginal. Note that partial IS-MU-ZF (without adaptive selection of dominant interfering) is significantly degraded compared to the adaptive one when the user density is relatively low (U/A <1/4).

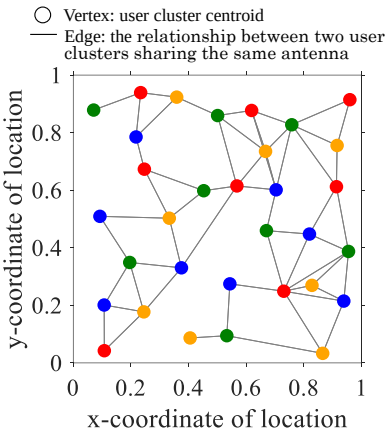

Fig. 9-6 Pilot assignment result.

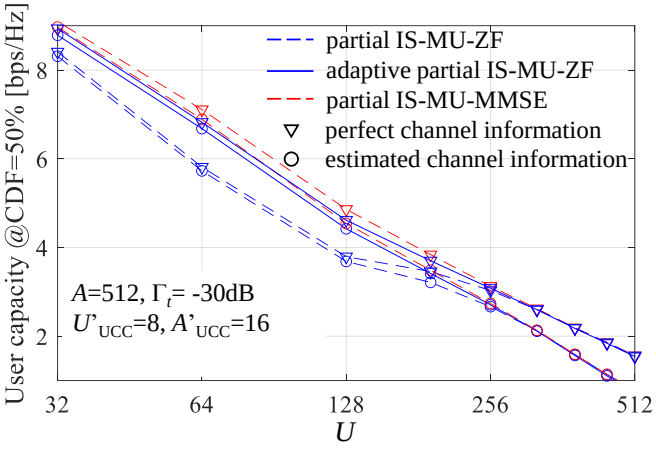

Fig. 9-7 Impact of channel estimation error.

II-9.4. Conclusion

The UCC approach utilizing partial IS-MU-MMSE/ZF with interference suppression capability enhances CF-mMIMO systems. It should be noted that the communication area size of the CF-mMIMO system is relatively small due to the limited computing power of the CPU. It is well-known that the cellular system is the most practical approach to accommodate a large number of users over a wide communication area and that by reducing the cell size (the coverage area size of each base station), the spectrum utilization efficiency can be improved. However, a straightforward significant reduction in cell size may not be realistic because the control data traffic related to hand-off, etc. increases significantly. The following cellular architecture combined with UCC-based CF-mMIMO could be a realistic solution [9]. Instead of reducing the cell size further than a macro-cell with a radius of several 100 meters, UCC-based CF-mMIMO is employed to form user clusters as user-centric virtual small cells within each CPU-controlled macro-cell. The size of the macro-cell can be determined by considering the computing power of each CPU (equivalent to the base station of cellular systems).

Acknowledgements

A part of this work was conducted under “R&D for further advancement of the 5th generation mobile communication system” (JPJ000254) commissioned by the Ministry of Internal Affairs and Communications in Japan.

REFERENCE

[1] I. Kanno, K. Yamazaki, Y. Kishi, and S. Konishi, “A Survey on Research Activities for Deploying Cell Free Massive MIMO towards Beyond 5G,” IEICE Trans. Commun., Vol. E105-B, No.10, pp. 1107-1116, Oct. 2022.

[2] E. Björnson and L. Sanguinetti, “Scalable Cell-Free Massive MIMO Systems,” IEEE Trans. Commun., Vol. 68, Issue 7, pp. 4247 – 4261, July 2020.
[3] R. Takahashi, H. Matsuo, S. Xia, Q. Chen, and F. Adachi, “Uplink Postcoding in User cluster-Centric Cell-Free massive MIMO,” IEICE Trans. Commun., Vol. E106-B, No. 9, pp. 784-757, Sep. 2023.
[4] Y. Huang, W. Lei, C. Lu, and M. Berg, “Fronthaul Functional Split of IRC-Based Beamforming for Massive MIMO Systems,” Proc. IEEE VTC2019-Fall, Honolulu, Hawaii, USA, 22–25 Sep. 2019.
[5] P. Bradley, K. Bennett, and A. Demiriz, “Constrained K-means clustering”, Microsoft Research Technical Report, May 2000.
[6] S. Xia, C. Ge, Q. Chen, and F. Adachi, “Cellular Structuring and Clustering for Distributed Antenna Systems,” Proc. WPMC2021, Okayama, Japan, 14-16 Dec. 2021.
[7] E. Björnson, J. Hoydis, and L. Sanguinetti, “Massive MIMO Networks: Spectral, Energy, and Hardware Efficiency,” Foundations and Trends in Signal Processing: Vol. 11, No. 3-4, pp. 154-655, 2017.
[8] S. Xia, C. Ge, R. Takahashi, Q. Chen, and F. Adachi, “Adaptive Interference Suppressing Multi-User ZF in Cluster-Centric Cell-Free Massive MIMO Systems,” IEEE Communications Letters, Vol. 28, No. 6, pp. 1422-1426, June 2024.
[9] F. Adachi, R. Takahashi, H. Matsuo, S. Xia, C. Ge, and Q. Chen, “On Design Concept of Cellular Distributed MU-MIMO for Ultra-dense RAN,” Proc. IEEE APCC2022, Jeju Island, Korea, 19-21 Oct. 2022.

II-10. Low-Complexity User-Centric TRP Clustering Method in Downlink Cell-Free MIMO with Regularized ZF-Based Beamforming

Kenichi Higuchi, Hiroki Kato, Takanori Hara
Tokyo University of Science
Satoshi Suyama and Satoshi Nagata
NTT DOCOMO, INC.

Abstract—This article investigates a computationally-efficient method for user equipment (UE)-centric transmission reception point (TRP) clustering in downlink cell-free multi-input multi-output (MIMO) using regularized zero-forcing (RZF)-based beamforming (BF). The proposed method selects a set of TRPs used for data transmission for each UE (user-centric TRP cluster) based only on the average path gain information between UEs and TRPs. Thus, no complex calculations for a downlink BF matrix are needed for TRP clustering. Since the proposed method takes into account the BF gain and spatial interference levels for the RZF-based BF, the achievable system-level throughput can be enhanced compared to that for conventional path loss-based TRP clustering. This is achieved by utilizing the average path gain information of the target and neighboring UEs. Computer simulation results assuming a realistic partial channel state information scenario show the effectiveness of the proposed method compared to conventional methods.

II-10.1. Introduction

In downlink cell-free or distributed multi-input multi-output (MIMO) [1, 2], the selection of transmission reception points (TRPs) for data transmission to each user equipment (UE), which is referred to as user-centric TRP clustering hereafter, significantly impacts the achievable system throughput. This paper investigates a computationally-efficient user-centric TRP clustering method.

User-centric TRP clustering can be categorized into two approaches. The first approach utilizes only the average path gain (or path loss) in the TRP clustering. References [1] and [3] investigated clustering methods that determine a set of TRPs in order of the highest average path gain between the target UE and each TRP. These methods achieve TRP clustering with low computational complexity since there is no need for complex calculations for a beam forming (BF) matrix. However, since the received signal and interference power levels after BF are not sufficiently considered during the TRP clustering, the achievable system-level throughput performance is not significant.

The second approach utilizes the instantaneous channel state information (CSI) in TRP clustering [4, 5]. Reference [4] investigated a TRP clustering method that maximizes the instantaneous channel gain of the target UE. This method is simple but

the received signal and interference power levels after BF were not sufficiently considered. Reference [5] investigated a TRP clustering method based on the received signal power after BF and interference to other UEs, which is referred to as the signal-to-leakage-and-noise ratio (SLNR)-based method hereafter. Since the SLNR-based method considers the BF gain during the TRP clustering, its achievable throughput performance is high. However, this method suffers from a significantly high level of computational complexity due to the complex BF matrix computations, such as channel matrix inversion. In addition, in a realistic scenario where the time interval for TRP clustering is longer than the coherence time of the wireless channel, the advantage of employing TRP clustering based on instantaneous CSI may be restricted due to the instantaneous fading variation during the TRP clustering interval.

We propose a low-complexity user-centric TRP clustering method for regularized zero-forcing (RZF)-based BF [3, 6]. The proposed method selects the TRP cluster for each UE based only on the average path gain information without the need for complex calculations for the downlink BF matrix. Since the proposed method takes into account the BF gain and spatial interference levels for the RZF-based BF, the achievable system-level throughput can be enhanced compared to that for conventional path loss-based TRP clustering. This is achieved by utilizing the average path gain information of the target UE and its neighboring UEs. Computer simulation results assuming a realistic partial CSI scenario show the effectiveness of the proposed method compared to conventional methods.

II-10.2. Proposed TRP Clustering Method

We consider downlink cell-free MIMO, where a set of TRPs, $\mathcal{L}$, and a set of users, $\mathcal{K}$, are distributed over the system coverage of interest. Each TRP and UE are equipped with a single antenna. All TRPs are assumed to be connected to a central processing unit (CPU), which allows joint data transmission using an arbitrary set of TRPs for each UE. For simplicity, we assume flat instantaneous fading in this paper. Let $h_{k,l}$ be the instantaneous CSI between UE $k \in \mathcal{K}$ and TRP $l \in \mathcal{L}$, where $h_{k,l} \sim CN(0, g_{k,l})$ and $g_{k,l}$ denotes the average path gain determined by the distance-dependent loss and random shadowing effect. The set of candidate TRPs for UE k clustering is denoted as $\mathcal{L}_k \subseteq \mathcal{L}$. We assume that $|\mathcal{L}_k|$ is fixed to L_{cand} for all UEs and $\mathcal{L}_k$ comprises TRPs with the L_{cand} highest average path gain between it and UE k. In this paper, a part of instantaneous CSI $h_{k,l}$ is assumed to be estimated and known at TRPs based on the uplink reference signal in a time division duplex (TDD) system. Let $S_k \subseteq \mathcal{L}_k$ be the set of TRPs that know the instantaneous CSI of UE k. Based on [3] and [5], we define S_k as the set of TRPs whose average path gain to UE k is higher than $g_{k,\max} - \Delta_{\text{CSI}}$ in decibels (dB), namely $S_k = \{l \mid g_{k,l} \geq g_{k,\max} - \Delta_{\text{CSI}}, l \in \mathcal{L}\}$, where $g_{k,\max}$ is the maximum average path gain between UE k and all TRPs, and Δ_{CSI} is a parameter that determines the range of instantaneous CSI acquisition.

We assume RZF-based BF [3, 6] in this paper. Let $\mathcal{T}_k \subseteq \mathcal{L}_k$ be the TRP cluster for UE k. The $|\mathcal{T}_k|$-dimensional channel vector of UE k, $\mathbf{h}_k(\mathcal{T}_k)$, is represented as

$$\mathbf{h}_k(\mathcal{T}_k) = [h_{k,[\mathcal{T}_k]_1} \quad h_{k,[\mathcal{T}_k]_2} \quad \cdots \quad h_{k,[\mathcal{T}_k]_{|\mathcal{T}_k|}}]^T, \qquad \text{Eq. (10-1).}$$

where $[\mathcal{T}_k]_l$ represents the l-th element of $\mathcal{T}_k$. Due to the partial CSI condition, $\mathbf{h}_k(\mathcal{T}_k)$ may contain unknown elements. We use the channel matrix muting method in [5] to determine the BF vector with partial CSI. The muting operation generates muted channel vector $\tilde{\mathbf{h}}_k(\mathcal{T}_k)$ by setting the l-th element of $\mathbf{h}_k(\mathcal{T}_k)$, $h_{k,[\mathcal{T}_k]_l}$, to zero if it is not known at the TRP.

Let $\mathcal{U}_k(\mathcal{T}_k)$ be the set of UEs other than UE k for which the instantaneous CSI to TRP set $\mathcal{T}_k$ is at least partially known. Thus, $\mathcal{U}_k(\mathcal{T}_k) = \{j \mid S_j \cap S_k \neq \varnothing, j \neq k \in \mathcal{K}\}$. The muted channel vector between set of TRPs $\mathcal{T}_k$ and UE $j \in \mathcal{U}_k(\mathcal{T}_k)$ is denoted by $\tilde{\mathbf{h}}_j(\mathcal{T}_k)$. Let $\tilde{\mathbf{H}}_k(\mathcal{T}_k)$ be the muted channel matrix with $\tilde{\mathbf{h}}_k^T(\mathcal{T}_k)$ and $\{\tilde{\mathbf{h}}_j^T(\mathcal{T}_k)\}$ aligned in the row direction. According to the principle of RZF [6], the BF vector to UE k can be obtained from the following matrix.

$$\mathbf{M}_k^{\mathrm{RZF}}(\mathcal{T}_k) = \tilde{\mathbf{H}}_k^H(\mathcal{T}_k)\left(\tilde{\mathbf{H}}_k(\mathcal{T}_k)\tilde{\mathbf{H}}_k^H(\mathcal{T}_k) + \xi\frac{N_0}{p_k}\mathbf{I}\right)^{-1}, \qquad \text{Eq. (10-2).}$$

where p_k and N_0 are the transmission signal power allocated to UE k and the noise power, respectively. Term $\xi N_0 / p_k \mathbf{I}$ is the regularization term and ξ is a nonnegative parameter that adjusts the magnitude of the regularization term. We note that ξ includes the effect of path loss. When $\tilde{\mathbf{h}}_k^T(\mathcal{T}_k)$ is placed in the first row of $\tilde{\mathbf{H}}_k(\mathcal{T}_k)$, the BF vector to UE k corresponds to the first column vector of $\mathbf{M}_k^{\mathrm{RZF}}(\mathcal{T}_k)$ after its norm is normalized to one.

When ξ is set to zero, RZF is equivalent to pure zero-forcing (ZF), which minimizes the interference power. When ξ is set sufficiently large, RZF is equivalent to maximum ratio transmission (MRT), which maximizes the received signal power. The performance of RZF is between pure ZF and MRT. By selecting an appropriate ξ value for a given channel, RZF can achieve performance close to that for the minimum mean squared error (MMSE)-based BF.

We propose a computationally-efficient TRP clustering metric suitable for RZF. The proposed metric comprises a weighted sum of two metrics suitable for pure ZF and MRT. These metrics are defined as the ratio of the achievable BF gain of UE k to the spatial interference levels (leakage power) imparted to other UEs in the neighborhood when applying pure ZF and MRC-based BF.

First, we derive a metric for pure ZF, which corresponds to RZF with ξ of zero. Pure ZF based on the Moore-Penrose generalized inverse of the channel matrix can be recognized as a concatenation of ZF and MRC of the effective channels after ZF. Thus, effective channel f_k after BF of UE k assuming the candidate TRP cluster, $\mathcal{T}$, is represented as

$$f_k = \sqrt{\sum_{i=1}^{|\mathcal{T}|-|\mathcal{U}_k(\mathcal{T})|} |\tilde{\mathbf{h}}_k^T(\mathcal{T})\mathbf{z}_k^i|^2} = \sqrt{\sum_{i=1}^{|\mathcal{T}|-|\mathcal{U}_k(\mathcal{T})|} \left|\sum_{l\in\mathcal{T}} z_{k,l}^i \tilde{h}_{k,l}\right|^2}, \quad \text{Eq. (10-3).}$$

where $\tilde{h}_{k,l}$ is the l-th element of $\tilde{\mathbf{h}}_k(\mathcal{T})$, $\mathbf{z}_k^i$ is the i-th normalized ZF vector that is orthogonal to all channel vectors of other UE $i \in \mathcal{U}_k(\mathcal{T})$, and $z_{k,l}^i$ is the l-th element of $\mathbf{z}_k^i$. The received signal power of UE k becomes

$$|f_k|^2 p_k = \sum_{i=1}^{|\mathcal{T}|-|\mathcal{U}_k(\mathcal{T})|} \left|\sum_{l\in\mathcal{T}} z_{k,l}^i \tilde{h}_{k,l}\right|^2 p_k . \quad \text{Eq. (10-4).}$$

The exact computation of Eq. (10-4) requires the calculation of the BF matrix. The proposed method applies the expectation operation to the received signal power to avoid complex calculation of the BF matrix ($\mathbf{z}_k^i$) during the metric calculation for TRP clustering, which is given by

$$\mathrm{E}[|f_k|^2 p_k] = \sum_{i=1}^{|\mathcal{T}|-|\mathcal{U}_k(\mathcal{T})|} \sum_{l\in\mathcal{T}} \mathrm{E}\left[\left|z_{k,l}^i\right|^2 \left|\tilde{h}_{k,l}\right|^2\right] p_k = \left\{\left(|\mathcal{T}| - |\mathcal{U}_k(\mathcal{T})|\right)/|\mathcal{T}|\right\} \sum_{l\in\mathcal{T}} g_{k,l} p_k . \quad \text{Eq. (10-5)}$$

The sum of the estimated interference power to other UE $j \in \mathcal{U}_k(\mathcal{L}_k)$ and the expected noise power are calculated as

$$\frac{1}{|\mathcal{U}_k(\mathcal{L}_k)|} \sum_{j\in\mathcal{U}_k(\mathcal{L}_k)} \sum_{l\in\mathcal{T}\setminus S_j} g_{j,l} \left(g_{k,l} \Big/ \sum_{l\in\mathcal{T}} g_{k,l}\right) p_k + \alpha N_0 . \quad \text{Eq. (10-6)}$$

The second term in Eq. (10-6) is the product of noise power N_0 and positive coefficient parameter α. It reflects the noise power and the interference from other TRP clusters. The proposed TRP clustering metric, $\lambda_k^{\text{Prop.ZF}}(\mathcal{T})$, of UE k for candidate TRP cluster $\mathcal{T}$ assuming pure ZF-based BF is obtained as

$$\lambda_k^{\text{Prop.ZF}}(\mathcal{T}) = \frac{\left\{\left(|\mathcal{T}| - |\mathcal{U}_k(\mathcal{T})|\right)/|\mathcal{T}|\right\} \sum_{l\in\mathcal{T}} g_{k,l} p_k}{\frac{1}{|\mathcal{U}_k(\mathcal{L}_k)|} \sum_{j\in\mathcal{U}_k(\mathcal{L}_k)} \sum_{l\in\mathcal{T}\setminus S_j} g_{j,l} \left(g_{k,l} \Big/ \sum_{l\in\mathcal{T}} g_{k,l}\right) p_k + \alpha N_0} . \quad \text{Eq. (10-7)}$$

Based on the same idea as in the derivation of $\lambda_k^{\text{Prop.ZF}}(\mathcal{T})$, the metric for MRT-based BF, $\lambda_k^{\text{Prop.MRT}}(\mathcal{T})$, which corresponds to RZF with sufficiently large ξ, is obtained. The proposed metric, $\lambda_k^{\text{Prop.MRT}}(\mathcal{T})$, of UE k for candidate TRP cluster $\mathcal{T}$ assuming MRT-based BF is represented as

$$\lambda_k^{\text{Prop.MRT}}(\mathcal{T}) = \frac{\sum_{l\in\mathcal{T}} g_{k,l} p_k}{\frac{1}{|\mathcal{U}_k(\mathcal{L}_k)|} \sum_{j\in\mathcal{U}_k(\mathcal{L}_k)} \sum_{l\in\mathcal{T}} g_{j,l} \left(g_{k,l} \Big/ \sum_{l\in\mathcal{T}} g_{k,l}\right) p_k + \alpha N_0} . \quad \text{Eq. (10-8)}$$

Finally, by taking the weighted sum of two metrics, $\lambda_k^{\text{Prop.ZF}}(\mathcal{T})$ and $\lambda_k^{\text{Prop.MRT}}(\mathcal{T})$, proposed metric $\lambda_k^{\text{Prop.}}(\mathcal{T})$ of UE k for candidate TRP cluster $\mathcal{T}$ for RZF-based BF is obtained as

$$\lambda_k^{\text{Prop.}}(\mathcal{T}) = \beta \lambda_k^{\text{Prop.ZF}}(\mathcal{T}) + (1-\beta) \lambda_k^{\text{Prop.MRT}}(\mathcal{T}) , \quad \text{Eq. (10-9)}$$

where β is a weight coefficient that ranges from zero to one. UE k selects its clustered TRPs that maximize $\lambda_k^{\text{Prop.}}(\mathcal{T})$.

II-10.3. Numerical Results

The user throughput of the proposed method is evaluated by computer simulation and compared to that for the conventional methods. TRPs and UEs are randomly placed in a wraparound 5 × 5-square kilometer (km^2) system coverage area according to the Poisson point process. The density of TRPs, L, of 25 and 50 per km^2 are tested. The UE density is set to 10 per km^2. The system bandwidth is 100 MHz, and the transmission signal power per UE is set to 30 dBm. The distance-dependent path loss with the decay factor of 3.76, random log-normal shadowing with a standard deviation of 8 dB, and instantaneous Rayleigh fading are simulated as the propagation channel model. The noise power density at the UE is set to −165 dBm/Hz. Term Δ_{CSI} is set to 10 dB in the partial CSI model. In addition to the proposed method with parameter β, the path loss-based method [1, 3] and SLNR-based method [5] are evaluated as conventional methods for comparison. Parameter α included in the metrics of the proposed and SLNR-based methods is set to 10^4. Term L_{cand} is set to 15 for all TRP clustering methods. Throughput is calculated based on Shannon's capacity formula. We tested two scenarios in terms of the time interval of the TRP clustering. The first scenario is referred to as fast TRP clustering, which has an interval within a coherent interval of the channel fading. The second scenario is referred to as slow TRP clustering, which has an interval that is much longer than the channel coherence time interval.

Figs. 10-1(a) and 10-1(b) show the cumulative probability of the user throughput when pure ZF (RZF with ξ of zero) is applied to the fast and slow TRP clustering scenarios, respectively. In the path loss-based method, the maximum number of TRPs in a cluster, denoted as U, is set to 5 and 7 for L of 25 and 50, respectively. Fig. 10-1(a) shows that the path loss-based method is significantly degraded at a low cumulative probability compared to the other methods. This is mainly due to the fact that the path loss-based method does not consider the degrees of freedom of the MIMO channel and the received signal power after BF. The proposed method achieves throughput close to that of the SLNR-based method while avoiding complex calculation of the BF matrix for TRP clustering. This is because the proposed method performs TRP clustering based on the estimated power gain at BF considering the degrees of freedom of the MIMO channel and the interference to other UEs in the neighborhood. Fig. 10-1(b) shows that the proposed method outperforms the two conventional methods in the slow TRP clustering scenario. In the SLNR-based method, which is based on the instantaneous channel condition, the optimal TRP clustering changes with instantaneous channel fading. Hence, the SLNR-based method tends to be degraded by the instantaneous fading variation after TRP clustering in the slow TRP clustering scenario. Since the proposed method is

based on the average channel conditions, the proposed method is particularly effective in a realistic slow TRP clustering scenario.

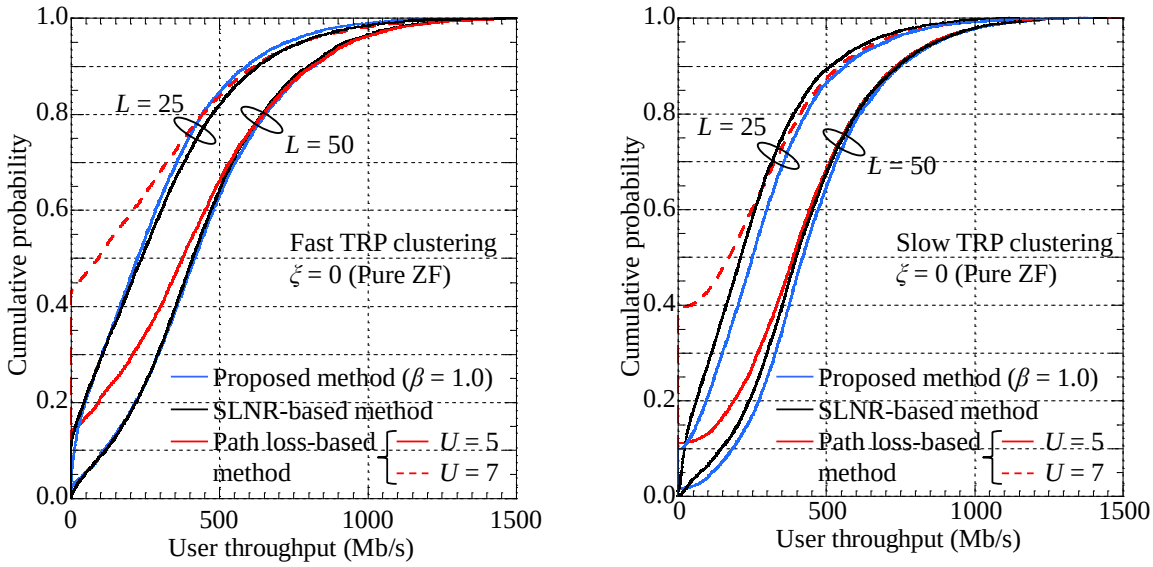

(a) Fast TRP clustering. (b) Slow TRP clustering.

Fig. 10-1 User throughput distribution at ZF-based BF.

Figs. 10-2(a) and 10-2(b) show the average and 5%-outage user throughput as a function of ξ, respectively. The slow TRP clustering scenario is assumed. The proposed method and conventional path loss-based method are compared. For each TRP clustering method, the average number of TRPs used per UE, N_{TRP}, is fixed at four by adjusting the maximum number of TRPs in the cluster. In the proposed method, β of 0.5, 1.0, and 0.0 are tested. Fig. 10-2(a) shows that the proposed method outperforms the path loss-based method regardless of ξ and L. The β value achieving the highest throughput varies depending on ξ. For instance, at ξ of 10^3 where the effect of RZF is greatest under the assumed channel conditions, the proposed method with β = 0.5 achieves the highest performance. Fig. 10-2(b) shows that the proposed method with β = 0.5 is most effective also in terms of the 5%-outage user throughput at ξ of 10^3.

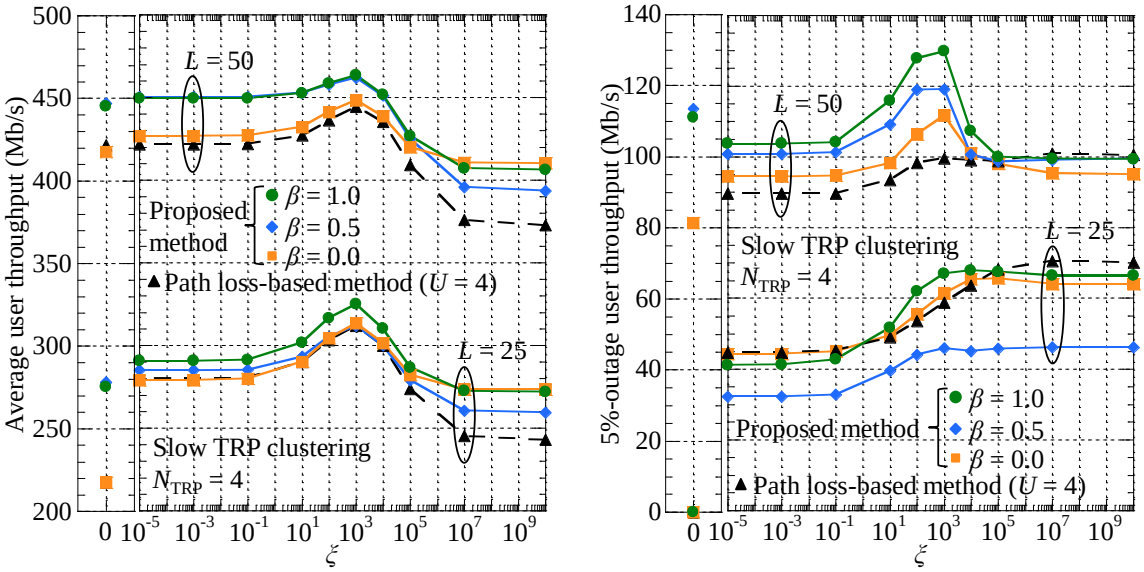

(a) Average user throughput. (b) 5%-outage user throughput.

Fig. 10-2 Average and 5%-outage user throughput as a function of ξ.

II-10.4. Conclusion

We investigated downlink cell-free MIMO in a partial CSI scenario and proposed a low-complexity user-centric TRP clustering method with RZF-based BF. The proposed method selects the TRP cluster for each UE based only on the average path gain information between UEs and TRPs. The proposed method does not require complex calculation of the BF matrix. The proposed method considers the BF gain and spatial interference levels, which is different from the conventional path loss-based method. Computer simulation results assuming a realistic partial CSI scenario show the effectiveness of the proposed method in terms of the achievable system-level throughput compared to the conventional path loss-based and SLNR-based methods.

REFERENCE

[1] E. Björson and L. Sanguinetti, "Scalable cell-free massive MIMO systems," IEEE Trans. Commun., vol. 68, no. 7, pp. 4247-4261, Jul. 2020.

[2] I. Kanno, K. Yamazaki, Y. Kishi, and S. Konishi, "A survey on research activities for deploying cell free massive MIMO towards beyond 5G," IEICE Trans. Commun., vol. E105-B, no. 10, pp. 1107-1116, Oct. 2022.

[3] M. Mojahedian and A. Lozano, "Subset regularized zero-forcing precoders for cell-free C-RANs," in Proc. IEEE EUSIPCO2021, Ireland, Aug. 2021.

[4] S. Buzzi, C. D'Andrea, A. Zappone, and C. D'Elia, "User-centric 5G cellular networks: Resource allocation and comparison with the cell-free massive MIMO approach," IEEE Trans. Commun., vol. 19, no. 2, pp. 1250-1264, Feb. 2020.

[5] Y. Oshima, A. Benjebbour, and K. Higuchi, “A novel adaptive interference admission control method for layered partially non-orthogonal block diagonalization for base station cooperative MIMO,” IEICE Trans. Commun., vol. E97-B, no. 1, pp. 155-163, Jan. 2014.

[6] C. B. Peel, B. M. Hochwald, A. L. Swindlehurst, “A vector-perturbation technique for near-capacity multiantenna multiuser communication-part I: Channel inversion and regularization,” IEEE Trans. Commun., vol. 53, no. 1, pp. 195-202, Jan. 2005.

[7] H. Q. Ngo, *et al.*, “Cell-free massive MIMO versus small cells,” IEEE Trans. Wireless Commun., vol. 16, no. 3, pp. 1834-1850, Mar. 2017.

II-11. Robust Massive MIMO Transmission Technology in Mobile Environments

Kazuki Maruta, Yuki Sasaki and Jin Nakazato, Tokyo University of Science
Tetsuya Iye, Shohei Takaya, Eisaku Sato and Yuki Susukida,
Kozo Keikaku Engineering Inc.
Chunh-Siang Huang and Koji Ikuta, Kyocera Corporation

Abstract— **Spatial multiplexing transmission technologies, such as MIMO and multi-user MIMO, mitigate interference between multiple signal streams by leveraging channel state information (CSI). In a mobile environment with varying channel conditions, the CSI could be changed rapidly and outdated over a short interval. Using such outdated CSI will introduce interference and cause conventional beamforming or null-steering methods to be degraded in performance. To address this challenge, we proposed a novel method called null-space expansion (NSE), which generates transmission weights by utilizing the rich spatial degrees of freedom available in Massive MIMO systems. This article introduces the concept of null-space expansion along with related research and development efforts.**

II-11.1. Introduction

Massive MIMO (Multiple-Input Multiple-Output), introduced in 5G mobile communications, dramatically improved spectral efficiency by enabling spatial multiplexing of multiple users. In the upcoming 6G mobile communication systems by 2030, Massive MIMO is still regarded as a core technology. However, for new services targeting high mobility users, channel time variation (i.e., CSI aging) becomes a major issue. Since channel state information (CSI) acquired at the base station (BS) is no longer accurate at the time of transmission, conventional beamforming struggles to suppress inter-user interference (IUI), which severely degrades system performance.

To address this problem, we proposed a novel spatial multiplexing transmission technique called Null-Space Expansion (NSE) and actively studied over the past decade. NSE utilizes the rich spatial degrees of freedom in Massive MIMO systems to place additional nulls in possible directions where interference is expected. By exploiting CSI from the past to the present time, NSE proactively suppresses the onset of IUI caused by CSI aging and achieves robust multi-user transmission ability even in fast-changing environments. This section presents an overview of NSE, its objectives, its application to multiuser MIMO, the underlying algorithms and equations, and its relevance to 6G.

II-11.2. Null-Space Expansion

II-11.2.1. Fundamental Theory

The null-space of a channel vector refers to the subspace of transmit signal vectors that result in zero received power at the receiver. Let M and K represent the number of base station (BS) antennas and users, respectively. Each user is assumed to have a single antenna. Given a channel vector $\mathbf{h}_k = (h_{k1},\ h_{k2},\ \ldots, h_{kM}) \in \mathbb{C}^{1\times M}$ for the k-th user at time t_0, the set of transmit vectors $\mathbf{w}_k(t_0) \in \mathbb{C}^{M\times 1}$ is designed to satisfy the following conditions:

$$\mathbf{h}_i(t_0)\mathbf{w}_k(t_0) \neq 0 \quad (i = k) \qquad \text{Eq. (11-1).}$$

$$\mathbf{h}_i(t_0)\mathbf{w}_k(t_0) = 0 \quad (i \neq k) \qquad \text{Eq. (11-2).}$$

In multiuser MIMO, beamforming vectors for each user are designed to avoid interference with others by placing beams in the null spaces of other users' channel vectors. In high-mobility environments, however, the channel state $\mathbf{h}_i(t)$ for undesired users, estimated at some time in the past, becomes outdated at transmission time $t + \Delta t$, and $\mathbf{h}_i(t_0 + \Delta t)\mathbf{w}_k(t_0) \neq 0$ may occur. This leads to residual interference and signal-to-interference power ratio (SIR) degradation.

NSE addresses this problem by expanding the null space in the time domain [1][2]. The concept of NSE is illustrated in Fig. 11-1. Specifically, it uses multiple past channel state information (CSI) vectors for undesired users and designs precoders that are orthogonal to all of them. That is, NSE places transmitting beams in the intersection of multiple null spaces, aiming to suppress interference resulting from future channel variation.

$$\mathbf{h}_i(t_0 - lT)\mathbf{w}_k^{\mathrm{NSE}}(t_0) = 0 \quad (i \neq k, l = 0, \ldots, L-1) \qquad \text{Eq. (11-3).}$$

where T denote the CSI acquisition period. l indicates the expansion order and represents the use of past CSI up to l time slots ago. If the number of antennas is large enough, these conditions can all be satisfied simultaneously; such a rich spatial degree of freedom (DoF) is typically available in Massive MIMO. As a specific implementation scheme, an extended channel matrix for the k-th user $\widehat{\mathbf{H}}_k \in \mathbb{C}^{\{L(K-1)+1\}\times M}$ is constructed by concatenating the current CSI vector of the desired user $\mathbf{h}_k^T(t_0)$ with multiple past and current channel vectors of other undesired users $\overline{\mathbf{H}}_k \in \mathbb{C}^{L\times M}$.

$$\widehat{\mathbf{H}}_k = [\mathbf{h}_k^T(t_0) \quad \overline{\mathbf{H}}_1^T \quad \cdots \quad \overline{\mathbf{H}}_{k-1}^T \quad \overline{\mathbf{H}}_{k+1}^T \quad \cdots \quad \overline{\mathbf{H}}_K^T] \qquad \text{Eq. (11-4).}$$

$$\overline{\mathbf{H}}_i = \begin{bmatrix} \mathbf{h}_i(t_0) \\ \mathbf{h}_i(t_0 - T) \\ \vdots \\ \mathbf{h}_i(t_0 - (L-1)T) \end{bmatrix} \qquad \text{Eq. (11-5).}$$

NSE suppresses interference toward undesired users even if the channel changes over time, by considering not only the current CSI but also past CSIs when designing transmitting beam patterns.

In NSE, the transmitting beam is designed to be orthogonal to multiple past channel vectors, where the system could preemptively suppress interference caused by future channel variations. This functionality of NSE requires rich spatial DoF, hence it is well-suited with Massive MIMO systems. Especially for a BS is equipped with a lot of antenna element. By designing orthogonality to multiple past channel vectors, the beam remains robust even if the channel fluctuates slightly due to mobility. In other words, NSE expands null-steering capability in spatial domain, even the channel varies over time. NSE improves the spatial multiplexing performance for multiuser MIMO system in mobility environments.

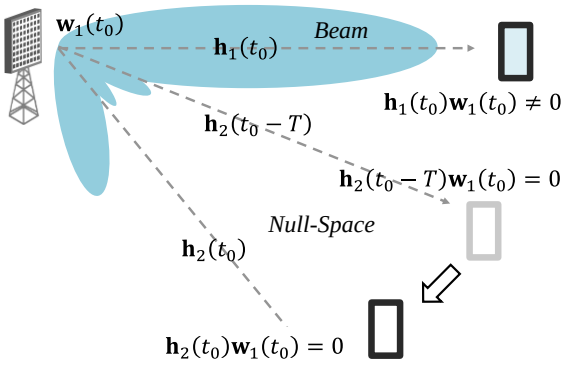

Fig. 11-1. Overview of null-space expansion.

II-11.2.2. Recent Advancement of Null-Space Expansion in Japan

NSE is applicable to both downlink and uplink multiuser MIMO [3], but it is especially beneficial for downlink multiuser MIMO systems in which the BS simultaneously serves multiple user terminals with large-scale antenna arrays. The following provides an overview of research related to NSE conducted within Japan. NSE reduces desired signal gain by consuming DoF for additional nulling. Literature [4] conceived to reduce the required null-space dimensions by extracting the interference subspace. A foundational study was provided to clarify the principles of NSE through a mathematical approach [5]. By appropriately selecting users based on the expanded null-space, the effectiveness of NSE in time-varying channel environments can be further enhanced [6]. Hardware implementation and laboratory experiments have validated the feasibility of receiver-side NSE [7]. Combining NSE with receiver-side beamforming significantly improves multiuser spatial multiplexing performance [8]. The iterative approximation of the pseudo-inverse matrix of $\widehat{\mathbf{H}}_k$ reduces the computational complexity while allowing some reduction in the NSE's interference suppression capability [9]. To compensate the performance degradation caused by such simplification, adaptive regularization based on Doppler characteristics has been introduced, maintaining robustness under channel variation [10].

II-11.2.3. Technical Challenges and Relevance to 6G

The practical implementation of NSE faces several challenges, foremost among them being the design of a CSI estimation framework that enables effective NSE implementation. This necessitates careful planning of reference signal placement to ensure accurate CSI acquisition. In the context of 6G, the anticipated use of higher frequency bands, such as the sub-terahertz band, will lead to the deployment of antenna arrays with a significantly larger number of elements. This evolution aligns with the concept of Extremely Large-Scale MIMO (XL-MIMO), which involves arrays with hundreds or even thousands of antennas. While XL-MIMO offers enhanced spatial resolution and capacity, it also introduces new challenges, including increased signal processing complexity, spatial non-stationarity, and near-field propagation effects that differ from traditional MIMO systems.

NSE addresses key design targets such as reliable high-mobility communication, interference-aware multi-user access, and support for dense terminal scenarios. It offers stable transmission performance in emerging use cases such as augmented and virtual reality (AR/VR) and connected automated vehicles (CAVs), where channel conditions vary rapidly. Furthermore, NSE aligns well with advanced 6G network architectures. In Cell-Free Massive MIMO, it helps suppress interference across spatially distributed antenna elements by expanding nulls over both space and time domains. Additionally, in systems assisted by Reconfigurable Intelligent Surfaces (RIS), NSE can serve as a complementary technique by further suppressing residual interference that remains after environmental control is applied. Overall, NSE is positioned as a fundamental technique for achieving robust, interference-resilient communication in 6G, particularly in scenarios requiring high capacity, high reliability, and dynamic interference control.

II-11.3. Toward Advanced V2X Communications in Millimeter-Wave Bands

In vehicle-to-everything (V2X) scenarios leveraging millimeter-wave (mmWave) communications, beamforming is essential for ensuring coverage as well as delivering high-definition sensor data to support safe automated driving via cooperative perception. Meanwhile, such a high mobility environment complicates beam tracking to target vehicles. One of our research and development project commissioned by Japan's Ministry of Internal Affairs and Communications (MIC) proposes a framework that integrates beam tracking with NSE to realize high-capacity mmWave V2X communication [11]. Its overview is depicted in Fig. 11-2. Two key aspects are emphasized:

(1) Coordinated Beam Tracking and Nulling in mmWave Environments

To address frequent Line-of-Sight (LoS) blockages caused by large vehicles or buildings, Roadside Units (RSUs) coordinate with vehicles to track beams and expand nulls using NSE based on past/predicted CSI including dynamic handover management. This

ensures robust communication and stable multiplexing even under rapid channel variation [12]. In addition, multi-point transmission can contribute to further enhancement of transmission capacity.

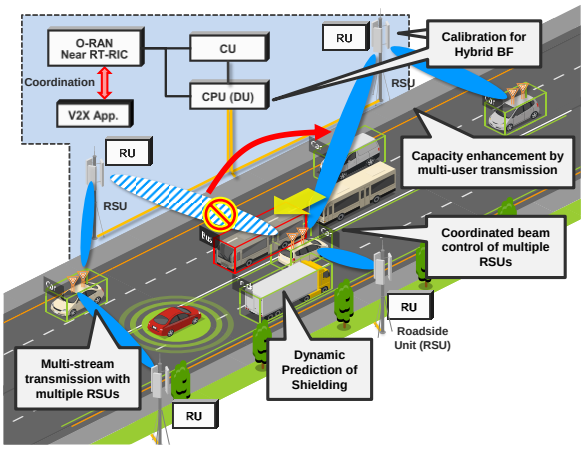

Fig. 11-2. Project overview.

(2) Site-Specific Propagation Modeling via Open Wireless Digital Twin

This work also develops an Open Wireless Digital Twin (OWDT) that integrates 3D geographic data, such as OpenStreetMap and PLATEAU, with mobility simulators like SUMO [13]. By combining these components, the OWDT enables realistic traffic modeling with time-synchronized vehicle trajectories, emulates ray-traced millimeter-wave propagation using tools such as Sionna and Wireless InSite (see Fig. 11-3). Although the platform currently supports single-input single-output (SISO) communication in the Sub-6 GHz band, further development will enable the evaluation of massive array beam tracking and interference suppression techniques under site-specific conditions. This advancement will support the realization of real-time adaptive beam control in 6G vehicular networks.

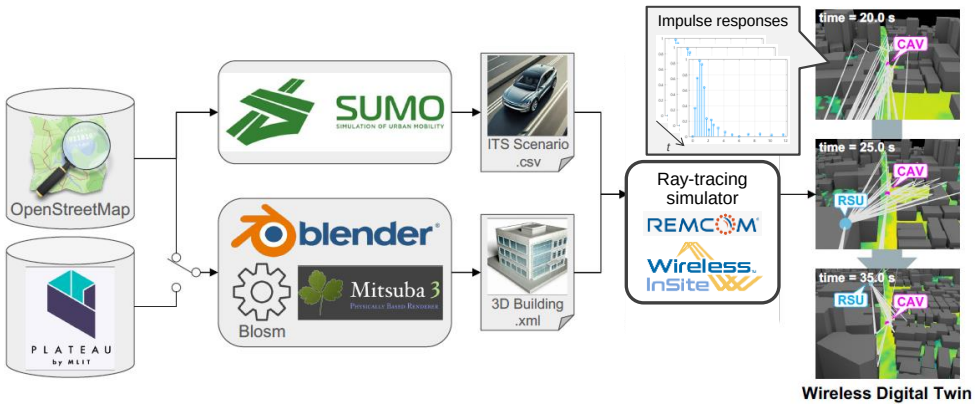

Fig. 11-3. Framework of open wireless digital twin (OWDT).

II-11.4. Implementation Challenges and NSE with Phase-only Adaptive Nulling

Full digital implementations allow flexible spatial precoding, such ways are costly with higher power consumption. To reduce implementation costs, hybrid beamforming architectures are widely adopted nowadays, as they have less RF chains and only contain analog phase shifters. To apply NSE under such constraints, we have proposed the Phase-Only Adaptive Nulling (POAN) based NSE [14]. This approach formulates beamforming/null-steering as a phase-only optimization problem using SIR as the

objective function. By iteratively updating the beamforming weights based only on phase weights, nulls can be placed in possible interfered directions without controlling amplitude weights in adaptive array antenna signal processing. The method extends the interference steering vector to include CSIs corresponding to the past or the predicted directions, enabling NSE even with phase-only constraints.

To assess the effectiveness of our proposal, a simulation study was conducted focusing on multiuser MIMO spatial multiplexing in a high-mobility scenario. The simulation schemes include the coordinated beam tracking combined with angular-based NSE, as described in Section II-11.3. . In Fig. 11-4(a), the simulation consists of a BS equipped with a uniform rectangular antenna array that serves two user terminals moving toward each other. The beam is directed toward the target user while additional nulls are formed in possible interfered directions. The radio channel is assumed to be free-space propagation condition, with a BS transmitting power of 30 dBm and a feeder loss of 3 dB. The beam tracking period is 20 ms, and CSI updating period is 200 ms. The dimension of the expanded null-space is set to five using past CSI, including the most recent one (L=5). Fig. 11-4(b) presents the simulation results in terms of the cumulative distribution function (CDF) of SINR. The black line is conventional null-steering based on QR decomposition, which does not expand the null space. The orange line is the basic NSE algorithm that utilizes past CSI to enhance interference suppression. The red line is the method that integrates beam tracking with NSE to compensate for beam misalignment due to mobility. The blue line is POAN-NSE, which realizes null-space expansion using phase-only control under analog beamforming constraints.

The above results show that conventional null-steering (black line) suffers from SINR degradation in mobile environments due to outdated CSI. On the other hand, NSE (orange line) improves SINR by utilizing multiple past CSIs, and when beam tracking is combined (red line), it could achieve the best performance. POAN-NSE (blue line), even

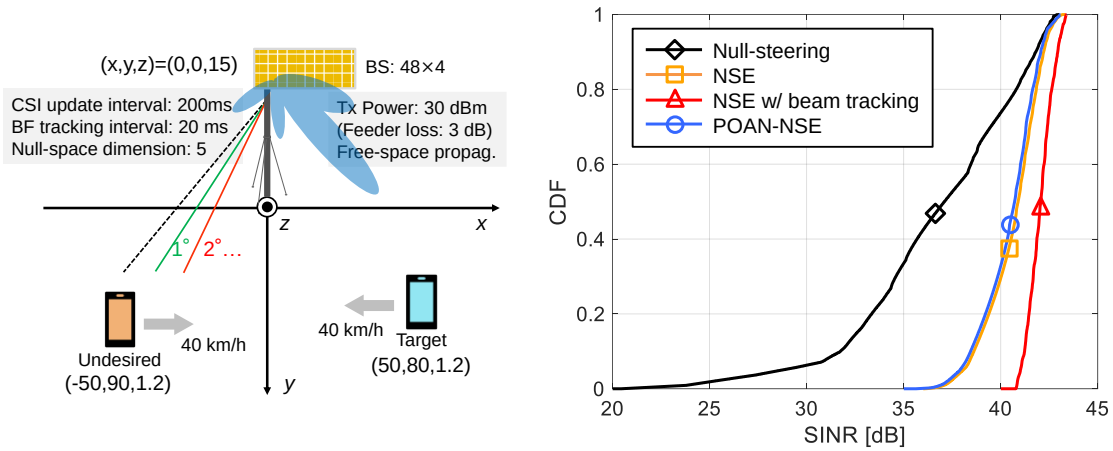

(a) Simulation condition (b) CDF of SINR

Fig. 11-4. Simulation example.

only controls phase weights, which could achieve a comparable result of SINR versus full digitally controlled NSE. Regarding the high hardware cost of full digital beamforming architecture, our result demonstrated that POAN-NSE can achieve interference suppression, with simplified architecture with lower cost.

As a summary, the simulations verified the core technology of NSE and its derivatives, which can significantly improve the robustness of spatial multiplexing in mobile scenarios. Our future work will aim to address practical limitations of POAN-NSE, including null accuracy degradation due to quantization error in phase weight control, and new challenges in extending nulling across broadband signals. At the meantime, the need for dynamic optimization of null directions in response to different user mobility and directions. From our perspective, POAN-NSE is a promising technique for achieving robust and providing interference suppression ability in cost-effective 6G massive MIMO systems.

II-11.5. Conclusion

This section introduced Null-space expansion (NSE), as a novel signal processing approach that enhances transmission robustness in mobile environments by utilizing the rich spatial degrees of freedom (DoF) in large-scale antenna systems. We explained the fundamental theory of NSE and gave a survey on this technique in the past decade. The latest studies are on beam tracking coordination and possible implementation using phase-only adaptive nulling control (POAN). There are still many open challenges, such as user mobility, and system-level integration, this technique remains a promising and valuable object to study. Its flexibility and potentiality can contribute toward realizing high-reliability, interference-resilient wireless communication in the 6G era.

REFERENCE

[1] T. Iwakuni, K. Maruta, A. Ohta, Y. Shirato, T. Arai, and M. Iizuka, "Null-space expansion for multiuser massive MIMO inter-user interference suppression in time varying channels," *IEICE Transactions on Communications*, vol. E100.B, no. 5, pp. 865–873, 2017.

[2] T. Iwakuni, K. Maruta, A. Ohta, Y. Shirato, and M. Iizuka, "Experimental verification of null-space expansion for multiuser massive MIMO via channel state information measurement," *IEICE Transactions on Communications*, vol. E101.B, no. 3, pp. 877–884, Mar. 2018.

[3] K. Arai, K. Maruta, and C.-J. Ahn, "Uplink null-space expansion for multiuser massive MIMO in time-varying channels under unknown interference," *IEEE Access*, vol. 8, pp. 224 292–224 305, Dec. 2020.

[4] N. Funaki, K. Maruta, and C.-J. Ahn, "Dimensionality reduction of interference subspace for multiuser massive MIMO null-space expansion," *Digital Signal Processing*, vol. 114, 103063, July 2021.

[5] H. Ban, D. Motegi, M. Taromaru, and M. Ohta, "A study on propagation model and mechanism on null-space dimension expansion for multi-user MIMO tolerant to channel fluctuation," Proc. *2017 Int. Workshop on Smart Wireless Commun. (SmartCom)*, vol. 117, no. 257, 2016, pp. 63–64.

[6] Y. Sasaki, K. Arai, J. Nakazato, and K. Maruta, "Time-series-aware user scheduling for multi-user massive MIMO null-space expansion," Proc. *IEEE International Conference on Communications (ICC 2024)*, June 2024.

[7] S. Kobayashi, Y. Ohi, H. Murata, M. Taromaru, T. Iwakuni, D. Uchida, T. Fujita, "Experimental Performance of Null-Space Expanded MIMO Reception Technique," Proc. *2024 IEEE 29th Asia Pacific Conference on Communications (APCC)*, pp. 300-302, Nov. 2024.

[8] Y. Sasaki, K. Arai, J. Nakazato, and K. Maruta, "Receiver maximum eigenmode beamforming-based null-space expansion for multi-user massive MIMO in time-varying channel," *IEEE Transactions on Vehicular Technology*, Feb. 2025.

[9] Y. Tsunoda, T. Suzuki, Y. Sasaki, K. Maruta, "Iterative Interference Replica Subtraction Based Low-Complexity Precoding for Multiuser Massive MIMO Null-Space Expansion," Proc. *The 2025 IEEE 101st Vehicular Technology Conference (VTC2025-Spring)*, June 2025.

[10] Y. Sasaki, S. Berra, S. Chakraborty, J. Nakazato, R. Dinis, K. Maruta, "Newmann Series-based Precoding Weight Design for Multi-User Massive MIMO Null-Space Expansion," Proc. *The 2025 IEEE 101st Vehicular Technology Conference (VTC2025-Spring)*, June 2025.

[11] J. Nakazato, T. Iye, Y. Susukida, E. Sato, Y. Sasaki, K. Maruta, M. Tsukada, "Toward 6G Mobility Network: Design of a Wireless Digital Twin for Connected Autonomous Vehicle," Proc. *IEEE Consumer Communications & Networking Conference (CCNC 2025)*, Jan. 2025.

[12] S. Ozawa, Y. Sasaki, J. Nakazato, K. Maruta, "Optimized Broad-Range Null-Steering Incorporated with O-RAN-Based Beam Tracking for Millimeter-Wave V2X," Proc. *IEEE Vehicular Technology Conference (VTC2025-Spring)*, June 2025.

[13] T. Iye, M. Sakamoto, S. Takaya, E. Sato, Y. Susukida, Y. Nagaoka, K. Maruta, J. Nakazato, "Open Wireless Digital Twin: End-to-End 5G Mobility Emulation in O-RAN Framework," *arXiv preprint* arXiv:2503.12177, 2025.

[14] T. Ikuta, K. Maruta, C. Huang, K. Ikuta, "Null-Space Expansion with Phase Control for Analog Beamforming Massive MIMO," *IEICE Tech. Rep.*, vol. 124, no. 409, RCS2024-257, pp. 7-12, March 2025.

II-12. Recent R&D Activities of Distributed MIMO (D-MIMO) Technologies in Japan

Koji Ishibashi
The University of Electro-Communications

Abstract— **Distributed multiple-input multiple-output (D-MIMO) technologies and their variants, such as cell-free massive MIMO, are emerging as promising enablers for enhancing capacity and achieving stable, reliable communications in 6G networks. These approaches address the limitations of conventional centralized architectures by distributing antennas across a wide area, which helps to mitigate interference and improve signal quality. In addition, they offer greater flexibility in network deployment and can adapt to diverse propagation environments. This article reviews recent research and development activities on D-MIMO in Japan.**

II-12.1. Introduction

D-MIMO, including cell-free massive MIMO, is a promising approach for 6G. To overcome the well-known cell-edge problem in traditional cellular systems, interference must be treated deterministically rather than stochastically. Consequently, cell-free massive MIMO, where all antennas are jointly controlled by a single central processing unit (CPU), has emerged [1]. Mathematically, cell-free massive MIMO is equivalent to a distributed antenna system without the other cells or small-cell configuration, namely highly dense BS placement with a single antenna, with full cooperation among BSs [2]. As obvious, this configuration does not have the *cell-boundary*, so that interference among different streams can be eliminated through beamforming. However, this centralized processing architecture leads to the remarkably high load at the CPU. Therefore, exchanged signal reduction based on clustering has been actively discussed [3]. Considering latency and cost for fronthaul links between APs and CPU, cell-free network with multiple CPUs has also been studied. This architecture is mathematically and conceptually equivalent to a cellular system with distributed antennas operating under full cooperation among base stations, as in virtual MIMO and network MIMO. Although D-MIMO systems and their variants have been explored for an extended period, market adoption has been limited. This is largely due to the high implementation costs, including the need for precise phase and time synchronization among UEs and APs, as well as the extensive fronthaul/backhaul infrastructure required. This article reviews recent research activities in Japan aimed at addressing these challenges.

II-12.2. Research on Hardware Limitations or Imperfections

As described above, addressing hardware limitations and imperfections in D-MIMO systems is essential. In response, research activities in Japan have been undertaken to

tackle these challenges. The most significant barrier to realizing these systems in practice is the finite capacity of both fronthaul and backhaul links. Every AP connects to a CPU via a dedicated optical fiber cable, known as the fronthaul. Since the fronthaul must transmit complex signals at the Nyquist symbol period, especially during uplink transmission, it must operate at a rate higher than the system's symbol rate. One effective solution to mitigate this high-rate requirement is to employ low-resolution analog-to-digital converters (ADCs) [4][5]. In [4], the uplink signal detection in cell-free networks subject to limited fronthaul link capacity and highly correlated channel condition has been discussed. In [5], joint channel and data estimation (JCDE) based on Bayesian inference was proposed for the uplink transmission of cell-free networks with limited fronthaul link capacity. Furthermore, the clustering design of D-MIMO systems by limiting the dedicated APs is actively discussed [6]. To further enhance the scalability, the system with multiple CPUs has been investigated [7], and further discussions under limited backhaul capacity can be found [8][9], revealing the actual gain achieved through multiple CPU cooperation. Moreover, achieving precise phase and time synchronization among UEs and APs is extremely challenging in practice. Consequently, various methods for synchronization have been actively discussed, e.g., [10][11].

II-12.3. Research on Duplex Techniques

Time division duplex (TDD) is considered a key enabler for massive MIMO technologies, as it allows the exploitation of channel reciprocity between uplink and downlink. This means that the overhead of channel estimation depends only on the number of UEs, not on the number of antennas, making it a scalable solution even with large antenna arrays. As a result, the majority of current research on D-MIMO is based on the TDD protocol.

On the other hand, frequency division duplex (FDD), which uses separate frequency bands for uplink and downlink and allows simultaneous transmission in both links, does not benefit from channel reciprocity and requires downlink pilot transmission and feedback for each antenna element. As the number of antennas increases, the overhead becomes a serious issue. To address this challenge, recent studies have proposed novel approaches that exploit angle reciprocity, enabling downlink channel estimation with limited feedback [12]. Nonetheless, a fundamental issue remains in FDD systems: the limited number of orthogonal pilot sequences. This constrains the number of simultaneously supported UEs and imposes a scalability bottleneck when the number of UEs becomes comparable to the number of available orthogonal pilots.

One possible solution to this problem is to implement in-band full-duplex technology at each AP. However, this approach requires remarkably complex signal processing and becomes less preferable, especially in cell-free architectures where a large number of APs are deployed. As an alternative without changing the hardware of the APs, Network-

Assisted Full-Duplex (NAFD) has been proposed [13][14][15][16], where each AP is assigned to either uplink or downlink to enable full-duplex transmission through the whole network. In [13][14], optimal AP configuration and the corresponding beamforming have been derived using convex optimization techniques, and it is shown that optimized NAFD significantly outperforms conventional TDD in terms of the sum spectral efficiency and user fairness. Since these papers assumed the perfect CSI in optimization, the AP configuration using large scale fading has been further investigated [15][16]. Especially, in [15], practical user-centric clustering and downlink power control have been proposed, where APs in a cluster for each UE must have the same transmission direction, namely either uplink or downlink, and clusters with the same transmission direction can share APs. NAFD-based cell-free network with this practical clustering remarkably improves the sum spectral efficiency when the fronthaul capacity is limited.

II-12.4. Conclusion

This article introduced recent research efforts in Japan aimed at addressing practical challenges of D-MIMO systems, including cell-free MIMO. In addition to the work mentioned above, there are ongoing discussions on advanced beamforming techniques [17] and the application of D-MIMO technologies in millimeter-wave communications [18]. While some remarkable contributions such as in the areas of distributed beamforming and CSI acquisition have successfully addressed fundamental issues, a significant gap still remains between theoretical insights and practical implementation. This underscores the need for further research and real-world experimentation to bridge this gap.

REFERENCE

[1] H. Q. Ngo, A. Ashikhmin, H. Yang, E. G. Larsson and T. L. Marzetta, "Cell-Free Massive MIMO: Uniformly great service for everyone," *2015 IEEE 16th Intl. Workshop on Signal Process. Adv. in Wireless Commun.* (SPAWC), Stockholm, Sweden, pp. 201-205, 2015.

[2] J. Hoydis, M. Kobayashi and M. Debbah, "Green Small-Cell Networks," *IEEE Veh. Technol. Mag.*, vol. 6, no. 1, pp. 37-43, March 2011.

[3] E. Björnson and L. Sanguinetti, "Scalable Cell-Free Massive MIMO Systems," *IEEE Trans. Commun.*, vol. 68, no. 7, pp. 4247-4261, July 2020.

[4] K. Ando, H. Iimori, T. Takahashi, K. Ishibashi, and G. T. F. de Abreu, “Uplink Signal Detection for Scalable Cell-Free Massive MIMO Systems With Robustness to Rate-Limited Fronthaul,” *IEEE Access*, vol. 9, pp. 102770 – 102782, July 2021.

[5] T. Takahashi, H. Iimori, K. Ando, K. Ishibashi, S. Ibi, and G. T. F. de Abreu, “Bayesian Receiver Design via Bilinear Inference for Cell-Free Massive MIMO with Low-Resolution ADCs,” *IEEE Trans. Wireless Commun.*, vol. 22, no. 7, pp. 4756-4772, July 2023.

[6] D. Ishii, T. Hara and K. Higuchi, "Throughput Maximization-Based AP Clustering Methods in Downlink Cell-Free MIMO Under Partial CSI Condition," in *IEICE Trans. Commun.*, vol. E107-B, no. 10, pp. 653-660, October 2024.

[7] R. Takahashi, H. Matsuo, F. Adachi, Joint Multi-Layered User Clustering and Scheduling for Ultra-Dense RAN Using Distributed MIMO, *IEICE Trans. Commun.*, 2021, E104.B vol. 9, p. 1097-1109, Sept. 2021.

[8] M. Ito, S. Fukue, K. Ando, I. Kanno, K. Yamazaki, and K. Ishibashi, “Clustering and Beamforming for User-Centric Cell-Free Massive MIMO With Backhaul Capacity Limitation,” *IEEE Access*, vol. 12, pp. 382-395, 2024.

[9] F. Ndimumahoro and K. Ishibashi, “Distortion-Aware Clustering for Cell-Free Massive MIMO Under Backhaul Capacity Limitation,” IEEE 22nd Consumer Communications & Networking Conference (CCNC), Las Vegas, NV, USA, 2025.

[10] R. Kanzaki, K. Ueda, T. Takahashi, and K. Ishibashi, "Joint Estimation Method of User-Activity, Carrier Frequency Offset, and Channel Coefficient for Cell-Free Massive MIMO," *IEICE Tech. Rep.*, vol. 124, no. 311, RCS2024-193, pp. 104-109, Dec. 2024.

[11] H. Iimori, T. Takahashi, K. Ishibashi, G. T. F. de Abreu, and W. Yu, “Grant-Free Access via Bilinear Inference for Cell-Free MIMO With Low-Coherence Pilots,” *IEEE Trans. Wireless Commun.*, vol. 20, no. 11, pp. 7694-7710, Nov. 2021.

[12] L. Miretti, E. Björnson and D. Gesbert, "Team MMSE Precoding With Applications to Cell-Free Massive MIMO," IEEE Trans. on Wireless Commun., vol. 21, no. 8, pp. 6242-6255, Aug. 2022.

[13] S. Fukue, H. Iimori, G. T. F. De Abreu and K. Ishibashi, “Joint Access Configuration and Beamforming for Cell-Free Massive MIMO Systems With Dynamic TDD,” *IEEE Access*, vol. 10, pp. 40130-40149, Apr. 2022.

[14] S. Fukue, G. T. Freitas de Abreu and K. Ishibashi, "Network-Assisted Full-Duplex Millimeter-Wave Cell-Free Massive MIMO with Localization-Aided Inter-User Channel Estimation," *2023 Intl. Conf. on Inf. Networking (ICOIN)*, Bangkok, Thailand, pp. 13-18, 2023.

[15] K. Okui, K. Ando, G. Abreu and K. Ishibashi, "Scalable Network-Assisted Full-Duplex Cell-Free Massive MIMO With Limited Fronthaul Capacity," *IEEE VTC2023-Fall*, Hong Kong, pp. 1-5, 2023.

[16] H. Iimori, J. Huschke, and J. Vieira, " Radio Unit Configuration for Dynamic Time Division Duplex in Distributed MIMO Systems," *IEEE GLOBECOM*, Kuala Lumpur, Malaysia, pp. 2543-2548, 2023.

[17] K. Ando, H. Iimori, G. T. F. de Abreu, and K. Ishibashi, “User-Heterogeneous Cell-Free Massive MIMO Downlink and Uplink Beamforming via Tensor Decomposition,” *IEEE Open J. Commun. Soc.*, vol. 3, pp. 740-758, Apr. 2022.

[18] S. Kamiwatari, M. Ito, I. Kanno, K. Ando and K. Ishibashi, "Interference-Aware Analog Beam Selection for Cell-Free Massive MIMO With Hybrid Beamforming Over Millimeter-Wave Channels," 2024 IEEE 21st Consumer Communications & Networking Conference (CCNC), Las Vegas, NV, USA, 2024, pp. 696-701.